

STATUS OF THESIS

Title of thesis

RESIDUAL STRENGTH ASSESSMENT OF CORRODED
PIPELINES

I, CHANYALEW TAYE BELACHEW
hereby allow my thesis to be placed at the Information Resource Center (IRC) of
Universiti Teknologi PETRONAS (UTP) with the following conditions:

1. The thesis becomes the property of UTP
2. The IRC of UTP may make copies of the thesis for academic purposes only.
3. This thesis is classified as

Confidential

Non-confidential

If this thesis is confidential, please state the reason:

The contents of the thesis will remain confidential for _____ years.

Remarks on disclosure:

Endorsed by:

Signature of Author

Signature of Supervisor

Permanent address:
Addis Ababa Institute of Technology
Addis Ababa, Ethiopia
P. O. Box 385

Name of Supervisor:
Assoc. Prof. Ir. Dr. Mokhtar Che Ismail

Date : _____

Date : _____

UNIVERSITI TEKNOLOGI PETRONAS
RESIDUAL STRENGTH ASSESSMENT OF CORRODED PIPELINES
by
CHANYALEW TAYE BELACHEW

The undersigned certify that they have read, and recommend to the Postgraduate Studies Programme for acceptance of this thesis for the fulfilment of the requirements for the degree stated.

Signature: _____

Main Supervisor: Assoc. Prof. Ir. Dr. Mokhtar Che Ismail

Date: _____

Signature: _____

Co-Supervisor: Dr. Saravanan Karuppanan

Date: _____

Signature: _____

Head of Department: Assoc. Prof. Dr. Ahmad Majdi Bin Abdul Rani

Date: _____

RESIDUAL STRENGTH ASSESSMENT OF CORRODED PIPELINES

by

CHANYALEW TAYE BELACHEW

A Thesis

Submitted to the Postgraduate Studies Programme

as a Requirement for the Degree of

DOCTOR OF PHILOSOPHY

MECHANICAL ENGINEERING

UNIVERSITI TEKNOLOGI PETRONAS

BANDAR SERI ISKANDAR,

PERAK

AUGUST 2011

DECLARATION OF THESIS

Title of thesis

RESIDUAL STRENGTH ASSESSMENT OF CORRODED
PIPELINES

I, CHANYALEW TAYE BELACHEW

hereby declare that the thesis is based on my original work except for quotations and citations which have been duly acknowledged. I also declare that it has not been previously or concurrently submitted for any other degree at UTP or other institutions.

Witnessed by:

Signature of Author

Signature of Supervisor

Permanent address:
Addis Ababa Institute of Technology
Addis Ababa, Ethiopia
P. O. Box 385

Name of Supervisor:
Assoc. Prof. Ir. Dr. Mokhtar Che Ismail

Date : _____

Date : _____

Dedicated to my beloved wife, Alem Gemechu

ACKNOWLEDGMENT

Above all, I praise the Almighty Father and Lord Jesus Christ who gave me His enabling grace to successfully undertake this challenging research work beyond my expectation.

It is with immense gratitude that I acknowledge the support of my supervisor AP. Ir. Dr. Mokhtar Che Ismail for his unreserved guidance and support as backbone for successful completion of this research work. I also would like to gratefully thank my co-supervisor Dr. Saravanan Karuppanan for his assistance and crucial contribution to this research work. It was a blessing for me to have such intimate and helpful supervisors.

It is my pleasure to thank UTP for providing grants and facilities for undertaking my research work. Furthermore, my great thanks goes to Addis Ababa University for granting me a study leave to pursue and make my graduate studies possible. I am also grateful to PETRONAS Sdn. Bhd. for providing pipelines and covering the major expenses to carry out the lab tests.

I owe my warm gratitude to UTP technicians who assisted me in the experimental part of the research work. All the tough jobs of burst test sample preparation and material tests were made possible due to the unreserved assistance of Mr. Jani Bin Aland Ahmad, Mr. Shaiful Hisham Bin Samsudin, Mr. Johan Ariff Bin Mohamed and Mr. Mohd Hafiz Bin Baharun. Special thanks also goes to Dr. Nasir Shafiq for his advice and facilitation of the lab test. I am indebted to thank all my friends and all my relatives who created conducive work environment and gave me moral support throughout my research period.

Last but not least, I thank my colleagues Mr. Aja Ogboo Chikere for proofreading this manuscript and Ms. Nor Nurulhuda Binti Md. Ibrahim for translating the abstract to Bahasa Melayu.

ABSTRACT

Pipelines are one of the most efficient means for transporting hydrocarbons from one point to the other point, which may be routed within onshore or offshore locations. There is a great risk while operating these pipelines due to defects occurring during the service life. Corrosion is one of the most common defects observed in many instants. At the point of corrosion, the wall of the pipe section becomes thinner and starts to lose its mechanical resistance. Therefore, appropriate defect assessment method is necessary in order to decide whether to keep them into continual operation or to make a shutdown for necessary maintenance or replacement of sections of the pipeline.

Methods for assessing metal loss defects have been available for many decades, as for instance the NG-18 equation and ANSI/ASME B31G code. Throughout the years, many modifications to the original equations have been made and newer methods like Modified B31G and RSTRENG were adopted. Moreover, these days, there are several in-house methods and commercial codes. A quantitative study on the prediction by five most applicable current assessment methods showed big bias and large scatters against burst test database. For example, the burst capacity prediction made by B31G criteria showed an average bias of about 31% under estimation with up to 72% lower predictions. Hence, these methods enforce either unnecessary maintenance or premature replacement of pipelines. But pipeline operators need a reliable defect assessment methodology not only to assure safe operation but also to implement optimum operation cost.

This research was conducted to develop a new method for the residual strength assessment of corroded pipeline based on burst test and a series of nonlinear finite element (FE) analyses. The burst test samples were taken from API X52 pipeline retired from service due to corrosion. Burst tests were conducted in order to study the failure mode and to validate the FE approach for the assessment of corroded pipelines.

The burst test showed that the failure of the corroded pipeline is due to plastic collapse. The FE simulations corresponding to the test samples well matched with burst test results within less than 5% error. Thus, the FE simulation was used as a complement to the burst test database in order to develop a new corrosion assessment method. Stress-based criterion based on plastic instability analysis was used to predict the failure pressure.

This research contributed to the development of an alternative corrosion defect assessment method. The New Method can predict the burst pressure of corroded pipelines with better accuracy than the currently used corrosion assessment codes and norms. The New Method agreed with the burst test database with predictions evenly distributed within about $\pm 7\%$ along the actual value with an average error of only about 0.30%. For the same burst test database, the Modified B31G gave conservative predictions with a mean bias of about 24% with as low as 52% predictions than the actual value. Therefore, pipeline operators and engineers will benefit from this research.

ABSTRAK

Saluran paip penyalur adalah salah satu cara yang paling efisien untuk memindahkan hidrokarbon dari satu tempat ke tempat yang lain, sama ada yang menyalurkan dalam lokasi onshore atau offshore. Terdapat risiko yang besar semasa mengendalikan paip penyalur tersebut kerana berlaku kerosakan dalam tempoh penggunaan. Kakisan merupakan salah satu masalah yang paling biasa terjadi. Pada bahagian berlakunya kakisan, dinding paip menjadi nipis dan mula hilang ketahanan mekanik. Oleh kerana itu, kaedah penilaian kerosakan yang sesuai diperlukan untuk memutuskan sama ada operasi akan tetap diteruskan atau berhenti dilakukan untuk penyelenggaraan atau menggantikan bahagian paip pergantian.

Kaedah untuk menguji kerosakan telah wujud sejak beberapa dekad, seperti persamaan NG-18 dan kod ANSI/ASME B31G. Sepanjang tahun banyak pengubahsuaian persamaan asal telah dibuat dan kaedah yang terbaru seperti B31G yang dimodifikasi oleh RSTRENG digunakan. Selain itu, terdapat beberapa kod yang digunakan oleh perseorangan dan industri. Satu kajian kuantitatif tentang ramalan dengan lima kaedah yang terbaru menunjukkan terdapat ralat yang besar dan taburan yang besar terhadap data ujian letupan. Sebagai contoh, ramalan kapasiti letupan yang diperoleh daripada kriteria B31G menunjukkan ralat purata sekitar 31% dan sekitar 72% dibawah perkiraan. Oleh kerana itu, kaedah ini tidak memerlukan penyelenggaraan atau penggantian paip pada awal operasi. Operator paip penyalur memerlukan kaedah penilaian kerosakan yang boleh dipercayai kerana tidak hanya untuk memastikan operasi dalam keadaan yang selamat tetapi juga untuk memastikan kos operasi adalah optimum.

Kajian ini dilakukan untuk membangunkan kaedah baru bagi penilaian kekuatan sisa paip yang kakisa berdasarkan tes letupan dan juga metode elemen hingga analisa. Sampel tes letupan diambil daripada paip API X52 yang tidak digunakan disebabkan kakisan. Tes letupan dilakukan untuk mengetahui model kegagalan dan untuk

mengesahkan pendekatan FE bagi penilaian paip yang berkarat. Tes letupan menunjukkan kegagalan paip yang terkakis disebabkan oleh kegagalan plastik. Simulasi FE yang sesuai dengan sample ujian sampel bersamaan dengan keputusan tes letupan iaitu kurang daripada 5% ralat. Dengan demikian, simulasi FE digunakan sebagai pelengkap untuk data tes letupan dalam rangka untuk mengembangkan kaedah penilaian baru bagi kakisan. Kriteria berasaskan tekanan berdasarkan analisis ketidak stabilan plastik digunakan untuk meramalkan tekanan letupan.

Kajian ini memberi sumbangan terhadap pembangunan kaedah penilaian pilihan bagi masalah kakisan. Kaedah Baru dapat meramal tekanan letupan untuk paip yang terkakis dengan ketepatan yang lebih baik berbanding kaedah penilaian terkakis kod dan aturan. Ramalan yang dihasilkan oleh Kaedah Baru bersamaan dengan data tes letupan dengan ramalan sekitar $\pm 7\%$ sepanjang nilai sebenar dengan purata ralat iaitu hanya sekitar 0.30%. Untuk data tes letupan yang sama, ramalan yang dihasilkan oleh B31G yang dimodifikasi memberikan ramalan yang paling aman dengan rerata simpangar sekitar 24% daripada nilai sebenar dengan anggaran setinggi 52% daripada nilai sebenar. Rumusannya, pembekal paip dan jurutera akan mendapat manfaat daripada kajian ini.

In compliance with the terms of the Copyright Act 1987 and the IP Policy of the university, the copyright of this thesis has been reassigned by the author to the legal entity of the university,

Institute of Technology PETRONAS Sdn Bhd.

Due acknowledgement shall always be made of the use of any material contained in, or derived from, this thesis.

© Chanyalew Taye Belachew, 2011
Institute of Technology PETRONAS Sdn Bhd.
All rights reserved

TABLE OF CONTENTS

STATUS OF THESIS	i
APPROVAL PAGE	ii
TITLE PAGE	iii
DECLARATION OF THESIS	iv
DEDICATION	v
ACKNOWLEDGMENT.....	vi
ABSTRACT.....	vii
ABSTRAK.....	ix
TABLE OF CONTENTS.....	xii
LIST OF TABLES	xvi
LIST OF FIGURES	xviii
LIST OF PLATES	xxi
NOMENCLATURES	xxii
Chapter 1: INTRODUCTION.....	1
1.1 Background.....	1
1.1.1 Corrosion in Pipelines.....	1
1.1.2 Overview of Corrosion Assessment Methods.....	2
1.1.3 Pipelines Inspection	4
1.1.4 Integrity Assessment.....	7
1.2 Motivation of the Research.....	7
1.3 Problem Statements	9
1.4 Objectives of the Research.....	9
1.5 The Scope of the Study	9
1.6 Research Methodology	10
1.7 Organization of the Thesis	11

Chapter 2: LITERATURE REVIEW	13
2.1 Corrosion Defect Assessment Methods	13
2.2 Deterministic Assessment Methods	16
2.3 Probabilistic and Reliability Methods	18
2.4 FE Methods	20
2.5 Defect Anomalies and Parameters	24
2.6 Defect Interaction and Limits	27
2.7 Summary	29
Chapter 3: APPRAISAL OF CORROSION ASSESSMENT METHODS	33
3.1 Introduction	33
3.2 Approximation of Corrosion Area	34
3.3 Uniformly Corroded Pipeline Sections	36
3.4 ANSI/ASME B31G Assessment	38
3.4.1 Original ASME B31G Criterion	39
3.4.2 Modified B31G Criterion (0.85dL Area)	41
3.4.3 RSTRENG Criterion (Effective Area Method)	42
3.5 DNV Criterion	42
3.6 PCORRC Assessment	44
3.7 Comparison of Assessment Methods	45
3.7.1 Problems with Scatter in the Data	45
3.7.2 Problems with Comparing the Methods	46
3.7.3 Comparison of Methods with Burst Test Database	46
3.8 Summary	52
Chapter 4: LABORATORY TESTS	55
4.1 Introduction	55
4.2 Corrosion Measurement	57
4.2.1 Inline Inspection	57
4.2.2 Metal Loss Inspection	58
4.2.3 Visual Inspection	59
4.2.4 UT Inspection	59

4.3	Burst Test	60
4.3.1	Modeling of Corrosion Defects	60
4.3.2	Machining of Simulated Defects	61
4.3.3	Burst Test Procedures	63
4.4	Instrumentation	64
4.4.1	Strain gauges	64
4.4.2	Pressure gauges	65
4.4.3	Thermocouple	66
4.4.4	CCTV Cameras	66
4.4.5	Safety Precaution	66
4.5	Material Characterization.....	67
4.6	Burst Test Results and Discussions	71
4.7	Conclusion	75
Chapter 5: FINITE ELEMENT ANALYSIS		77
5.1	Nonlinear FE Analyses	77
5.1.1	Geometrical nonlinearities	78
5.1.2	Material Nonlinearities	78
5.2	FE Analysis Procedures	79
5.3	FE Modeling	80
5.3.1	Coupled Degrees of Freedom	80
5.3.2	Plane Strain Modeling.....	81
5.3.3	Axisymmetric Modeling	82
5.3.4	Flat-bottomed Rectangular Defect Modeling	84
5.4	Computational Tools for Modeling and Automatic Analysis of Defects	85
5.4.1	Use of Log Files.....	85
5.4.2	Solution Algorithms.....	86
5.4.2.1	Pre-processing Phase	86
5.4.2.2	Solution Phase.....	86
5.4.2.3	Post-processing Phase	88
5.5	Mesh Convergence Study	88
5.6	Failure Analyses.....	89

5.6.1	Failure Criteria	90
5.6.1.1	Strain-based Criterion	90
5.6.1.2	Stress-based or Instability-based Criterion	90
5.6.2	Failure Prediction.....	91
5.6.3	Sample of FE Analyses	93
Chapter 6:	PARAMETRIC STUDY	101
6.1	Geometric Parameters	101
6.2	Mathematical Model	107
6.3	Benchmarking of the Findings.....	111
6.3.1	Comparison with the Available Methods	111
6.3.2	Comparison with Burst Test Database.....	115
6.4	Chapter Summary	116
Chapter 7:	CONCLUSIONS AND RECOMMENDATIONS.....	117
7.1	Conclusions.....	117
7.2	Contributions of the Research.....	120
7.3	Recommendations for Future Work.....	121
References		122
Appendix A:	BURST TEST DATABASE.....	129
Appendix B:	BURST TEST SAMPLES DRAWING	139
Appendix C:	BURST TEST RECORDS.....	143
Appendix D:	BURST TEST PHOTOS.....	145
Appendix E:	SAMPLE OF FE SIMULATION RESULTS	149
Appendix F:	FE SIMULATION RESULTS	159
Appendix G:	LIST OF PUBLICATIONS	162

LIST OF TABLES

Table 2.1 Defect Anomaly [19]	26
Table 3.1 Summary of mean bias and scatterings of various prediction methods.....	47
Table 4.1 Summary of tensile test results	68
Table 4.2 Summary of Burst Test Results	71
Table 5.1 von Mises stress near burst point in axial groove.....	98
Table 5.2 von Mises stress near burst point in circumferential slot.....	99
Table 5.3 von Mises stress near burst point in flat bottomed defect.....	100
Table 6.1 Material and geometric parameters analyzed	102
Table A.1 Actual and theoretical burst pressure of defect-free pipelines.....	129
Table A.2 Actual and predicted burst pressure of corroded pipeline	131
Table E.1 A sample of FE simulation results for plane strain defect model [$D = 274mm, t = 12mm, d/t = 0.5$ and $w/t = 10$]	149
Table E.2 A sample of FE simulation results for an axisymmetric defect model [$D = 274mm, t = 12mm, d/t = 0.5$ and $L/t = 15$]	153
Table E.3 A sample of FE simulation results for a flat-bottomed rectangular defect model [$D = 274mm, t = 12mm, d/t = 0.5, L/D = 0.75$ and $w/t = 10$].....	157
Table E.3 A sample of FE simulation results for a flat-bottomed rectangular defect model [$D = 274mm, t = 12mm, d/t = 0.5, L/D = 0.75$ and $w/t = 10$] (continued)	158
Table F.1 FE results summary for plane strain models ($D = 274mm$ and $t = 12mm$)	159
Table F.2 FE results summary for axisymmetric models ($D = 274mm$ and $t = 12mm$)	159

Table F.3 FE results summary for flat-bottomed rectangular defects: effect of defect width ($D = 274mm$, $t = 12mm$ and $d/t = 0.5$).....	160
Table F.4 FE results summary for flat-bottomed rectangular defects: effect of defect length ($D = 274mm$, $t = 12mm$ and $w/t = 6.0$).....	160
Table F.5 FE results summary for flat-bottomed rectangular defects: effect of defect depth ($D = 274mm$, $t = 12mm$ and $w/t = 6.0$).....	161

LIST OF FIGURES

Figure 2.1 Orientation of a corrosion defect.....	25
Figure 2.2 Nomenclature of metal loss defect [66].....	25
Figure 2.3 Graphical presentations of metal loss anomalies per dimension class [19]	26
Figure 2.4 Projection view of two nearby corrosion defects [68].....	28
Figure 3.1 Pictorial representation of corrosion defect [12].....	35
Figure 3.2 Theoretical versus actual failure pressure for intact pipelines.....	38
Figure 3.3 Actual failure pressure versus B31G predictions.....	48
Figure 3.4 Actual failure pressure versus Modified B31G predictions.....	49
Figure 3.5 Actual failure pressure versus RSTRENG predictions.....	50
Figure 3.6 Actual failure pressure versus DNV predictions.....	51
Figure 3.7 Actual failure pressure versus Modified PCORRC predictions.....	52
Figure 4.1 Corrosion defect anomaly classes.....	56
Figure 4.2 Schematic drawing of burst test sample.....	63
Figure 4.3 Strain gauges placement.....	65
Figure 4.4 Tensile properties of the API X52 grade steel pipe material.....	70
Figure 4.5 Burst test, T1.....	72
Figure 4.6 Total strain distribution, T2.....	73
Figure 4.7 Total strain distribution, T1.....	74
Figure 5.1 Idealized longitudinally extended slot.....	82
Figure 5.2 Plane strain idealization.....	82
Figure 5.3 Idealized circumferentially extended groove.....	83
Figure 5.4 Axisymmetric FE model.....	83
Figure 5.5 Idealized flat-bottomed rectangular defect.....	84
Figure 5.6 FE quarter model and mesh close view at the defect.....	85
Figure 5.7 Automatic defect modeling and analyses command lines.....	86

Figure 5.8 Convergence of mesh number in the ligament	89
Figure 5.9 von Mises stress distribution through the ligament	92
Figure 5.10 von Mises plastic strain distribution through the ligament	93
Figure 5.11 von Mises plastic strain distribution through the longitudinal slot	94
Figure 5.12 von Mises plastic strain distribution through the circumferential groove	94
Figure 5.13 von Mises plastic strain distribution through the rectangular defect.....	95
Figure 5.14 von Mises stress distribution through the longitudinal slot.....	96
Figure 5.15 von Mises stress distribution through the circumferential groove	96
Figure 5.16 von Mises stress distribution through the rectangular defect	97
Figure 5.17 The variation of von Mises stress through the slot near failure pressure	98
Figure 5.18 The variation of von Mises stress through the groove near failure pressure	99
Figure 5.19 The variation of von Mises stress through the defect near failure pressure	100
Figure 6.1 <i>RSF</i> versus defect depth for longitudinal defects	103
Figure 6.2 <i>RSF</i> versus defect width for longitudinal defects	103
Figure 6.3 <i>RSF</i> versus defect depth for circumferential defects	104
Figure 6.4 <i>RSF</i> versus defect length for circumferential defects	105
Figure 6.5 <i>RSF</i> versus defect width for flat-bottomed rectangular defects	106
Figure 6.6 <i>RSF</i> versus defect length for flat-bottomed rectangular defects	106
Figure 6.7 <i>RSF</i> versus defect depth for flat-bottomed rectangular defects.....	107
Figure 6.8 FE results versus the <i>LSF</i> for $L/D \leq 1$	110
Figure 6.9 FE results versus the <i>LSF</i> for $1 < L/D \leq 2$	110
Figure 6.10 Comparison of <i>RSF</i> predictions with the FE results	112
Figure 6.11 Comparison of <i>RSF</i> predictions by different methods ($d/t = 0.3$).....	112
Figure 6.12 Comparison of <i>RSF</i> predictions by different methods ($d/t = 0.5$).....	113
Figure 6.13 Comparison of <i>RSF</i> predictions by different methods ($d/t = 0.7$).....	113
Figure 6.14 Comparison of <i>RSF</i> predictions by different methods ($L/D = 0.75$).....	114
Figure 6.15 Comparison of <i>RSF</i> predictions by different methods ($L/D = 1.50$).....	114
Figure 6.16 Benchmarking of the new method with the actual <i>RSF</i> values	116

Figure B.1 Burst test sample drawing, T1	139
Figure B.2 Burst test sample drawing, T3	140
Figure B.3 Burst test sample drawing, T4	141
Figure B.4 Burst test sample drawing, T5	142
Figure C.1 Burst test, T3.....	143
Figure C.2 Burst test, T4.....	143
Figure C.3 Total strain distribution, T3	144
Figure C.4 Total strain distribution, T4	144

LIST OF PLATES

Plate 4.1 Sample prepared for test	67
Plate 4.2 Ductile failures of corroded pipe sections	75
Plate D.1 Sections of abandoned pipeline.....	145
Plate D.2 Simulated defect.....	145
Plate D.3 Surface preparation and strain gauges placement	146
Plate D.4 Test sample setup: (a) Clamping on saddle support (b) Monitoring device	147
Plate D.5 Samples ruptured at the defect: (a) T3 and (b) T1	148

NOMENCLATURES

Abbreviations

AGA	American Gas Association
APDL	ANSYS Parametric Design Language
API	American Petroleum Institute
ASME	American Society of Mechanical Engineers
BG	British Gas
DNV	Det Norske Veritas
FE	Finite Element
FFS	Fitness-for-Service
IP	Intelligent Pig
LSF	Lost Strength Factor
MAOP	Maximum Allowable Operating Pressure
MFL	Magnetic Flux Leakage
PCORRC	Pipe Corrosion Failure Criterion
RSF	Remaining Strength Factor
SMTS	Specified Minimum Tensile Stress
SMYS	Specified Minimum Yield Stress
UT	Ultrasonic
UTP	Universiti Teknologi PETRONAS
UTS	Ultimate Tensile Strength

Symbols

A	Corrosion metal loss area along the longitudinal axis
d	Depth of corrosion defect

D	Nominal outside diameter of the pipe
E	Modulus of elasticity of the pipe material
F	Design factor (ASME: B31.4, B31.8 or B31.11)
L	Axial extent of the defect
M, Q	Folias factor
n, α	Ramberg-Osgood constants
P	Pressure
P_{corr}	Allowable corroded pipe operating pressure
StD	Standard deviation
t	Nominal wall thickness of the pipe
T	Temperature de-rating factor
w	Circumferential width of metal loss defect
ΔP	Incremental applied load vector
Δu	Incremental displacement vector
γ_d	Partial safety factor for corrosion depth
γ_m	Partial safety factor for model prediction
ε	Strain
ε_d	Fractile value for the corrosion depth
σ	Stress
φ	Burst pressure correction factor

Subscripts

b	Burst
c	Cross-section
e	Effective (von Mises)
f	Failure
u	Ultimate
max	Maximum
r, L, θ	Radial, Longitudinal and Circumferential (hoop) directions
0	Original (plain)
y	Yield

CHAPTER 1

INTRODUCTION

Metallic pipelines are widely used as the most efficient and safest way of high-volume oil and gas transportation systems. However, like other structures, pipelines deteriorate over time, therefore to ensure their integrity is a great challenge. This natural deterioration in a metallic pipeline usually occurs as a result of metal loss from the pipe wall due to corrosion. Generally, the most dominant cause of high pressure gas and oil pipeline rupture is corrosion [1]. Corrosion is a time dependent electrochemical process and depends on the local environment within or adjacent to the pipeline [2]. Operating aged pipelines is an expensive and risky task because of corrosion and its potential damaging effects [3]. Therefore, a reliable defect assessment methodology has been sought in order to ensure safe operation.

The principal aim of this research was to develop a new method for the remaining strength analysis of corroded pipelines. The background information, objectives of the research and the research methodology are presented in the following sections.

1.1 Background

1.1.1 Corrosion in Pipelines

The historical performance of pipelines has been outstanding but their increasing age has led to concern regarding the occurrence and growth of corrosion defects [4]. The numbers of accidents are increasing with the increasing number of operating pipelines [5]. The integrity of these pipelines is very important due to costly investment and to prevent fatality and environmental hazard because of their failures. Since most

pipelines operate at remote areas, failures rarely cause fatalities to the public, but they can disrupt an operator's business, either by loss of supply or by necessary remedial work. They are also extremely costly in terms of replacement and repair. The economic consequences of a reduced operating pressure, loss of production due to downtime, repairs or replacement can be severe and, in some cases not affordable [6]. For instance, recently, due to BP's Mexico Gulf Oil pipeline spilling, 0.6 to 1.2 million gallons of oil was leaking from the bottom of the sea per day. The total financial loss was estimated to be 23 billion USD and moreover huge environmental disasters have been showing up [7].

On pipelines' surface, mostly corrosion appears as either general corrosion or localized corrosion. General corrosion usually creates more or less uniform loss of material thickness from the pipe surface. Whereas, localized corrosion results in a non-uniform or localized metal loss. Pitting is a typical form of localized corrosion, which is found to be very destructive. This is mainly because pitting corrosion usually occurs in limited areas and results in the formation of deep pits, which may completely perforate pipeline walls. In most cases, pits are relatively small in diameter and are covered with corrosion products and hence are difficult to detect. The presence of chemical compounds such as species of CO₂, H₂S, O₂ and Acetic acids (HAc) with water inside the pipeline are some of the prominent factors causing internal corrosion [8].

1.1.2 Overview of Corrosion Assessment Methods

Many pipeline failures in the past have commanded to the need for assessing flawed pipes. Nowadays, failures due to corrosion have been one of the greatest concerns for pipeline operators. Accurate predictions of the residual strength for corroded piping systems remain essential in fitness-for-service (FFS) analysis of oil and gas transmission pipelines [9]. When pipeline infrastructure gets older, metal loss due to corrosion become a major source of material degradation. Therefore, it reduces its burst strength with increased potential for catastrophic failure [10, 11].

Methods for assessing corrosion metal loss defects have been available since early 1970's, as for instance the NG18 equation and ANSI/ASME B31G code. Most of the current methods like ASME B31G [12], Modified B31G [13], RSTRENG [14], DNV-RP-F101 [15], and some in-house codes were developed based on modification of the original NG18 equation [16].

These defect assessment codes and standards provided simplified acceptance criterions for corroded pipelines. They were derived based on limit-load solution for a blunted axial crack-like flaw in a pressurized vessel or pipe. These codes are empirical and semi-empirical formulas based on experimental tests [17]. However, the methods are known to be conservative. In most cases their usage gives essentially low estimates of the remaining strength of the corroded pipeline segments and enforcing premature cut outs [18]. Their application scopes are also limited as they are dependent on material properties, pipeline geometries and defect geometries. These facts imply that any change in either of these properties will require the development of a large number of tests to update the empirical solutions [19].

Pipeline operators need reliable defect assessment methodology not only to ensure safe operation but also to implement optimized operation cost. Currently researchers are working towards developing a more reliable and advanced corrosion assessment methods. Motivated by these observations, in the recent years various specific solutions have been proposed; mostly based on FE studies and burst tests [20]. Realistic burst pressure prediction can be achieved if the nonlinearities due to material properties and due to large-deformation are taken into consideration during the FE analyses [21]. The material nonlinearities due to an elastic-plastic deformation can be represented as rate-independent plasticity model [22]. Failure criterion like stress-based or plastic instability and strain-based were used to decide the failure point while executing the FE analyses [9].

Inspection techniques developed during the last decade have enabled the accurate location and sizing of pipeline wall corrosion [23]. In parallel, modern numerical methods have enabled the modeling of realistic defect shapes and nonlinear material behavior [24]. But, the conventional procedures used to assess the integrity of corroded piping systems generally employ simplified defect geometries and a plastic

collapse failure mechanism incorporating the tensile properties of the pipe material [9]. Thus, realistic defect geometries were proposed for better accuracy.

In order to evaluate the accuracy of currently accepted corrosion assessment procedures and to develop a new method of assessment, an experimental database is necessary [25]. Such database is also necessary to validate models, particularly if they are to be the basis of any code or standard. Many of the reported tests with detailed measurements involve artificial or machined defect with simple geometries such as grooves and notches. These type of tests were important stepping-stone in the development of numerical methods and understanding of the defect behavior. But the complexity of real corrosion defects may not be accurately represented with simpler shapes.

1.1.3 Pipelines Inspection

There are millions of kilometers of transmission pipelines operating all over the world. Many of these pipelines operate in harsh environments and transport hydrocarbon products with different species of chemical compounds. The reaction between water and compounds like CO_2 and H_2S result in formation of corrosive by-products leading to extensive corrosion damage. Inspection and rehabilitation are, therefore, critical for ensuring continuous, safe and reliable operation [2, 26]. In order to increase the safety level of operating pipelines and to reduce failures imposing harmful consequences, it is necessary to inspect and to repair critical corroded segments timely [1].

Through past researches and developments, different pipeline inspection techniques had been invented. Some of these techniques like caliper pigs, inertial pipe mapping, Magnetic Flux Leakage (MFL), and Ultrasonic (UT) inspection are extensively employed in the industries [27]. Pipeline inspection techniques are in general costly processes. Currently, many new and advanced pipeline inspection technologies are at various stages of development. The MFL continues to be the most common method for pipelines inspection because it is relatively inexpensive and is well understood technique [28].

The working principle of MFL is by using powerful magnets which magnetize the pipe wall to saturation. At any location where the wall is thinner, the pipe wall cannot retain all of the magnetic flux. Therefore, the flux leaks out from both the outer side and the inner side of the pipe. Pigs with magnetic sensors measure the leakage flux and analysis programs convert the measurements to metal loss. The main disadvantage of MFL is it lacks accuracy. MFL measures the fraction of metal lost relative to the nominal pipe wall thickness feed into the device. Therefore, any error in the nominal pipe wall thickness results in inaccurate remaining wall thickness measurement. The measurements are said to have accuracy of +/- 10% at 80% confidence level. Better accuracy is achieved by inspection methods that can make direct measurements of the remaining wall thickness, as for instance, the UT inspection.

UT inspection pigs were developed because MFL inspection measurements are not accurate enough to measure the remaining wall thickness [23]. UT inspection measures the remaining wall thickness. These results can be directly used in formulations such as B31G, RSTRENG, or FE calculations to determine the remaining strength of the corroded pipeline.

In the past, conservatism of the defect assessment criterion was appropriate due to the low resolution of inspection tools used in pipeline examination. Currently, high resolution in-line inspection tools are being introduced which permit the accurate measurement of corrosion damage in pipelines. These tools provide data that are sufficiently accurate to allow estimation of corrosion growth rates from subsequent inspection and development of long-term maintenance plans. However, the present corrosion assessment procedures are too simplified to permit such detail data. Therefore, multi-level assessment procedures have been proposed in order to reduce the degree of conservatism in the assessment for increasing accuracy [26].

Pipeline operators depend on internal inspection of a transmission pipeline using IP as a means of both maintaining their pipelines and ensuring that their major asset has a long and efficient life [16]. After a high-resolution inspection an operator needs to determine future safe operating conditions and the remaining life of the pipeline. Inspection can reveal defects in the pipelines; therefore, the operator needs to assess

the significance of the defects in order to maintain a safe pipeline. Consequently, one must consider maintenance measures that are both cost effective and prevent failures or large repair bills.

The following points identify the four main issues that determine the need of maintenance and inspection activities. The strategies which must be developed to ensure a robust and economic means of undertaking these activities are also suggested [29].

- *Safety and environmental issues:* Effective maintenance and inspection is essential to minimize the environmental risks caused by pipeline failure. It is also essential to ensure maintenance and inspection activities, minimize impact on the safety of the public, staff and contractors.
- *Security of supply:-* The system must deliver its product in a continuous manner. The life cycle of a pipeline can be considered to follow the 'bath tub' failure probability curve with higher incidences of failure in early life followed by a fairly constant failure rate which gradually increases towards the end of the pipeline's life. With pipelines, early life failures generally result from damage associated with construction and commissioning. A constant failure rate is then generally observed during the operating life. A gradual increase in failure rate then may be caused by age and duty related damage mechanisms. Maintenance and inspection strategy should be applied to accommodate the early failures, minimize and respond to random failures, anticipate and avoid predictable failures due to age and duty deterioration mechanisms.
- *Cost effectiveness:-* The system must deliver the product at an attractive market price, and generate an acceptable rate of return on the investment. The maintenance and inspection strategy should ensure transportation and delivery of the product to the satisfaction of the operator and/or the customer. It should be robustly planned to optimize performance by increasing the overall life and ensuring that the probability of failure remains at an acceptable level whilst minimizing overall operating costs.

- *Legislative compliances:-* The operation of the system must satisfy all legislation and regulations. An operator must ensure that all risks associated with the pipeline are low and is reasonably practicable. In the past, an operator will detect or become aware of defects in their pipeline occasionally. Therefore, these had caused several expensive shutdowns and repairs of corroded pipelines.

1.1.4 Integrity Assessment

Pipeline integrity is ensuring that the pipeline is safe and secure. It involves all aspects of a pipeline's design, inspection, management and maintenance. A detailed integrity assessment can provide much valuable information. For example, on the condition of a pipeline and the ability of the team maintaining the line to keep it in good condition, it can inform any rehabilitation plan. A key part of the integrity assessment is an assessment of the FFS or fitness-for-purpose (FFP) of the pipeline [30]. Since early 1970s, a number of pipeline integrity assessment criteria were developed. Basically the purposes of these criteria are the following.

- Provide the operator with best possible understanding of the current condition of the pipeline, and whether it is safe to continue operation.
- Identify degradation mechanisms and give conservative estimates of the rate of degradation.
- Identify other issues that may affect the feasibility of repair or rehabilitation (e.g. location).

1.2 Motivation of the Research

The overall target of pipeline operators is to maintain safe pipeline for operation at the design working pressure to maximize throughput and revenue. Many pipeline systems in service today are getting older and also experiencing corrosion. Corrosion fault reduces the pipeline pressure carrying capacity and if it is allowed to proceed, the

pipeline may eventually leak or rupture. Failure of pipelines has a tremendous impact on the environment which may lead to high costs for repair and ecological compliances. Thus, there is a demand for an accurate guideline or code to assess the condition of corroded pipelines. This guideline shall prevent pipe leakage or rupture, but not enforce an excessive amount of premature repair or replacement of the corroded pipes.

Though, it has been said that the current defect assessment methods are conservative, they are still employed by the industries. The excess conservatism of current corrosion assessment criteria and the cost associated with unnecessary repair or replacement of corroded pipe motivated researchers to look for more reliable guidelines. Therefore, some pipeline operators are funding research centers and universities in order to develop less conservative engineering procedures for assessing corroded pipelines. For example, the Korean Gas Corporation (KOGAS) is funding Sungkyunkwan University [31, 32] and likewise PETROBRAS is supporting National Laboratory for Scientific Computing (LNCC/MCT) [22, 33]. It is obvious that these findings will remain copyright procedure for the corresponding funding pipeline operators until they may be commercialized. Therefore, it is viable for UTP to find a new or customized defect assessment method for one of the giant pipeline operators, PETRONAS Sdn. Bhd.

So far, some pipeline operators have performed burst test to develop in-house engineering procedures in order to assess corrosion damage on high pressure oil and gas transmission pipelines. This creates some concerns as to the uniformity of the collected data and the liability of the engineering assessment procedure. However, it was doubtful that testing can provide information on all pipe and defect geometries, material properties and service conditions that pipeline field engineers will require. Therefore, efficient numerical techniques have an important role in generating additional information through parametric studies over the full range of pipe geometries and grades of steels used by the pipeline industry. Numerical models also permit additional information to the database of experimental results by simulating defects which are complex to produce. However, testing cannot be neglected in order to ensure that no mode of failure is overlooked in the numerical modeling.

1.3 Problem Statements

This research was mainly targeted to address the following main problems.

- Aged pipeline can leak or rupture if it operates at a design pressure due to reduced wall thickness by corrosion.
- Failure of a pipeline can cause huge disaster on the environment and exposes the operator to unbearable costs of ecological compliances and fatalities.
- Conservative corrosion assessment methods impose premature repair or replacement of costly pipelines.

1.4 Objectives of the Research

The main objective of this research was to develop a new method for the residual strength assessment of corroded pipeline based on full scale burst test and an intensive nonlinear FE analyses. The burst test samples are taken from a pipeline retired from service due to corrosion and from pipeline sections with simulated corrosion defects.

1.5 The Scope of the Study

The scope of the study was bounded by the following specific studies:

1. investigation of current defect assessment methods as practiced by industry and identification of their limitations
2. evaluation of credibility of intelligent pig (IP) inspection tally by advanced UT-Scan inspection techniques
3. conducting experimental burst tests on pipe section with natural complex corrosion defects removed from service and with simulated predefined corrosion defects

4. developing FE models for common types of the corrosion defects and conducting intensive nonlinear FE simulations which permit a complementary study of experimental results and supplementing the experimental program by investigating cases not considered in the testing
5. studying the effect of corrosion defect parameters on the burst strength of pipeline in order to develop a simplified representation of their effect
6. developing a less conservative defect assessment method and validating the new method with a credible burst test database available in published literatures

1.6 Research Methodology

The flowchart for the research is shown in Figure 1.1. It starts with collection of available information and data from open literatures. Based on the investigation of some of the most popular available assessment methods, modified methods were suggested if possible. In case the modified assessment methods are not satisfactory, new method based on FE analysis and burst test is developed. Finally, the new method is validated with burst test database.

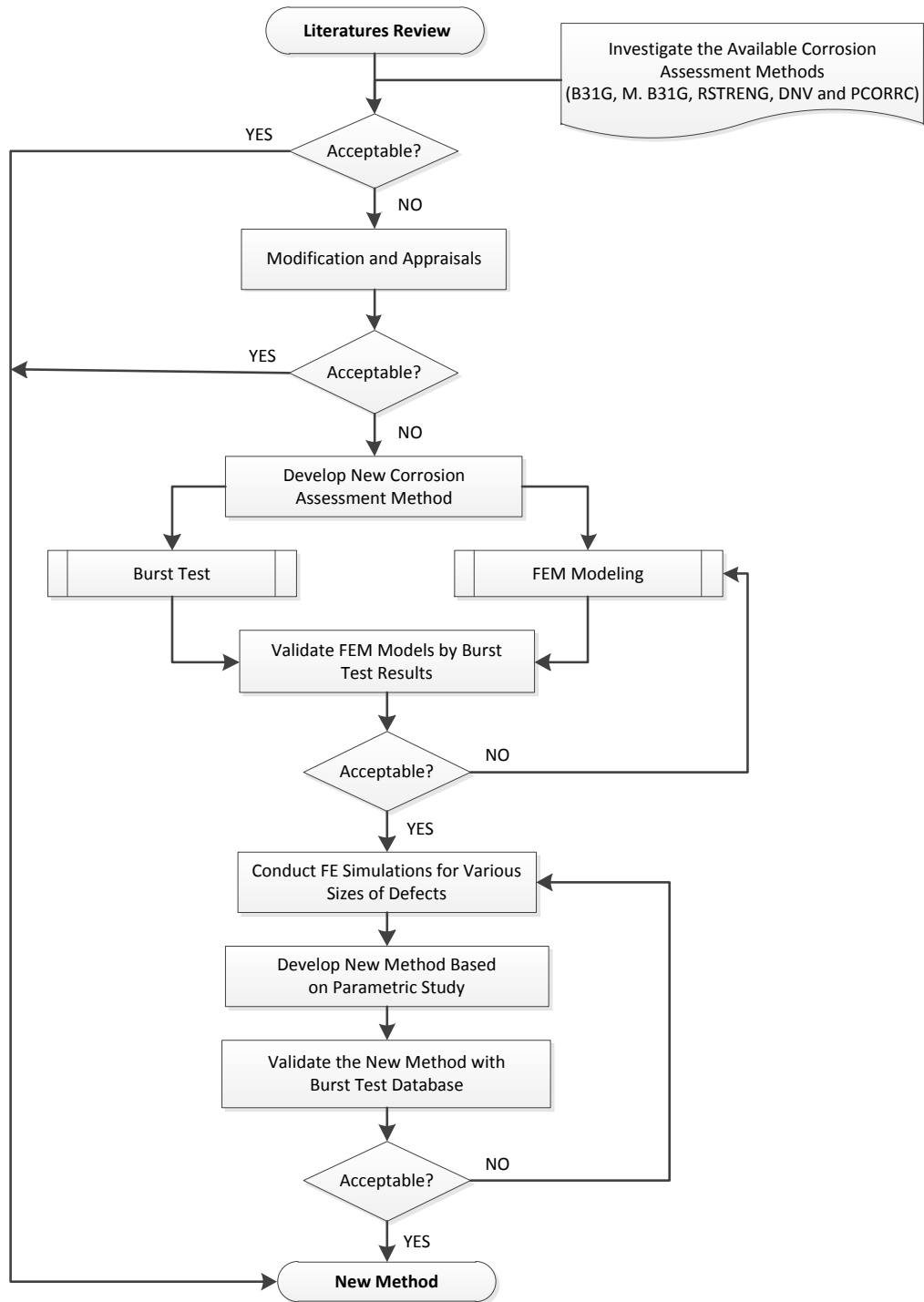


Figure 1.1 Research Methodology Flowchart

1.7 Organization of the Thesis

This thesis is presented in seven chapters. The historical overview of corrosion problems in pipelines, corrosion assessment methods and pipeline inspection

techniques are presented in Chapter 1. The motivations for the research and the objectives to be achieved are also highlighted in this chapter.

The literature review of related research works are presented in Chapter 2. The common approaches towards developing corrosion assessment methods were broadly categorized into three classes as deterministic approach, probabilistic or reliability approach and the FE approach. Further, in the same chapter, the different types of defect anomalies and rules for defect interaction and limits were revised.

In Chapter 3, brief quantitative studies and investigation of the current pipeline defect assessment methods are presented. The quantitative study focused on five most popular and most frequently utilized codes by pipeline operators. These codes were ASME B31G, Modified B31G, RSTRENG, DNV and PCORRC. The chapter is concluded with comparison of predictions made by the codes with the actual results from burst test database.

The lab test procedures and results are reported in Chapter 4. The observations based on comparison of visual and UT-Scan inspections with the IP inspection are discussed in the first half of the chapter. The burst test setup, the material characterization and test results are also discussed in the remaining sections of the chapter.

Chapter 5 presents the FE analyses procedures. The details of nonlinear FE analyses and the FE modeling of defects with the basic assumptions are also discussed. Further, the discussions for the development of the computational tools for modeling and automated analyses of defects are given. Finally, the failure criteria used to predict the failure points and demonstration of the FE analyses is shown.

The final results and discussions are presented in Chapter 6. The mathematical model developed based on the parametric study and the validations of findings with the burst test database are also included in this chapter. The thesis is concluded by Chapter 7, presenting the final conclusions, contribution of the research and recommendations for future research.

CHAPTER 2

LITERATURE REVIEW

Hydrocarbons are mainly transported by underground or undersea pipelines. As a result, pipelines are susceptible for corrosive environments. Metal loss due to corrosion is one of the most common situations leading to the loss of pipeline integrity. There are various mechanisms for both external and internal corrosion, which may cause local reductions in wall thickness. Failure occurs when the nominal wall thickness of the pipe becomes smaller than the safe operating wall thickness. Basically there are two ways of pipeline corrosion risk assessment methods which are known as deterministic methods and probabilistic methods. The deterministic methods are based on either qualitative and/or semi-quantitative risk assessment. In the probabilistic methods quantitative risk assessment methods are employed. But, recently with the advancement of computational technology, alternative methods based on numerical analyses have been proposed.

The purpose of this summary review was to highlight on the prevailing defect assessment methods available to the industry. For comprehensive revision, the various methods are categorized into three basic approaches namely deterministic methods, probabilistic and reliability methods and FE methods.

2.1 Corrosion Defect Assessment Methods

The overall goal of assessing corrosion defect is to estimate the service life (remaining strength) of corroded pipelines. In the past, a number of solutions have been developed for the assessment of corroded pipelines based on burst test results. Therefore, some of these solutions are known to be dependent on material properties and pipeline geometries [31, 34, 35]. In the recent years, series of experiments

combined with the FE methods were also used to determine the burst pressure as a function of material and geometric parameters of different pipes and defects [10, 11]. The first FFS work in the area of pipelines was conducted because it was first recognized that safety was of utmost importance in this industry. The methodology was later developed for process plants and then recorded in API 579 as FFS [36]. Its simplicity and ease of use makes it a valuable tool for plant piping today.

In the late 1960s, a major long-line gas transmission Pipeline Company in conjunction with the Battelle Memorial Institute in Columbus, Ohio, began a research effort to examine the fracture initiation behavior of various kinds of corrosion defects in line pipe. This includes determining the relationship between the size of a defect and the level of internal pressure that would cause the defect to leak or rupture. Beginning in the early 1970s, the American Gas Association (AGA) Pipeline Research Committee assumed responsibility for this activity and began developing methods for predicting the pressure strength of line pipe containing various sizes of corrosion defects. The basic foundation for the ASME B31G was set in the late 1960s and early 1970s in a project sponsored by AGA-NG-18.

The testing by the Gas Pipeline Company and Battelle demonstrated that there was indeed a possibility of developing methodology and procedures to analyze varying degrees of corrosion of existing pipelines. From this, an operator could make a valid determination as to whether the pipelines could safely remain in service or should be repaired or replaced. As the awareness of this research program grew, other transmission companies began to express considerable interest [4].

The first and most popular research output in the assessment of corrosion defects was the ASME B31G criterion [12]. The basics of this technology was the number of burst tests conducted at the Battelle Memorial Institute [37]. The corrosion assessment codes in Canada, the United States and Europe were based on this criterion. In the late 1980's, a major improvement to B31G was introduced by Kiefner. The method is iterative and evaluate the failure pressure of corrosion defects using a program known as RSTRENG [14]. New definition for bulging factor and the material flow stress were introduced and a more detailed consideration of the shape of the corrosion was used to reduce the conservatism in the B31G criterion [13].

In 1991, researchers from university of Waterloo published one of the pioneer works based on the application of the FE method for the analysis of corrosion defects in pipeline [38]. This work was continued at the University of Waterloo with experimental burst tests on pipe with single pits and groups of interacting single pits [4]. Natural corrosion defects of simple geometry were also considered. Based on application of the three-dimensional FE analysis on these defects, various failure criteria were evaluated. Defect interaction rules were also proposed based on the experimental results.

British Gas (BG) Technology performed more than 70 burst tests in a research project in the 1990s, and developed a failure criterion based on FE analyses. More detailed FE results of simple shaped defect behaviour and failure criteria were published [17, 21]. The criterion has been included in BS 7910 [39]. To date, extensive numerical analyses of these defects have been carried out at various universities and institutions with the goal of using the results to develop a less conservative defect assessment method. Many other researchers have proposed new methods of assessment based on analyses of simple two-dimensional defects, or the numerical analyses of simple, three-dimensional defects [20].

Elsewhere, the Det Norske Veritas (DNV) in collaboration with BG Technology developed a unified guideline for the assessment of corrosion in pipelines know as recommended practice (RP-F101) [40]. Other methods like PCORRC, the LPC (Line Pipe Corrosion Equation) and company standards like Shell-92 were proposed independently from those efforts. PCORRC was proposed to predict the remaining strength of corrosion defects in moderate to high-toughness steels that fail due to the mechanism of plastic collapse. RSTRENG and ASME B31G equations are recommended for steels with lower yield strengths and the SHELL-92, PCORRC and LPC equations are more suitable for high strength steels. Thus, LPC equations are said to be not suitable for low toughness pipes and pipes with transition temperatures.

2.2 Deterministic Assessment Methods

Deterministic approach generally uses lower bound data like maximum corrosion rate, minimum wall thickness, peak depth of corrosion and minimum material properties data without considering the existing uncertainties [41]. These assessment codes can be used to evaluate the pipeline condition by calculating the remaining allowable operating pressure in order to determine the serviceability of pipeline impaired by corrosion. Most of the ASME corrosion assessment methods are based on this deterministic analysis.

The basis for the ASME B31G was on a semi-empirical fracture-mechanical formula for calculating the remaining strength of a metal loss defect. The original formula was modified and known as B31G, and there have been made several minor modifications to the criterion. While B31G has been very helpful in evaluating the integrity of corroded pipe, it has been found to be overly conservative. Throughout the years many modifications to the original B31G equations has been made. As a result newer deterministic methods like Modified B31G [13], RSTRENG [42] and several in-house codes were developed.

In principle, there are two equations of interest in defect assessment methods which are classified as capacity equation and design equation. Capacity equation is the equation which can be used to predict the capacity of a corroded pipeline as precisely as possible, for known pipeline dimensions, defect shape and size, and material properties. On the other hand, design equation or acceptance equation is used to estimate the allowable operating pressure which is the safe operational pressure of a corroded pipeline. Most of the deterministic methods belong to the design type of equations. For example, the PCORRC and the DNV-RP-F101 part B equations are capacity equations [43]. But the B31G is a design equation.

The ANSI/ASME B31G code is limited to thin wall pipes (0.25" to 0.5") and containing small areas of metal loss. The experimental data was dominated by low strength and high toughness steel materials [17]. However, modern pipelines have high strength and the corrosions are interacting. Therefore, new methods are necessary for assessment of high strength and low toughness pipeline materials.

In the past, the conservatism of the B31G criterion was appropriate due to the low resolution of inspection tools used in pipeline examination. Currently, high resolution in-line inspection tools are being introduced, which permit the accurate measurement of corrosion damage in pipelines. Such tools provide data that are sufficiently accurate to allow estimation of corrosion growth rates from subsequent inspection and development of long-term maintenance plans. However, present corrosion assessment procedures are too simplified and conservative to allow such a procedure to be economically viable. Therefore, multi-level assessment procedures were proposed by several authors in order to reduce the degree of conservatism [2]. As the corrosion assessment became more essential to the pipeline operators, a Joint Industry Project (JIP) which was sponsored by different international oil and gas companies was carried out. The objective was to develop a Pipeline Defect Assessment Manual (PDAM), in order to provide the best available techniques for the assessment of pipeline defects and service life [2, 26].

In continuous improvement effort of the assessment methods, new approaches have been implemented. With the move towards reliability based design and assessment, there is a need to understand the behavior of corrosion defect before they become critical. The DNV-RP-F101 equations were derived by a probabilistic calibration by considering the defect measurement and burst capacity [44]. The equations account directly for the accuracy in sizing of the corrosion defect. DNV-RP-F101 code was recommended for the assessment of corroded pipelines subjected to internal pressure and longitudinal compressive stresses [45]. In addition, DNV-RP-F101 provides assessment for single defect, interacting defects and complex-shaped defects.

Burst test conducted by various researchers demonstrated that failure of older pipe from natural corrosion occurs due to plastic collapse. Furthermore, the use of nonlinear FE techniques was successful in predicting plastic collapse of corroded pipes with single and multiple corrosion defects. Therefore, the FE technique was proposed for the highest level of corrosion assessment [17, 46]. Though it is accurate, years back, such assessment was time consuming and required large computing resources. Thus, a simplified technique was proposed as a transition from an empirical

to a nonlinear assessment of corroded pipe. This simplification aims at producing a suitable stress field for the lower bound theorem of limit analysis at the current yield locus. The concept of a modified elastic modulus has been incorporated in an elastic FE analysis as a simplified nonlinear analysis. An improved FE analysis together with the ANSI/ASME defect judgment was used to determine the limit carrying capacity of gas pipelines having corrosion defects [47, 48].

2.3 Probabilistic and Reliability Methods

There is a high degree of uncertainty associated with all the factors contributing to pipe failure, especially the corrosion growth rates. The traditional deterministic approach using point estimates (or fixed values) to estimate factor of safety is generally not sufficient. It requires a detailed uncertainty analyses to quantify the probability of pipe failures at a given time in order to plan for maintenance and repair strategies. Therefore, one way to deal with this phenomenon is through probabilistic modeling of the material loss as a nonlinear function of time. Probabilistic approaches deal with uncertainties in the input data by employing probability density distributions.

During service, pipeline can be affected by a range of corrosion mechanisms, which may lead to reduction in its structural integrity and eventual failure. The economic consequences of a reduced operating pressure, loss of production due to downtime, repairs, or replacement can be severe and, in some cases, not affordable. However, there are several pipelines kept in operation even though signs of corrosion are visible on their external surface [11]. Most of these pipelines were allowed to operate after recalculating the maximum admissible internal pressure of the product being transported.

Reliability methods are a powerful and useful tool when assessing corrosion defects in pipelines. The basis of a probabilistic assessment is the capacity equation, the model uncertainty and the distributions of all variables, including loading and the sizing accuracy of the inspection tool. There are a number of open literatures on reliability based assessments of corroded pipelines, but it was observed that in many of these papers, the model uncertainties or the sizing accuracies were omitted. A

proposed approach for probabilistic assessments of corroded pipelines was given by Bai and Bjornoy [44]. The model uncertainties were also specified for the BG/DNV simplified capacity equation.

Burst test data are usually used to determine the model uncertainties. The mean and standard deviation of the predicted burst pressure from the actual value can be calculated. In order to have a good estimation of the model uncertainty, a reasonable number of test results should be available. Preferably, the tests should cover the validity range of the capacity model, not only a limited range. Various authors had published burst test results, but these tests cover only a limited range of material and pipe and defect dimensions [4, 25, 43]. BG Technology performed a large number of burst tests, which were used in the development of the BG/DNV criterion, and of vital importance for confidence in the method [17]. Unfortunately, as the burst test is a costly process, simplified FE analyses results covering the whole validity range were used in combination with the burst tests results to determine the model uncertainties.

Ahammed and Melchers had published a number of papers on the application of probability approach for the assessment of corroded pipelines. Estimation of service life of pipelines subjected to pitting corrosion based on the loss of liquid through pit holes during transportation was described as a methodology for the assessment of the service life of liquid carrying metallic pipelines [49, 50]. The rate of corrosion pits growth was modeled by a two-parameter exponential function having time dependency and a decreasing rate of pit growth [51]. Parameters, which are related to corrosion, pipeline dimension and liquid flow, externally applied loading like traffic loading, temperature and axial bending of pipelines and internal pressure were treated as probabilistic variables [52]. Thus, a probabilistic approach is adapted and the associated variables are represented by normal or non-normal probabilistic distributions. The advanced first-order second moment method was employed to estimate the probability of failure and the relative contribution of the various uncertain parameters [53, 54].

Characterization of the actual condition of pipelines vulnerable to metal loss corrosion is depending on the interpretation of in-line inspection data collected using MFL tools. Pandey presented a probabilistic analysis framework to estimate the

pipeline reliability incorporating the impact of inspection and repair activities planned over the service life [55]. The framework was applied to determine the optimal inspection interval and the repair strategy that would satisfy a target reliability requirement. To update the pipeline failure probability after maintenance, a practical approximation was developed and validated using Monte Carlo simulation results.

Locating internal corrosion damage in pipelines is difficult due to the presence of large uncertainties in flow characteristics, pre-existing conditions, corrosion resistance, elevation data, and test measurements. A methodology to predict the most probable corrosion damage location along the pipelines and then update the prediction using inspection data was presented Kale *et al.* [56]. The approach computes the probability of critical corrosion damage as a function of location along the pipeline using physical models for flow, corrosion rate, and inspection information as well as uncertainties in elevated data, pipeline geometry and flow characteristics. The corrosion rate was defined to be a linear combination of three candidate corrosion rate models with separate weight factors. Monte Carlo simulation and the first-order reliability method (FORM) implemented in a simple spreadsheet models were used to perform the probability integration [35, 57]. Bayesian updating was used to incorporate inspection information and update the corrosion rate model weight factors and thereby refine the prediction of most probable damage location.

Early research on the corrosion damage considers either uniform corrosion or a corrosion pit of a uniform depth, infinitely long groove, where the depth is equal to the maximum depth of the corrosion defect. In such cases the result represents only the lower limit for the failure pressure of a pipe with a corrosion defect. In reality since corrosion depth is not uniform, the predicted failure pressure calculated from these limits using available codes resulted in conservative estimation [58].

2.4 FE Methods

The computational analysis with the FE approach has shown to be one of the most efficient tools for precise evaluation of structural integrity of defected pipes [4, 21, 22, 58]. It allows the direct simulation of the physical phenomena involved in the failure

of the pipe. It provides more precise results those obtained through semi-empirical methods and much faster and cheaper results than those from experiments [59]. Better approaches in order to reduce the premature rejection of defective pipelines' sections can be obtained by joint implementation of up-to-date methods of in-line inspection with modern methods of numerical analyses. Current computational technique and capabilities provide high efficacy of this joint implementation.

Unlike the experimental methods and the code procedures, numerical analysis allows the consideration of all forms of loads into defective pipeline calculations. Some of these loads are internal pressure, thermal deformation, distributed forces from ground influence, static and dynamic loads of ground-surface, initial strains of pipeline welded joints and residual strains of elastically-curved pipes. In addition, there is wind load for above-ground pipelines and external water pressure for underwater pipelines [60].

Since the burst test revealed that failures of pipes defected by corrosion occurs by plastic collapse, the nonlinear FE techniques is practical method to be used in predicting plastic collapse. Accurate application of the FE method involves the use of large number of solid elements to correctly model the corrosion geometry, and the use of large displacement, elastic-plastic analysis to model the material response. The computational simulation by the FE method permits a more realistic modeling representation of the defects [33, 59, 61]. Though this approach is accurate, in the past such an assessment was time consuming and required large computing resources. Currently with the invention of large and high speed computational tools, the FE method is primarily used as a research tool to assess specific corrosion geometries as it provides detailed insight into the behavior of the defect.

The earlier uses of the FE method was based on simple corrosion shapes like pits and longitudinally or spirally oriented grooves in line pipe using simplified 2D and 3D models [38, 62]. With the use of actual material properties and groove geometry, the FE method predictions were found to be within acceptable accuracy of experimental burst pressures. The material was modeled with incremental plasticity (Prandtl-Reuss) from tensile test data [63]. Failure was predicted when the strains in the corrosion ligaments began increasing in an asymptotic manner.

The behavior of longitudinally aligned and circumferentially aligned corrosion pits were studied by a series of burst tests [46, 64]. It was verified that as the distance between adjacent corrosion pits decreases, they began to interact and thus reducing the burst strength of the pipe. The effect of this interaction is a function of the pit dimensions, their separation and the loading conditions. As a complement to burst tests, the FE method was used to analyze the test data and to investigate geometric parameters not considered experimentally. Isoperimetric parabolic hybrid elements with reduced integration and large deformation theory were used in the FE model. Usually, pipeline materials were modeled using incremental plasticity and failure was predicted when the stress exceeded the ultimate tensile strength of the material through the full thickness of the corrosion ligament.

FE model based on shell elements was developed for the analysis of corrosion defects at Battelle Memorial Institute [20, 65]. This simplification allows a complex defect to be modeled with fewer elements than a full three-dimensional analysis but it is only a good approximation in specific cases. This method is limited to blunt defects which have no stress concentrations within the defects. The use of shell elements assumes that the corrosion defect can be represented as an equivalent amount of material loss on external and internal surface of the pipe. The corrosion defect was assumed to be of uniform depth over each element, with discontinuous changes in depth between elements. Application of this method to large, flat-bottomed defects has produced reasonable results. This will not be the case for small, deep defects in which there are through-thickness stress variations and plasticity in the corrosion ligament. Such cases can't adequately modeled using shell elements.

Simplified approach based on weighted depth difference (WDD) method, which accounts for the defect geometry and any interaction with adjacent defects for the prediction of failure pressure for complex corrosion defects was proposed Cronin and Pick [58]. The failure pressure of a plain pipe represents an upper limit of the failure pressure of a pipe with a corrosion defect. On the other hand, the failure pressure of a uniform depth and infinite groove with the depth is equal to the maximum depth of the defect, represents lower limit. The results indicate that this method provides more accurate burst pressure predictions than the currently accepted corrosion defect assessment procedures.

As the cost of full scale burst test is expensive, Netto *et al.* made an evaluation of the residual strength of pipelines with single longitudinal corrosion defects through a series of small-scale experiments [11]. In parallel, a three-dimensional nonlinear FE model was developed to predict the burst pressure of intact and corroded pipes [10]. The model was first validated by reproducing numerically the physical experiments performed and was subsequently used to carry out an extensive parametric studies. The data set was then reduced to a very simple curve that relates the main geometric parameters of the pipe and defect to its residual pressure capacity. After calibration was conducted, based on the experimental results, the model was used to determine the burst pressure as a function of material and geometric parameters of different pipes and defects.

Recent corrosion defect assessments methods are more specific in terms of pipeline materials and defect geometries and are called specific solution. Choi *et al.* proposed a FFP type specific solution for calculating the limit load for corroded gas pipelines made of X65 steel [31]. The basis for the specific solution was seven burst tests conducted with various types of machined. FE simulations were carried out to derive an appropriate failure criterion. Then, further FE analyses were performed to obtain the FFP type limit load solution for corroded X65 gas pipeline.

Conventional procedures used for the integrity assessment of corroded piping systems with axial defects generally employ simplified failure criteria based upon a plastic collapse mechanism incorporating the tensile properties of the pipe material. It was suggested that the use of stress-based criteria based upon plastic instability analysis of the defect ligament is a valid engineering tool for integrity assessments of pipelines with axial corroded defects [9].

It has been said that FE method approach is the most efficient tool and allows the direct simulation of the physical phenomena involved in the failures of pipes. However, FE method analysis requires specific knowledge and training that may not be expertise of all pipeline engineers. The process of creating good computational models for a defect includes precise representation of the geometry of the defect and the generation of an appropriate mesh which demands intense manual labor from the engineer. It is also slow and extremely repetitive; therefore, it is very error prone.

Normally, this process is repeated from the very beginning for each new defect to be analyzed, in a clear waste of qualified human resources [22].

Cabral *et al.* developed a computational tool called PIPEFLAW which is used to model defects for automatic analyses by commercial FE method programs [59]. The tool was developed based on MSC.PATRAN pre and post-processing program, and was written with Patran Command Language (PCL). The program for the automatic generation of models (PIPEFLAW) has a simplified and customized graphical interface, so that an engineer with basic notions of computational simulation with the FE method can generate rapidly models that result in precise and reliable simulations.

In a similar manner, Silva *et al.* developed a program called PIPE in order to provide a friendly graphical interface for ANSYS software to perform FE analysis of pipe with multiple rectangular defects in arbitrary position [33]. The code allows a quick solid modeling and nonlinear analyses to obtain the failure pressure. It has also an error estimation tool to carry out a mesh refinement strategy. However, these PIPEFLAW and PIPE computational tools are not commercialized yet.

2.5 Defect Anomalies and Parameters

A defect is a material or geometric discontinuity or irregularity that is detectable by inspection in accordance with the requirements of the applicable codes and standards. Different codes and standards give different warranty of rejection of defects. A non-acceptable defect is an imperfection of sufficient magnitude to warrant rejection based on the requirements of the code, standard or other method used for the assessment of that defect. Schematics representation of the orientation of most common form of metal loss defect is shown in Figure 2.1. The overall defect dimensions and metal loss profile are shown in Figure 2.2.

The measurement capabilities of non-destructive examination techniques depend on the geometry of the metal loss anomalies. In order to allow a proper specification of the measurements of the IP, these metal loss anomaly classes have been described in Table 2.1. The graphical presentations of anomalies according to the dimension

classes are shown in Figure 2.3. Each anomaly class permits a large range of shapes. Within that shape a reference point is defined at which the probability of detection (POD) is specified.

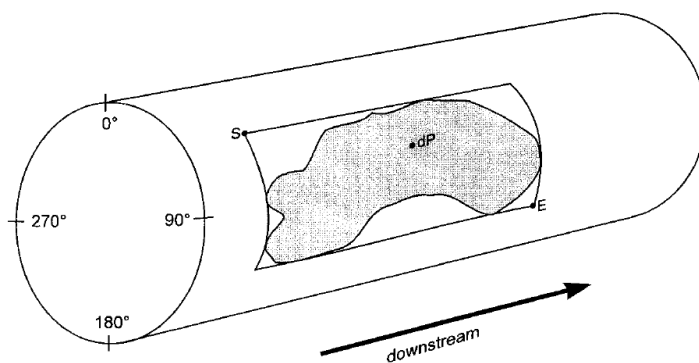
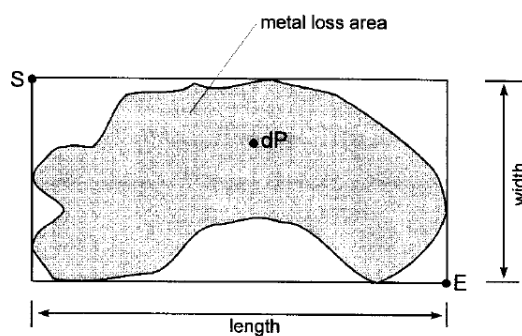
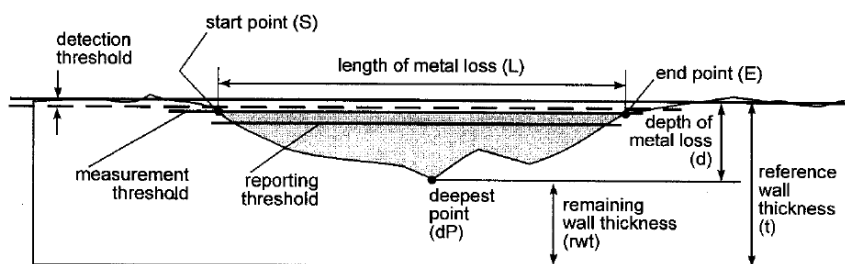


Figure 2.1 Orientation of a corrosion defect



(a) Actual defect and overall defect dimension



(b) Metal loss profile

Figure 2.2 Nomenclature of metal loss defect [66]

Table 2.1 Defect Anomaly [19]

Anomaly dimension class	Definition	Reference point/size for the POD in terms of $L \times W$
General	$W \geq 3t$ and $L \geq 3t$	$4t \times 4t$
Pitting	$(t \leq W < 6t$ and $t \leq L < 6t$ and $0.5 < L/W < 2)$ and not $(W \geq 3t$ and $L \geq 3t)$	$2t \times 2t$
Axial grooving	$t \leq W < 3t$ and $L/W \geq 2$	$4t \times 2t$
Circumferential grooving	$L/W \leq 0.5$ and $t \leq L < 3t$	$2t \times 4t$
Pinhole	$0 < W < t$ and $0 < L < t$	$0.5t \times 0.5t$
Axial slotting	$0 < L < t$ and $L \geq t$	$2t \times 0.5t$
Circumferential slotting	$W \geq t$ and $0 < L < t$	$0.5t \times 2t$

Note: If the wall thickness of the pipe $t < 10\text{mm}$, $t = 10\text{mm}$ would be set in the above expressions

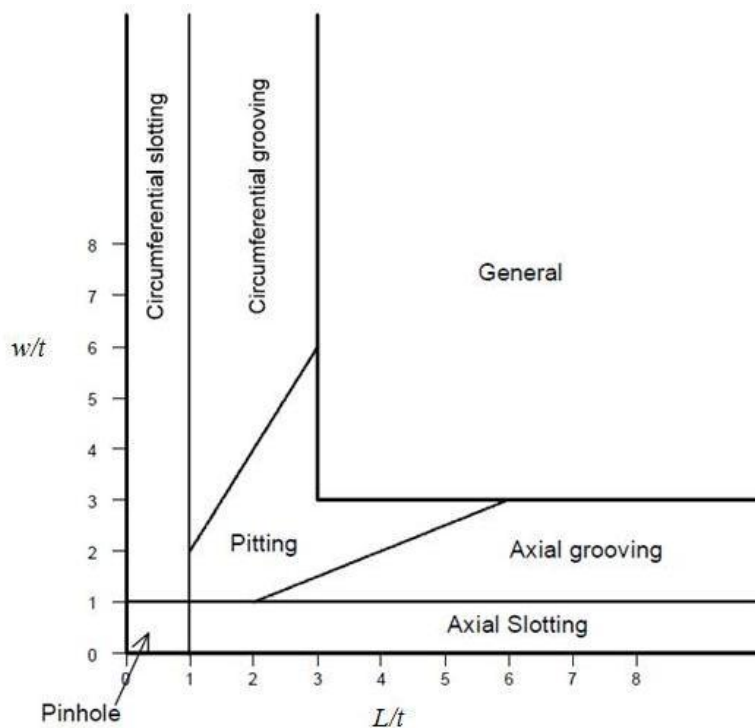


Figure 2.3 Graphical presentations of metal loss anomalies per dimension class [19]

A number of important parameters such as defect depth and material strength have been recognized as significant in the remaining strength of corroded pipe but the relative importance of each parameter is difficult to quantify. With the development of numerical techniques, parametric studies have been carried out to determine the effect of different parameters [11]. It was reported that the parameters in order of significance are internal pressure, pipe diameter, wall thickness/defect depth, ultimate strength, defect length, defect shape characteristics, yield strength/strain hardening characteristics, defect width and fracture (Charpy) toughness [67].

British Gas (BG) has reported similar results, but they indicated that the order of the above list was somewhat arbitrary [21]. It was generally accepted that the circumferential width of the defect does not play a significant role in the failure of blunt corrosion defects and this parameter is neglected in B31G. The above also lists that the toughness is not considered important. This is expected for typical pipeline steel which generally exhibits good toughness. But, this may not be true for low toughness steels such as older and lower grade material where fracture toughness was not a manufacturing requirement.

2.6 Defect Interaction and Limits

Most accepted methods of defect assessment require complex-shaped natural corrosion to be represented by a simplified geometry often enveloping the corrosion defect. Accurate assessment of corroded pipe requires the interaction of defects to be considered since most complex corrosion consists of interaction and defect simplification rules. This is useful since failure initiation of corrosion defect is generally localized. The local initial failure may be followed by a rupture that is governed by the full corrosion geometry; however it is the initial failure that must be predicted.

The interaction of corrosion defects has been investigated by a number of authors and a number of different sets of rules have been suggested [26, 61]. It is well understood that the presence of adjacent defects may reduce the burst pressure of a particular defect. On the other hand, application of the B31G criterion based solely on

the maximum length and depth of a group of defects neglects islands of thicker or full-thickness material which may reinforce the defect and result in a higher burst pressure. To simplify complex corrosion geometries and reduce the conservatism in the failure predictions, defect interaction need to be investigated.

Adjacent defects can interact to produce a failure pressure that is lower than the failure pressure of each of the isolated defects if they were treated as single defect. A projection view of two corrosion defects on the surface of the pipeline is shown in Figure 2.4. DNV states that two defects can be treated as an isolated defect if any of the following criterions are satisfied.

- The defect depth of one or both defects is less than 20% of the wall thickness
- The circumferential spacing between adjacent defects, $\phi > 360\sqrt{t/D}$ (degrees)
- The axial spacing between adjacent defect, $s > 2\sqrt{Dt}$

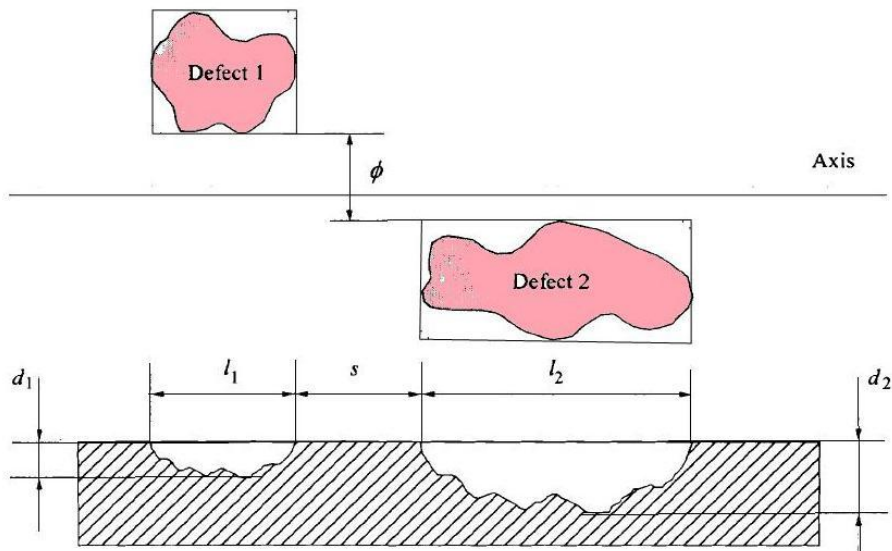


Figure 2.4 Projection view of two nearby corrosion defects [68]

These interaction rules were proposed to be valid for defects subjected to only internal pressure loading. The rules may be used to determine if adjacent defects interact under other loading conditions, at the judgment of the user. However, using these interaction rules may be non-conservative for other loading conditions.

One of the problems associated with defect interaction was that the number of possible geometries is infinite. As a result, early studies focused on the interaction of simple defects such as adjacent longitudinally oriented grooves. Some of the past works in this area focused on the interaction of machined grooves of various lengths [69]. They proposed two criteria for longitudinally oriented defects; i.e. defects separated by a longitudinal distance greater than the length of the shortest defect do not interact and defects separated by a circumferential distance greater than the width of the narrowest defect do not interact.

Kiefner *et al.* also suggested some interaction and evaluation guidelines [13]. They suggested that corrosion defects with a maximum depth less than 20% of the wall thickness are safe and corrosion defects that exceed 80% of the wall thickness must be removed from service or repaired. Their interaction guidelines suggested defects separated by more than 25.4mm of uncorroded material in the longitudinal direction do not interact, defect separated by a distance of 6 times the wall thickness in the circumferential direction do not interact and defects occurring within a region of general corrosion can be treated as defects within a reduced wall thickness pipe.

2.7 Summary

As discussed in the previous sections, methods for assessing corrosion metal loss defects have been available since early 1970s and still the effort to discover new methods are continued. Generalized overview is given by categorizing the efforts made through half a century into three chronological eras as, the beginning (1960 to 1980), the mid-age (1980 to 2000) and the recent (after 2000). Before 1980, pipeline operators were well aware of the risk of operating corroded pipelines and researches for corrosion assessment were started. Through some of those earlier efforts, researches delivered codes and methodologies which have been in use since 1980s.

During the mid-age (1980 to 2000), several methods had been proposed based on major modifications on the models developed earlier. In addition, several burst tests were conducted and FE method was also came to attention as an alternative approach. Recently the focus of the researches has been towards developing less conservative defect assessment methods. Some of the fundamental literatures are revised as follows.

- *1960 to 1980*

- In the late 1960s, a major long lines gas transmission Pipeline Company in conjunction with the Battelle Memorial Institute in Columbus, Ohio, began a research on the fracture mechanics of corrosion defects in pipe.
- Beginning in the early 1970s, the AGA Pipeline Research Committee assumed responsibility for this activity and began developing methods for predicting the pressure strength of line pipe containing various sizes of corrosion defects.
- The basis for the well-known ASME B31G was made in the late 1960s and early 1970s in a project sponsored by AGA-NG-18.

- *1980 to 2000*

- The first and most popular research in the assessment of corrosion defects was conducted by Kiefner and Vieth which resulted in what is known as the ASME B31G criterion for the evaluation of part-wall defects [12]. The basic of this technology was the number of burst tests performed at the Battelle Memorial Institute [37].
- In the late 1980's, a major improvement to B31G was introduced by Kiefner. This method was iterative and evaluate the failure pressure of corrosion defects using a program known as RSTRENG [14].
- In 1991, researchers in university of Waterloo published a pioneer work based on the application of the FE method for the analysis of corrosion defects in pipeline [38]. This work was continued at the University of Waterloo with experimental burst tests on pipe with

single pits and groups of interacting single pits [4].

- BG Technology performed more than 70 burst tests in a research project in the 1990s, and developed a failure criterion based on FE analyses. More detailed FE results of simply shaped defect behaviour and failure criteria were published [17, 21].
 - Elsewhere, the DNV in collaboration with BG Technology developed a unified guideline for the assessment of corrosion in pipelines known as RP-F101 [40]. Other methods like PCORRC, the LPC and company standards like Shell-92 were developed.
- ***2000 to date***
- Multi-level assessment procedures were proposed by many authors in order to reduce the degree of conservatism [2].
 - The use of nonlinear FE techniques succeeded in predicting plastic collapse of pipe with single and multiple corrosion pits, and complex-shaped corrosion, and was proposed for the highest level of assessment.
 - An improved FE analysis together with the ANSI/ASME defect judgment was used to determine the limit carrying capacity of gas pipelines having corrosion defects [47, 48].
 - Development of graphical interface program PIPEFLAW [59] and PIPE [33] for quick solid modelling and nonlinear analysis of defected pipelines.

CHAPTER 3

APPRAISAL OF CORROSION ASSESSMENT METHODS

3.1 Introduction

There are several methods available for the capacity prediction of corroded pipelines. However, as it was introduced in the previous sections, these methods are conservative. Thus they enforce unnecessary repair and underutilization of resources. Most of the published papers just conclude that the methods are conservative with none or limited quantitative analysis of the extent of the biased predictions. To date, as the researchers are studying for the development of less conservative methods, the available methods are still in use in most of the pipeline operations. Therefore, it is worthwhile to study the precision range of these assessment methods for any necessary precaution.

In this research some of these methods have been discussed to demonstrate quantitative study and appraisal procedures. Detail description of the methods can be found in published literatures. The selection of the methods was based on the popularity of their applicability in the industries. For example, the ASME B31G and DNV codes are widely used in the industry including PETRONAS Sdn. Bhd. pipeline operation.

The following methods are summarized in the following discussion.

- i.* ASME methods: ASME B31G [12], Modified B31G (RSTRENG 0.85) [70] and RSTRENG [14]
- ii.* DNV-RP-F101[15]
- iii.* PCORRC [20]

Basically, all of these methods are primarily concerned with the longitudinal extent of the corroded area and internal pressure loading and the DNV-RP-F101 method can be applied to corrosion subject to axial and bending loads. The methods are empirical or semi-empirical; the ASME methods are based on the original Battelle part-wall failure criterion (the NG-18 equations), whilst the DNV and PCORRC methods are partly developed from extensive numerical studies validated against limited number of test data.

3.2 Approximation of Corrosion Area

Corrosion defects are orientated and spaced in a random manner over the internal or external surface of the pipeline. In the analysis of such a defect an attempt is made to characterise the corroded area by its projected length and depth. The difficulty in describing a three-dimensional corroded area by a few parameters introduces large scatter in comparisons of predictions to actual failure pressure. The scatter is significantly reduced by the use of assessment methods based on a river-bottom profile, but there is still more scatter than for flat-bottomed defects [71]. River-bottom methods (such as RSTRENG and those given in DNV-RP-F101) are based on iterative algorithms and are not suited to hand calculations. The methods based on a simple geometric approximation are closed-form methods.

The original ASME B31G criterion, Modified B31G criterion, DNV-RP-F101, and PCORRC define simple approximations to the exact corroded area, based on the maximum length and the maximum depth of the defect. Corrosion typically has an irregular profile and the most conservative idealisation is a rectangular profile (as in DNV-RP-F101 and PCORRC). ASME B31G assumes a parabolic profile (2/3 factor in the equation) and modified B31G assumes an arbitrary profile (0.85 factor in the equation). The methods for assessing a river-bottom profile are also approximations, because a river-bottom profile is an idealisation of the actual three-dimensional shape of a corroded area. A pictorial representation of an arbitrary corrosion with basic dimensions is shown in Figure 3.1.

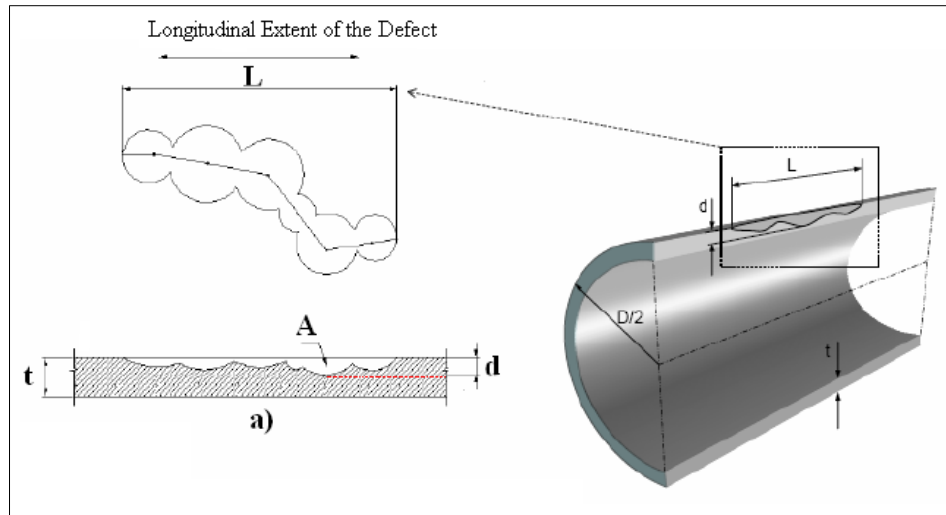


Figure 3.1 Pictorial representation of corrosion defect [12]

All of the methods considered here assumed that failure is due to a flow stress dependent mechanism therefore, it can be described by the tensile properties (yield strength or ultimate tensile strength) of the pipe steel. The methods, except PCORRC, are all similar in their general form, being based on the NG-18 equation for the failure of a part-wall flaw, but they are different in respect of assumptions and simplifications made in their derivation. These differences were due to different assumptions of the following factors:

- The flow stress
- The geometry correction factor (also referred to as the Folias factor, or the length correction factor, or the bulging correction factor)
- The defect profile

According to Stephens *et al.* two categories of corrosion defect assessment methods can be described [20]. These are:

- i. Empirically calibrated criteria that have been adjusted to be conservative for almost all corrosion defects, irrespective of the toughness of the line pipe (these criteria are variously based on the yield strength, the flow stress, or the ultimate tensile strength). ASME B31G and related methods are by contrast based on curve fits to empirical data.

- ii. Plastic collapse criteria that are only appropriate for blunt defects in moderate to high toughness line pipe (these criteria are based on the ultimate tensile strength). DNV-RP-F101 and PCORRC should be regarded as belonging to this category of assessment method. They were developed from curve fitting to the results of simplified FE analyses of blunt, part-wall defects. These are theoretically calibrated methods (i.e. calibrated to average data in the form of an experimentally validated FE model and associated numerical failure criterion).

3.3 Uniformly Corroded Pipeline Sections

The simplified equation for burst capacity of intact pressurized pipeline can be developed based on maximum hoop stress theory. It is assumed that the pressurized pipeline will rupture when the flow stress exceeds the maximum allowable hoop stress and this is more accurate for thin-walled pipelines. In operating pipelines, general corrosion can be as high as 12% of the total corrosion (refer section 4.1). As it was observed from an IP inspection, the wall thickness of operating pipeline is reduced almost uniformly, in the downstream pipeline sections. Therefore, we may assume a pipeline subjected to general corrosion as an intact pipeline with reduced wall-thickness to the average wall thickness.

ASME B31G and the DNV-RP-F101 methods suggested the reference pressure (maximum allowable internal pressure for a defect free pipe), P_o , as given by Eq. (3.1) and Eq. (3.2), respectively.

$$P_o = \sigma_{flow} \frac{2t}{D} \quad (3.1)$$

$$P_o = \sigma_{flow} \frac{2t}{(D-t)} \quad (3.2)$$

In open literatures, the flow stress (σ_{flow}) is expressed in several ways. In the B31G manual [12], the flow stress is defined as $1.1 \times SMYS$ and as $SMYS + 69MPa$ according to Kiefner and Vieth [14]. Furthermore, some sources estimate the flow

stress to be the average of *SMYS* and *SMTS*. In all these cases, the values we obtain are not the same. Therefore, multiple burst pressure estimations were obtained for the same pipe. In order to avoid these ambiguities, a consistent and realistic burst pressure estimation based on linear regression of 19 burst test result database is proposed by this research. The database consists of the most widely applicable API pipelines grades of X46, X52 and X60 steels. These data are obtained from burst test conducted during this study and from published literatures. Detail description of the pipe geometries and test results are given in Table A.1 (Appendix A).

Most often, by analogy, internally pressurised pipelines are approximated as pressure vessel. Theoretically, the burst pressure of a pressure vessel subjected to internal pressure can be determined by considering the maximum hoop stress theory. But in reality there is small discrepancy, and in order to compromise for the difference, we may assume a correction factor, φ . Thus, the reference pressure for a uniform cross-section pipeline can be described by Eq. (3.3).

$$P_o = \varphi P_{max} = \varphi SMTS \frac{2t}{(D-t)} \quad (3.3)$$

The correction factor, $\varphi = 1.0$ to 1.2 gave acceptable predictions. The best fit was obtained for $\varphi = 1.05$ with correlation factor of 0.98 by a linear regression of the true burst pressure versus the theoretical maximum pressure as shown in Figure 3.2. Therefore, we suggest the reference pressure of intact or uniformly corroded pipeline can be best estimated by Eq. (3.4). Once again, the flow stress is shown to be greater than the *SMYS* of the material. This delay of yielding can be justified due to strain hardening of the pipeline material.

$$P_o = 1.05 \times SMTS \frac{2t}{(D-t)} \quad (3.4)$$

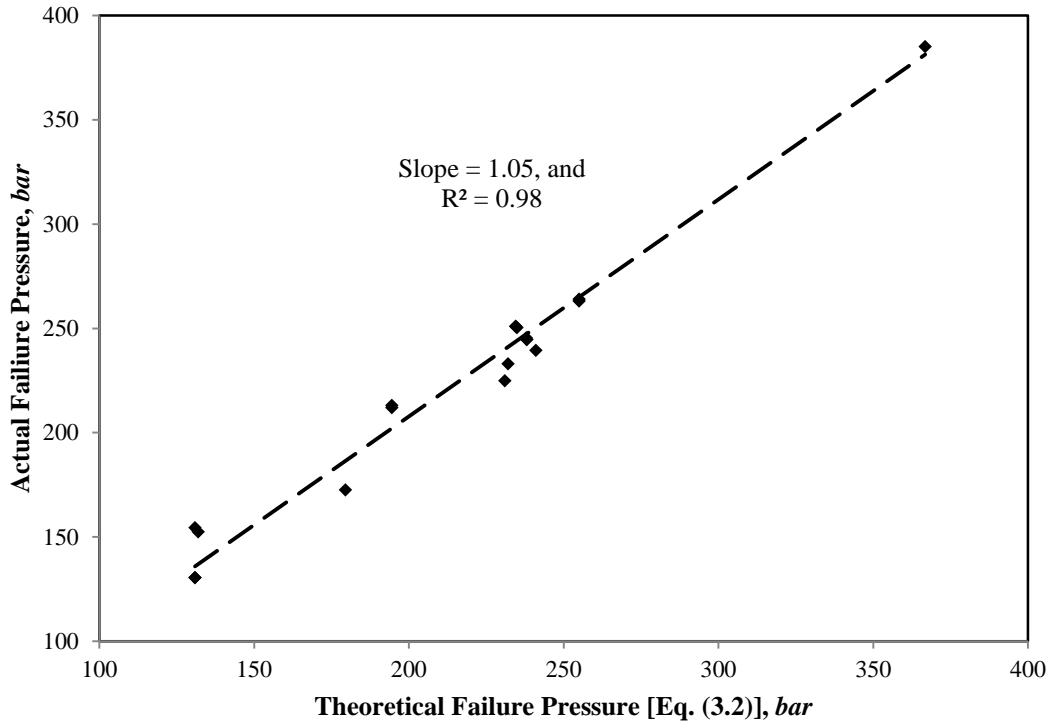


Figure 3.2 Theoretical versus actual failure pressure for intact pipelines

3.4 ANSI/ASME B31G Assessment

The ASME B31G criterion was developed based on full scale burst tests of pressured to failure corroded pipes [12]. It is used to estimate the Maximum Allowable Operating Pressure (MAOP) of corroded pipes. The origin of ANSI/ASME B31G equation is the NG18 equation, which was first developed in 1971. It is obvious that pipeline technology has been advanced a lot since then, but the B31G equation which was developed in 1991 it is still in use.

This equation also incorporates a design factor F , which is normally equal to 0.72. This design factor was never based on a rational assessment of operational stresses; but can be tracked back to the 1935 B31 codes, the working pressure was limited to 80% of the mill test pressure which itself has a design factor up to 0.9. Thus the total design factor will be 0.72. This number has since been used directly in some codes such as the DNV of the 1977 or the 1958 version of B31.8 for on-land pipelines [72].

Several modifications have also been proposed to these guidelines, e.g. changes in proposed flow-stress, corrosion area definition or proposed bulging factor. The modification of one or more parameters introduces adverse effects on the prediction. When some parameters are modified in order to obtain a better adaptation to existing and newer results have introduced a negative effect for other design cases with a different geometry and corrosion configuration [45].

This equation is clearly simple to use and implement. All variables go right into the equation for safe maximum pressure, and calculations are trivial. The equation is also versatile in the way that it can handle corrosion depths from 10% to 80% of the original pipe wall thickness. It doesn't however handle a real life problem such as system effects when more than one corrosion defect occurs. This is a very realistic problem, and it is a fact that the pipeline reliability is dependent on the number of failures found. The compatibility criterion is automatically fulfilled since the B31G equation has been the standard of practice for many years. On the other hand, the equation still needs exact data on the size of the corrosion damage. This data is only available through inspections. Coupled with the inconsistency in the results, the workability is not the good side of this approach. The engineering tools required to record data for utilization of this equation such as instrumented pigs are well developed. Therefore, the method can be said to be feasible.

3.4.1 Original ASME B31G Criterion

A continuous corroded area having a maximum depth of more than 10% but less than 80% of the nominal wall thickness of the pipe should not extend along the longitudinal axis of the pipe for a distance greater than that calculated from:

$$L = 1.12B\sqrt{Dt} \quad (3.5)$$

where, B in Eq. (3.5) is a constant and its value can be determined from:

$$B = \sqrt{\left(\frac{d/t}{1.1d/t - 0.15}\right)^2 - 1} \quad (3.6)$$

The value of B must not exceed 4. If the corrosion depth is between 10% and 17.5%, $B = 4.0$ can be used.

If the measured maximum depth of corroded area is greater than 10% of the nominal wall thickness but less than 80% of the nominal wall thickness and the measured longitudinal extent of the corroded area is greater than the value determined by Eq. (3.5), A is calculated by using Eq. (3.7).

$$A = 0.893 \left(\frac{L}{\sqrt{Dt}} \right) \quad (3.7)$$

The Folias factor (M) which accounts for the curvature of the pipeline section is determined using Eq. (3.8).

$$M = \sqrt{A^2 + 1} = \sqrt{1 + 0.8 \left(\frac{L}{\sqrt{Dt}} \right)^2} \quad (3.8)$$

For values of $A \leq 4$ (i.e. $L \leq \sqrt{20Dt}$), the corrosion is considered as short defect. Therefore, the complicated shape of corroded area is approximated by a parabolic shape and the failure pressure can be predicted by Eq. (3.9).

$$P_f = 1.1P_{max} \left[\frac{1 - \frac{2d}{3t}}{1 - \left(\frac{1}{M} \right) \frac{2d}{3t}} \right], \quad P_f \leq P_{max} \quad (3.9)$$

However, the $MAOP$ can be limited to a multiple of the estimated failure pressure by the design factor, F as given in Eq. (3.10).

$$P_{max} = MAOP = SMYS \times \frac{2t}{D} \times F \times T \quad (3.10)$$

For values of A greater than 4 ($L > \sqrt{20Dt}$), the defect is considered as infinite length and the corrosion area is approximated by a rectangular shape. The failure pressure estimation can be further simplified as shown in Eq. (3.11).

$$P_f = 1.1P_{max} \left[1 - \frac{d}{t} \right], P_f \leq P_{max} \quad (3.11)$$

If the established *MAOP* is equal to or less than P_f , the corroded region may be used for service at that *MAOP*. If it is greater than P_f , then a lower *MAOP* that does not exceed P_f should be used or the corroded region should be repaired or replaced.

3.4.2 Modified B31G Criterion (0.85dL Area)

The B31G method was found to be too conservative and has been modified, the new method is called Modified B31G (0.85dL) area method. One of the most significant changes to the original B31G method is the defect geometry approximation. Corrosion area is defined by 0.85dL.

This method removes some limitations by modifying the flow stress limit equal to $SMYS + 69MPa$. This is very close to the conventional fracture mechanism definition of the flow stress which is the average of the yield and ultimate strength. This modification results in the change of the failure equation, which is also dependent on the limit of defect length. The equation to calculate the failure pressure is modified and given as shown in Eq. (3.12).

$$P_f = (SMYS + 69.1MPa) \frac{2t}{D} \left(\frac{1 - 0.85 \frac{d}{t}}{1 - 0.85 \frac{1}{M} \frac{d}{t}} \right) \quad (3.12)$$

For $L \leq \sqrt{50Dt}$, the Folias factor is given by Eq. (3.13).

$$M = \sqrt{1 + 0.6257 \left(\frac{L}{\sqrt{Dt}} \right)^2 - 0.003375 \left(\frac{L}{\sqrt{Dt}} \right)^4} \quad (3.13)$$

For $L > \sqrt{50Dt}$, the Folias factor is given by Eq. (3.14).

$$M = 3.3 + 0.032 \left(\frac{L}{\sqrt{Dt}} \right)^2 \quad (3.14)$$

3.4.3 RSTRENG Criterion (Effective Area Method)

RSTRENG (Remaining Strength) of corroded pipe is a modification of the B31G code based on real shape of corrosion defects. The basic difference between the Modified B31G and RSTRENG is the geometry description [73]. The Modified B31G method can be considered as a simple calculation with an approximate geometric shape, while RSTRENG takes into account the actual profile of the defect. Therefore, in cases of real corrosion assessment, more measurements have to be done to determine the river-bottom profile.

Such area assessment results in better failure pressure prediction, which is given by Eq. (3.15).

$$P_f = (SMYS + 69.1MPa) \frac{2t}{D} \left(\frac{1 - \frac{A_c}{A_0}}{1 - M^{-1} \frac{A_c}{A_0}} \right) \quad (3.15)$$

The Folias factor M is the same to the factor used in modified B31G.

3.5 DNV Criterion

The DNV guidelines are still under development, and the latest version of the DNV-RP-F101 released in 2004 is considered in this discussion [15]. It provides guidance on single and interacting defects under pressure only and combined loading. The DNV-RP-F101 provides two methods of analysis i.e. a partial safety factor method and an allowable stress design method. The allowable corroded pipe pressure of a single metal loss defect subjected to internal pressure loading is given by acceptance equation as in Eq. (3.16).

$$P_f = \gamma_m SMTS \frac{2t}{D-t} \left(\frac{1 - \gamma_d \left(\frac{d}{t}\right)^*}{1 - \gamma_d \frac{1}{Q} \left(\frac{d}{t}\right)^*} \right) \quad (3.16)$$

The relative corrosion depth and the Folias factor Q are given by Eq. (3.17) and Eq. (3.18), respectively.

$$\left(\frac{d}{t}\right)^* = \left(\frac{d}{t}\right)_{mean} + \varepsilon_d StD \left(\frac{d}{t}\right) \quad (3.17)$$

$$Q = \sqrt{1 + 0.31 \left(\frac{L}{\sqrt{Dt}}\right)^2} \quad (3.18)$$

In the allowable stress design approach, the failure pressure of the pipe is calculated and multiplied by safety factors. These factors may be based on design factor and take into consideration the uncertainties discussed above. The uncertainties caused by the presence of a corrosion defect, can be described by the additional 0.9 factor. This is a commonly used approach because of its simplicity and is given as in Eq. (3.19).

$$P_f = 0.9F \times SMTS \frac{2t}{D-t} \left(\frac{1 - \frac{d}{t}}{1 - \frac{1}{Q} \frac{d}{t}} \right) \quad (3.19)$$

The expression of the burst capacity of single longitudinally oriented, rectangular corrosion defect was developed based on a large number of FE analyses, and a series of full scale burst tests. By using FE analyses the effect of each important parameter was investigated, while the accuracy of the analyses was verified by a large number of full-scale burst tests. The equations used in the development of this recommended practice and in the calibration are fairly complex. For practical use a simplified capacity equation of a single rectangular shaped defect was given by Eq. (3.20).

$$P_f = 1.05 \sigma_u \frac{2t}{D-t} \left(\frac{1 - \frac{d}{t}}{1 - \frac{1}{Q} \frac{d}{t}} \right) \quad (3.20)$$

This capacity equation represents the mean (best) estimate of the capacity of a pipe with a rectangular shaped corrosion (metal loss) defect. This implies that on average the equation should represent the capacity lower pressure, and some at a slightly higher pressure, than predicted.

The accuracy of the capacity equation had to be known for establishing the appropriate safety factors, and the above mentioned effects were accounted for. If the equation is used for irregular or parabolic defect shapes, and the maximum depth and lengths are used, the equation in general underestimate the failure pressure, as the defect is not as large as the rectangular shaped defect assumed in the capacity equation. This will result in a conservative estimate of the failure pressure capacity for defects with shapes other than rectangular.

3.6 PCORRC Assessment

The PCORRC method was developed by Battelle as part of on-going research into the fundamental mechanisms driving failure of pipeline with corrosion defects. The focus was to derive a more analytical, as opposed to empirical method for predicting failure of general and complex locally thinned areas (LTA). A FE analyses tool called PCORRC was developed to aid in the research. The procedure presented here is the final closed form model for the failure of blunt defects in pipelines that are general in nature and that can be applied to critical defect problems in the pipeline industry. The method is only applicable to high toughness steels, so its flexibility is limited.

The original approach of PCORRC method was designed to predict the failure pressure of damaged pipe by using an exponential function defined as is shown in Eq. (3.21).

$$P_f = \sigma_u \frac{2t}{D} \left\{ 1 - \frac{d}{t} \left[1 - \exp \left(-c \frac{L}{\sqrt{R(t-d)}} \right) \right] \right\} \quad (3.21)$$

As it is given in the original formula, from the curve fitting of the FE simulation results, the value for c is given to be 0.142 to 0.224 depending on the defect depth. The value of ultimate tensile strength, σ_u , is also suggested to be 95% of $\sigma_{u, test}$ for less conservative estimation. However, in practice, due to material anisotropy the ultimate tensile strength can have different values from sample to sample. Moreover, the need of the tensile data in the equation makes this method less usable. Therefore, we suggested a modified method based on the original PCORRC approach by curve fitting of more than 110 burst test database. This new method is described by *SMTS* of the material instead of the ultimate tensile strength. The modified assessment criterion is given by Eq. (3.22).

$$P_f = 1.1 SMTS \frac{2t}{D} \left\{ 1 - \frac{d}{t} \left[1 - \exp \left(-0.137 \frac{L}{\sqrt{R(t-d)}} \right) \right] \right\} \quad (3.22)$$

3.7 Comparison of Assessment Methods

3.7.1 Problems with Scatter in the Data

There are large scatters in the predictions of the burst strength of real corrosion by using the above discussed methods. Because these methods were based on a simple geometric idealisation, like rectangular and parabolic shapes. The maximum depth and maximum length are insufficient to describe the irregular shape of a real corrosion defect. Therefore, comparison of the methods with actual burst pressure of real corrosion defects resulted in high scattered predictions.

3.7.2 Problems with Comparing the Methods

There is insufficient data in the published literature to do a thorough comparison of the methods with each other. If there were enough detailed data, then the simplest comparison would be burst tests of simulated flat-bottomed corrosion defects. In order to avoid scatters associated with approximations to an irregular profile:

- The approach would be to consider those tests which are known to have failed by plastic collapse (i.e. reference stress is equal to the ultimate tensile strength as discussed in section 5.5)
- Define an appropriate failure criterion
- Then identify those tests which do not follow the predictions of the criterion
- Finally, determine what is different about these outliers and then define the limitations of the failure criterion. Only then would the methods can be compared against burst tests of real corrosion defects

3.7.3 Comparison of Methods with Burst Test Database

To get better understanding of different reviewed guidelines, a quantified comparison of the methods is necessary. The burst pressure capacity by the methods for various pipelines and corrosion sizes were reviewed. Since the real corrosion sizes are random, the comparison of methods is somewhat complicated for continuous ranges if any of these variables are to be studied. However, the continuous range of variables was studied based on FE simulation results as discussed in section 6.1.

The five methods described were compared with burst test database from 119 tests. For B31G and DNV equations, all the safety factors were set to unity in order to compare the burst pressure. The summary of results for mean error (bias) and standard deviation of the error (scatterings) of predictions against burst test database are shown in Table 3.1. Detail descriptions of the tests database are shown in Table A.2 (Appendix A).

Table 3.1 Summary of mean bias and scatterings of various prediction methods

Methods	Bias (%)	Pipeline Material Grade					Overall
		X42	X46	X52	X60	X65	
B31G	Mean	37.23	27.92	34.67	34.66	18.73	30.80
	StD	13.74	7.31	13.29	11.07	10.27	11.70
M. B31G	Mean	30.43	21.46	27.93	21.21	15.53	23.90
	StD	10.55	9.21	9.48	7.63	4.73	9.80
RSTRENG	Mean	35.70	26.77	25.81	28.88	24.08	27.00
	StD	12.93	11.56	9.38	5.42	7.36	10.80
DNV	Mean	27.16	18.62	33.10	29.20	21.72	25.65
	StD	13.77	9.93	12.00	6.32	4.93	12.06
Modified	Mean	12.08	8.50	18.68	17.62	2.65	12.90
PCORRC	StD	13.37	5.96	13.39	4.56	2.34	10.80

On the basis of the different guidelines reviewed here; it may be difficult to say which one is the “best” guideline. Apart from the overall results for mean bias and scatterings of predictions, the following criteria may need to be considered:

- *Simplicity*: ease of use and implementation
- *Versatility*: the ability to handle a wide variety of real problems
- *Compatibility*: readily integrated into common engineering and operational procedures
- *Workability*: the information and data required for input is available or economically attainable, and the output is understandable and can be easily communicated
- *Feasibility*: the available engineering instrumentation, maintenance tools and techniques are sufficient for application of the approach
- *Consistency*: the approach can produce similar results for similar problems when used by different engineers

Prediction versus actual failure pressure for B31G criteria according to Eq. (3.9) or Eq. (3.11) is shown in Figure 3.3. The overall mean error of 30.80% and standard deviation of the error of 11.70% was observed. All the predictions were less than the actual failure pressure and highly scattered up to 72.10% lower than the actual burst pressure. Unlike the recommendation of this method for lower grade steels, the quantitative study showed no better precision for X42 or X52 grade pipelines. Relatively better predictions were observed for flat-bottomed simulated corrosion defects. For example, better predictions were obtained for all X65 and some X52 flat-bottomed burst test samples.

The simplicity and workability of B31G criterion is good, but it is limited to the assessment of non-interacting longitudinal corrosion defect under internal pressure.

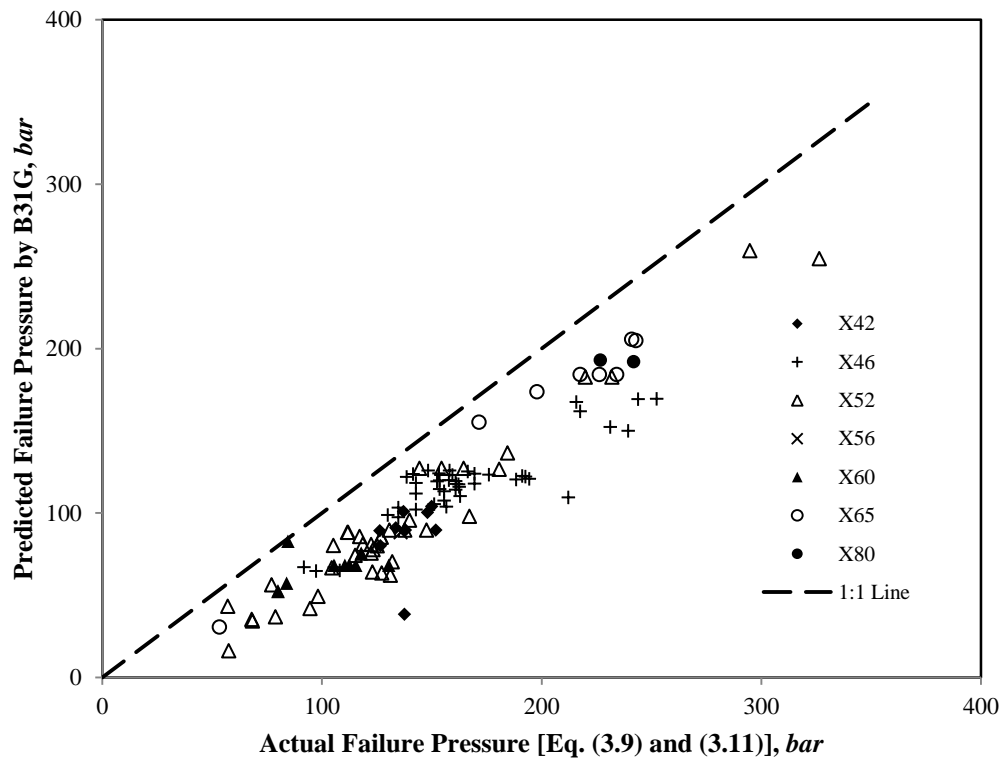


Figure 3.3 Actual failure pressure versus B31G predictions

Prediction versus actual failure pressure by Modified B31G criteria, Eq. (3.12) is shown in Figure 3.4. An overall mean error of 23.90% with standard deviation of an error of 9.80% was observed. Although the Modified B31G criteria gives better prediction than the original B31G code, there is still high scatters up to 51.90% of

under estimation. Like the original B31G code, this method is recommended to be used for lower grade steels. But the quantitative study showed no better precision for X42 or X52 grade pipelines. But better predictions were observed for flat-bottomed simulated corrosion defects. For example, better predictions were obtained for all X65 flat-bottomed burst test samples.

The simplicity and workability of this criterion is good, but it is also limited to the assessment of non-interacting longitudinal corrosion defect under internal pressure.

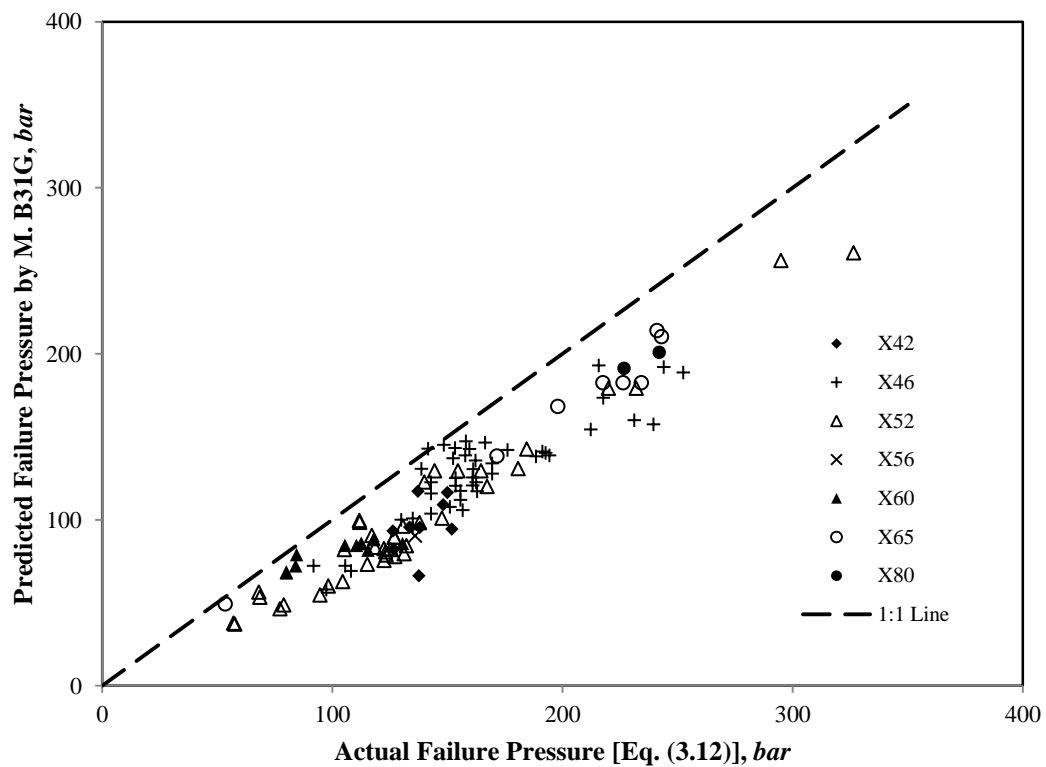


Figure 3.4 Actual failure pressure versus Modified B31G predictions

Prediction versus actual failure pressure by RSTRENG criteria, Eq. (3.15) is shown in Figure 3.5. An overall mean error of 27.00% and standard deviation of the error of 10.80% was observed. For the identified database, the method gave no better predictions as compared to the Modified B31G criteria. The scatters are also as high as 61.80% under estimation. Unlike the recommendation of this method for lower grade steels, the quantitative study show no better precision for lower grade pipelines. As the method is based on the actual defect area, better predictions were observed for flat-bottomed simulated corrosion defects. For example, for a flat-bottomed simulated

defect of X65 grade still pipeline, an average error was 24.08% and a consistent prediction (with only 7.36% of standard deviation of the error) was observed.

In practice, calculation of the actual area is not easy, therefore, a computer program called KAPA was developed for the utilization of this criterion [73]. Like other ASME methods it is limited for prediction of burst capacity of non-interacting defects.

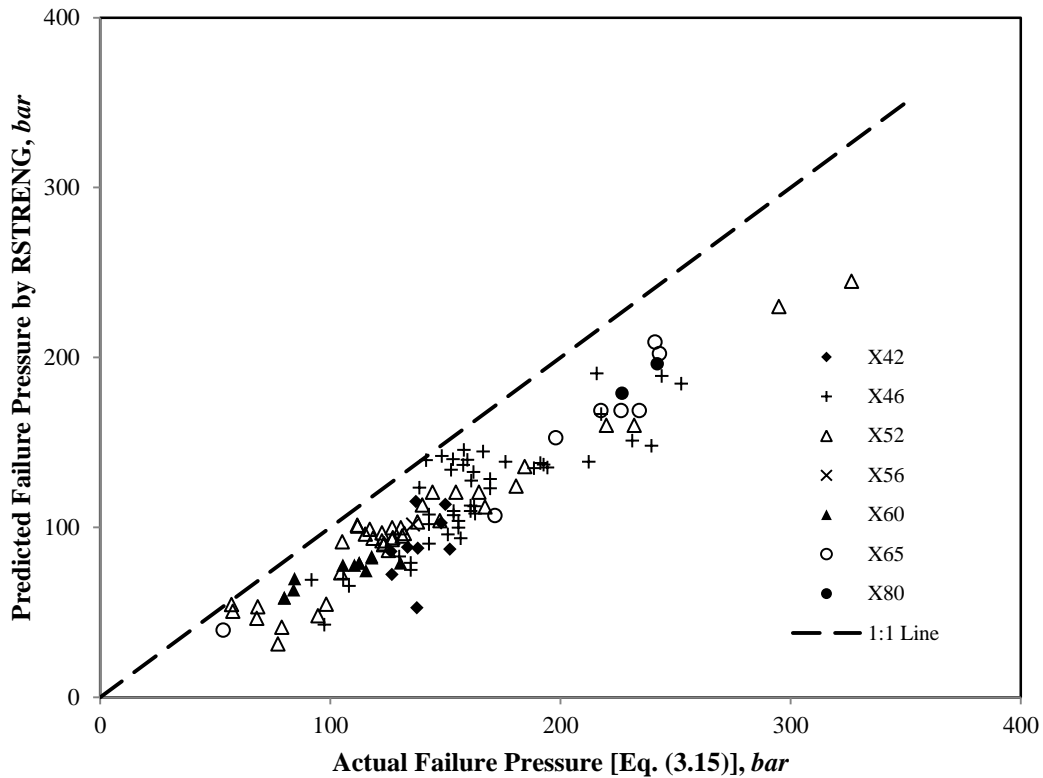


Figure 3.5 Actual failure pressure versus RSTRENG predictions

Prediction versus actual failure pressure for DNV method, Eq. (3.20) is shown in Figure 3.6. The overall mean error of 25.65% and standard deviation of an error of 12.06% was observed. Even though this method is new and several considerations were taken into account, for the identified database gave no better predictions than the ASME codes. The scatters are also as high as 62.20% under estimation. Unlike the recommendation of this method for higher grade steels, the quantitative study showed no better precision for higher grade pipelines. Rather, relatively better prediction with mean error of 18.62% and standard deviation of the error of 9.93% was predicted for X46 grade steel.

The DNV method is not as convenient as the ASME codes for application. There are a number of additional factors to be considered in the formulation; therefore, depending on the specific factors assumed, the prediction may not be consistent. Unlike the ASME codes, the method is not limited for prediction of burst capacity of single (isolated) longitudinal corrosion defect under internal pressure. The burst pressure of interacting defects and multiple loads can be treated by this approach; therefore, the versatility of this method is better.

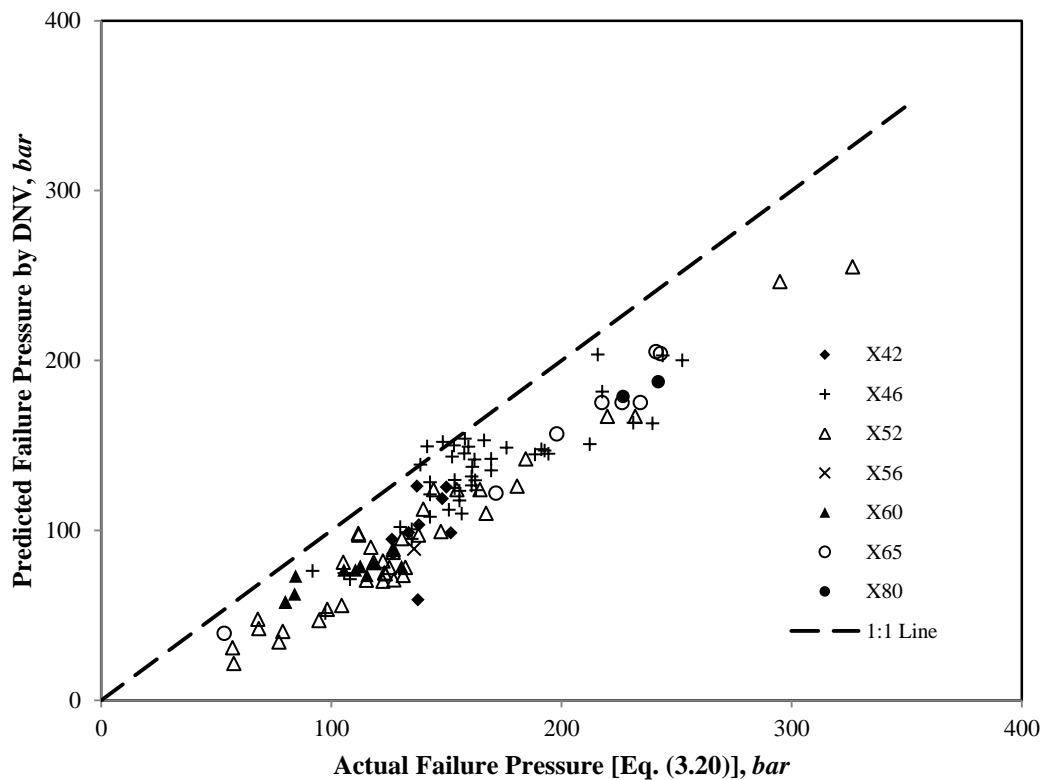


Figure 3.6 Actual failure pressure versus DNV predictions

Prediction versus actual failure pressure by Modified PCORRC method, Eq. (3.22) is shown in Figure 3.7. This method predicted the burst pressure by mean error of 12.90%, and with standard deviation of the error of 10.80%. A maximum error up to 57.70% is observed. Even though the mean deviation of the prediction seems better than the previously discussed methods, in some cases the prediction is greater than the actual burst pressure. The best prediction is made for simulated flat-bottomed rectangular defects. For example, in the case of X65 steel pipeline, the mean error was only 2.65% and the standard deviation of the error was as low as 2.34%.

The method is simple to be used and the workability of this criterion is good, but it is limited to prediction of single (isolated) longitudinal corrosion defect under internal pressure.

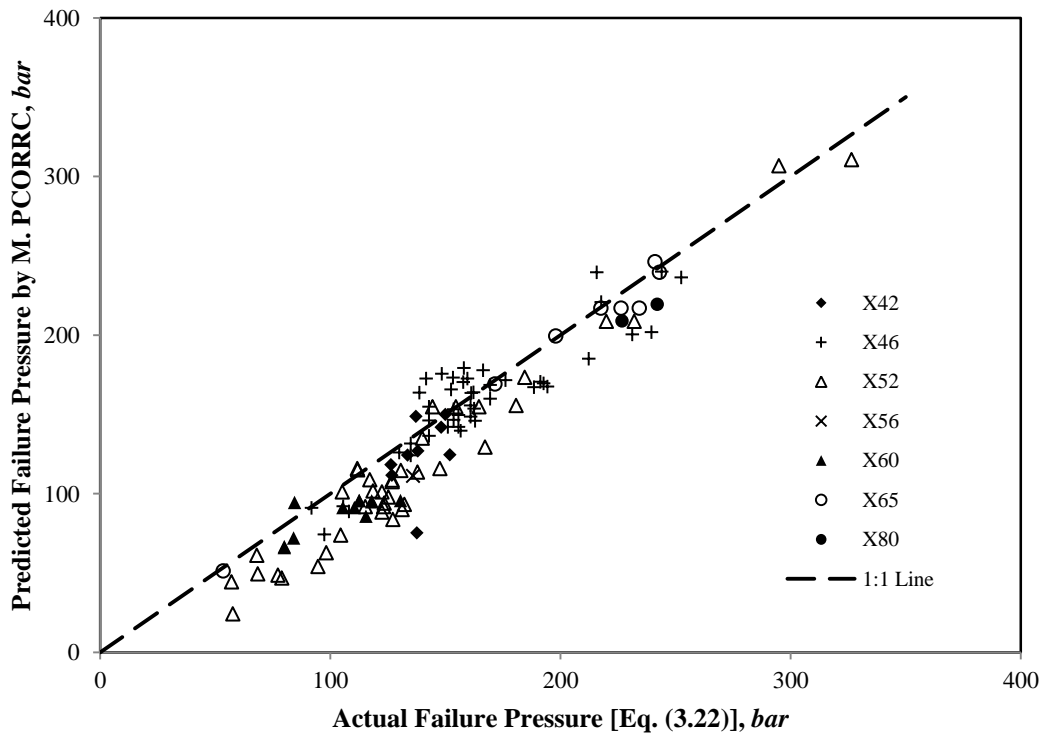


Figure 3.7 Actual failure pressure versus Modified PCORRC predictions

3.8 Summary

The failure pressure predictions for corroded pipelines were investigated by most popular current assessment methods. The predictions were compared with the actual values from the burst test database. Based on the comparison, the following conclusions were drawn:

- All the current assessment methods gave conservative and inconsistent predictions.
- For all methods, better predictions were observed for simulated flat-bottomed rectangular defects. This is because in the case of flat-bottomed rectangular defects, the defect area can be determined precisely. Therefore,

in order to get better predictions, the defect area should be determined accurately.

- The proposed Modified PCORRC criterion predicted the burst pressure with relatively less bias, but the scatters of the predictions are still very high.

As one can observe the predictions through Figure 3.3 to Figure 3.6, all the current methods showed conservative results. Based on the trends of the comparison with the burst test database, we suggested modified criterions using scale factor for each method. The scale factor was determined according to the average bias of each method. These scale factors are given as a multiplication factor to the equations describing the methods. Therefore, the modified criterions corresponding to B31G, Modified B31G, RSTRENG and DNV are suggested to be 1.45, 1.30, 1.35 and 1.35, respectively. For example, the modified RSTRENG equation can be given as 1.35 times the value given by Eq. (3.25). However, even after modification by using the scale factors, the inconsistency of predictions by the modified methods are still big.

CHAPTER 4

LABORATORY TESTS

4.1 Introduction

In order to develop and validate a new method for the assessment of corrosion defects, an experimental database is necessary [17, 25, 43]. Such database is also necessary to evaluate the accuracy of currently accepted corrosion assessment procedures. Much of the published burst test data is incomplete with only nominal pipe dimensions and material properties, and inaccurate representations of the corrosion defects. In addition, many of the reported tests with detailed measurements involved artificial or machined defect with simple geometries such as grooves and notches. These types of tests are an important stepping-ground in the development of numerical methods and understanding defect behavior. Unfortunately, the complexity of real corrosion defects may not be accurately represented with simpler shapes.

Corrosion management, inspection and monitoring rely on IP data obtained from the scheduled pigging exercise to provide feedback on the integrity of the pipeline. The IP metal loss data provide a means for engineers to conduct FFS assessment based on the available codes. Since the FFS assessment depends on the accuracy of the IP data, it is of utmost importance to have confidence on the IP data. An overestimation of metal loss by IP means premature retirement of the pipe and an underestimation of the metal loss means hazardous operations. Furthermore, the codes used also contain inherent conservativeness which also affects the assessment; therefore, there is a need to establish understanding of the accuracy of IP and the degree of conservativeness of the codes.

UTP had conducted a study on residual strength of severely corroded section of an abandoned 10” crude oil pipeline, which had been serving for more than 25 years. A 10” diameter pipeline of 6.9km length carrying wet and semi processed crude oil between two platforms was operating in South-China Sea. It was commissioned for a design life of 20 years. The MAOP of the pipeline was de-rated to 40bar from a design pressure of 93bar based on the FFS assessment performed two years before retirement. The pipeline had been operated at an average Operation Pressure (OP) of 28.0bar by the time of retirement.

An inline inspection using MFL tool reported 10,804 metal loss defects; where 10,803 internal defects concentrated at 700 meters from the upstream platform. The major portion of the defect was due to pitting corrosion. There was only one external defect reported at the riser of the upstream platform. The different class and distribution of metal loss anomalies are summarized as shown in Figure 4.1.

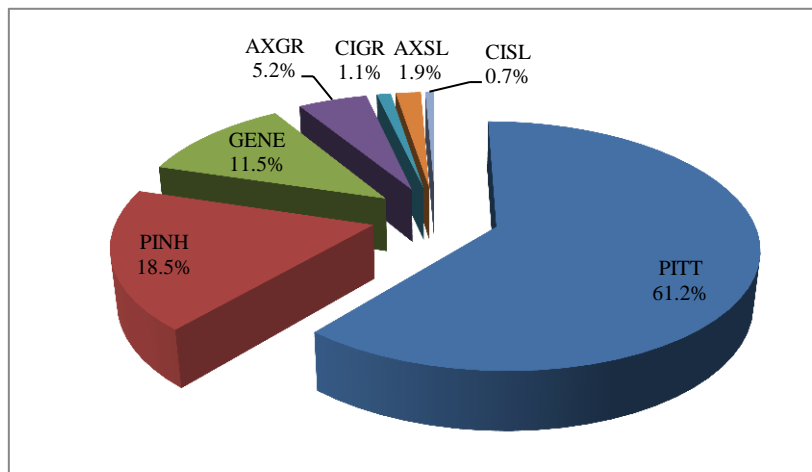


Figure 4.1 Corrosion defect anomaly classes

(Definition of acronyms: PITT: Pitting, PINH: Pinhole, GENE: General Corrosion, AXGR: Axial Grooving, AXSL: Axial Slotting, CIGR: Circumferential Grooving and CISL: Circumferential Slotting)

Based on the FFS assessment conducted by using DNV-RPF-101 Part A, 17 defects were reported with allowable corroded pipe OP (P_{corr}) lower than the MAOP and at 8 locations the P_{corr} was calculated as zero. Furthermore, 10 groups of interacting defects having $P_{corr} = 0$ were also reported. All the identified defects were located within 100 to 350 meters section from the upstream platform. Accordingly, the operator replaced the so called critical section from log distance 93 to 850 meters

due to single and interacting defects having $P_{corr} = 0$ and it contains the highest density (88%) of the defects.

Further investigation was conducted in order to justify the decision made by the operator. The output will be valuable for future handling of a vast pipeline network. Thus, about 100 meters of this abandoned pipe section was delivered to UTP for the study. First of all, the sections of the pipeline were inspected visually and photographic records of some of the unique features were taken. Next, UT C-Scanning and P-Scanning were done on sections of interest as identified by IP inspection and the critically corroded sections were identified. These sections were then used for the calculation of the burst strength and the MAOP for the pipeline system. The burst strength was determined by full scale burst test of five samples cut out from this section. Finally, these burst test results were used to validate the FE approach used to simulate the burst pressure prediction of corroded pipelines.

4.2 Corrosion Measurement

Accurate measurement of the corrosion defects is the most important but the most difficult stage of the test procedure. For the case of three dimensional FE analyses, the data can simply be used directly to create an appropriate FE model. A simplification is made for B31G where only the total length and maximum depth are used to quantify the defect. An intermediate approach is by using RSTRENG where a river bottom path through the corrosion defect is defined to represent the corrosion defect. While this incorporates detailed measurements of the corrosion defect, the circumferential extent and position of adjacent metal loss regions is neglected since the river bottom path is projected onto longitudinal axis.

4.2.1 Inline Inspection

Today, the use of inline inspection tools is a standard procedure for the collection of pipeline data required for integrity assessment and FFP studies. Their major task is to provide accurate geometric information regarding the length, width, depth, orientation

and location of the flaw. The major advantage of inline inspection tools is their capability to survey the entire pipe circumference whilst the pipeline remains in operation. They are usually pumped through the pipeline to be inspected (i.e. free-swimming tools) and do not require their own drive.

4.2.2 Metal Loss Inspection

Metal loss inspection encompasses finding and accurately sizing of flaws and wall thickness losses due to corrosion or gouging. The data obtained, e.g. length, depth, width, and others are then used for integrity assessment, for corrosion growth assessment or for determination of the service intervals.

All measurement principles have specific characteristics regarding their accuracy and error margin. The better the accuracy and the more reliable (less errors) the method, the better the suitability for use in any integrity assessment work. An important factor here is the confidence level. The confidence level quoted for ultrasound technology is usually 95%, compared to an average value of 80% for MFL method.

Accuracy of MFL tools is usually around 90% of wall thickness, although there are some tools available that quote a 95% accuracy regarding the detection of internal flaws. With the latest technology ultrasound tools depth resolutions of 0.06mm can be achieved. For example, for a pipeline of 11.1mm nominal wall thickness, an accuracy of 99.4% can be achieved by this latest technology. Regarding the detection, sizing and comparison of flaws based on corrosion or grooving, this is a major advantage of tools utilizing ultrasound technology.

Another advantage is owed to the fact that ultrasound tools can quantitatively measure the contour of a metal loss flaw. This implies that the "shape" of the bottom of a corrosion or gouge can be measured as a true river bottom. This is an added advantage for higher level of MAOP calculations, such as RSTRENG or calculations based on the DNV code. This technical ability also provides an option to use the geometric data provided as input for the modeling of the geometry for FE calculations.

4.2.3 Visual Inspection

Visual inspection was made on about 100 meters of the abandoned pipeline section delivered to UTP. For ease of transportation, the section was cut into 10 spools of approximately 10 meters. On the cut spools, the orientation and flow directions were indicated. About 60 meters of this section was taken from the most upstream location and the remaining 40 meters section was taken from the most downstream section of the abandoned pipeline section.

The visual inspection of the pipes was recorded in reference to the markings on the pipelines in terms of the O'clock orientation and log distance. Corrosion was found to be minimal and distributed between 3 O'clock to 9 O'clock (bottom half) of the pipe. However, there was no localized and deep corrosion of any form. Corrosion debris, solid precipitates and scale like deposits were observed along 6 O'clock line (bottom line) of the pipe. Most of the external surface of the pipeline was free from corrosion due to the protecting rubber coating. However, rusting due to sea water infiltration under the newly wrapped rubber laminations was observed. These newly wrapped rubber laminations were made after inspections and maintenance activities.

4.2.4 UT Inspection

Based on the IP tally, some heavily corroded sections were identified for UT inspection. UT thickness mapping using C-Scan technique and an advanced UCS/P-Scan were conducted on the identified sections.

An UT probe detachable light emitting diode (LED) was used for scanning the area under inspection. The LED emits infra-red light of narrow band-width that provides the means for camera to track the movement of the probe and hence its coordinates. By monitoring the back wall signal in gate, the area scanned can be marked with its corresponding thickness indicated in color on the screen. Thus a record is preserved and a topographic mapping (also called a C-Scan) of the area covered is obtained. The scanning was conducted on 8 sections each with 200mm length.

The comparison showed that the IP overestimated the defect size by about 20% as compared to the C-Scan result. This measurement is acceptable according to the 80% confidence level recommendation by MFL tool producers and vendors. In order to compare the IP tally with the C-Scan result, the reference point must match precisely. However, if the scan test section is limited to 200mm, the comparison is error prone and possibility of mismatching sections is higher. Therefore, to minimize the error due to mismatching of sections, it was decided to conduct more advanced UT scan in a continuous and longer section.

Two continuous sections of total length of 18.42 meters were chosen for an advanced UCS/P-Scanning. The scanning was handled by sub dividing each section into 11 segments of about 860mm in length. Unlike C-scan, UCS/P-Scan is faster and the probe is operated by automatic controller. The result showed that, the minimum wall thicknesses measured by IP in these sections was less only about 12.5% and the average wall thickness was 10% less than the P-Scan measurements. Therefore, it is concluded that, the IP tally was acceptable within a precision level of up to 87.5%.

4.3 Burst Test

The experimental part of this research consists of burst tests of API X52 corroded pipes removed from service field and pipes with simulated corrosion defect. Details of the pipe and corrosion geometry, material properties and the conditions surrounding failure locations were recorded. Results of these burst tests combined with experimental results available in the published literatures were used to establish and validate the relationships between burst pressure of the pipe and corrosion geometries, grades of steel and loading conditions. Furthermore, the experimental results were used to validate FE models used to simulate the failure of corroded pipe.

4.3.1 Modeling of Corrosion Defects

Researchers have attempted to simplify the experimental testing of complex corrosion defects by representing them with a large flat-bottomed patch with a depth equal to

the maximum defect depth and a length equal to the overall defect length [31, 43]. In terms of metal loss, this is a conservative representation of a complex corrosion defect and is appropriate for conservative assessment of a defect. However, experimental testing and numerical analysis of these defects has shown that the failure mode differs from that of natural corrosion defects. The flat-bottomed defects were machined as smooth surfaces so that no significant localization of stress occurs within the defect. Consequently, the patch behaves in a similar fashion to a curved plate subjected to pressure on one side and fixed around its edges. The abrupt change from the maximum defect depth to full pipe wall thickness at the edges of the defect results in a large degree of restraint.

In contrast, natural corrosion defects have local variations in depth which result in stress localization and localized failure at one of these deepest points. If failure occurs by rupture, the fracture generally propagates in the longitudinal direction although it may change circumferential position to follow the deepest path in the defect [58].

The use of artificial defects to represent natural corrosion was justified for smaller defect sizes [4]. The maximum allowable size for machined defect to behave as a complex corrosion defect has not been investigated. Nevertheless, it can be said that tests which fail by rupture around the edge of the machined defect are not representative of natural corrosion defect. Such tests should not be used to represent natural corrosion defects or to validate failure prediction models. In some cases, such as in preliminary investigations, it may be necessary to use large flat-bottomed defects due to their simplicity in shape.

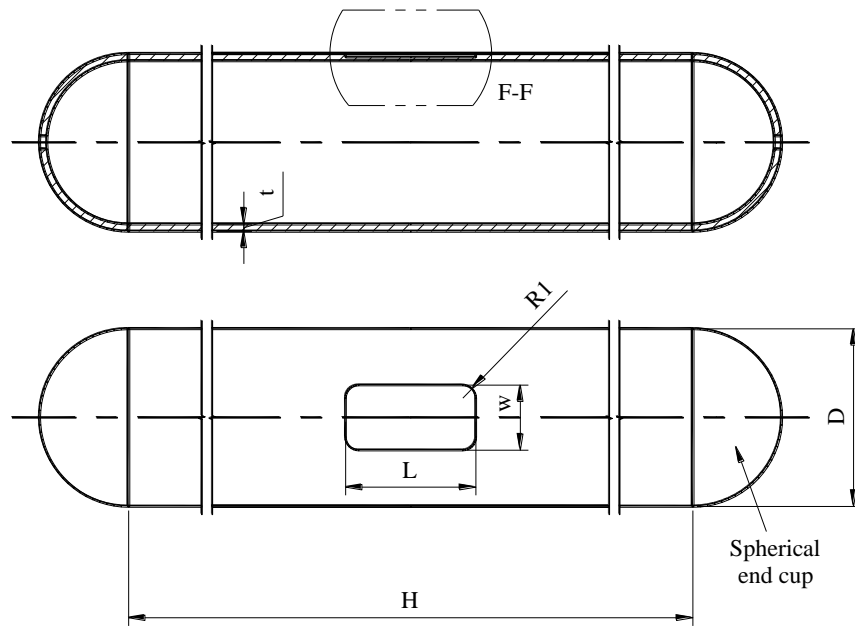
4.3.2 Machining of Simulated Defects

There are two most commonly used methods to induce artificial (simulated) defects on the pipe surface. These are mechanical machining and electro-chemical machining. Electro-chemical machining utilizes an electrode in the shape of the defect to be machined. An electrolyte is continuously pumped between the electrode and pipe surface, while a power supply is used to provide the necessary current for the artificial corrosion process. Although this process is more representative of the natural

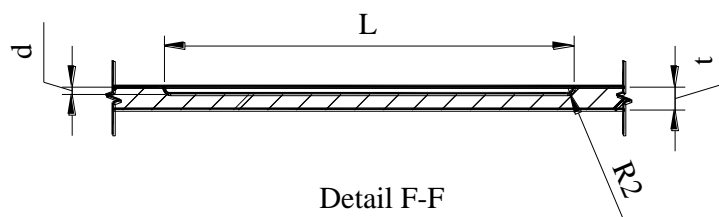
corrosion process, it can be difficult to achieve a smooth surface due to the accumulation of debris and variations in the flow of the electrolyte.

Mechanical machining can be done on a mill with a mechanical cutter. In this research CNC mill was used to machine the flat-bottomed defect on the external surface of the pipe. Although it is accurate, it can be difficult to achieve uniform depth in the circumferential direction due to the curvature of the pipe. It has also been suggested that this process may introduce residual stresses into the defect. In order to minimize the possible stress concentrations at the ligament, appropriate fillet radius was provided. Actually, residual stress may have no significant effect on the failure analysis due to larger degree of plasticity in the defect prior to failure.

A total of five burst test samples were prepared. One of these test samples (T2) was with general corrosion distributed over the internal surface and four of which were with simulated longitudinal corrosion defect. The defects had a smooth surface and all edges were made with a small radius. The surfaces were also grinded slightly to obtain a smoother surface for ease of thickness measurements and attachment of strain gauges. At each end of the test specimens a spherical end cap was welded to the pipe. The inlet for internal pressure and mounting of the pressure transducer were at the end flanges. Schematic drawing of the burst test samples with basic geometric dimensions are shown in Figure 4.2. Detail drawings for all samples are attached in Appendix B.



(a) Overall drawing



(b) Defect close view

Figure 4.2 Schematic drawing of burst test sample

4.3.3 Burst Test Procedures

The burst tests were performed under closed-ended conditions according to the following procedures:

- *Corrosion measurement:* All defects on the pipe surface were accurately mapped using surface scanners (see Section 4.2.4).
- *Material properties:* The material properties were measured with tensile test specimens in the circumferential and longitudinal directions (see Section 4.5).

- *Pipe dimensions:* The pipe wall thickness and diameter were measured at multiple locations for each pipe section tested.
- *Burst testing:* All pipes were closed with end caps and filled with water. The pipes were then pressurized to approximately 50% of the predicted burst pressure and inspected for leaks. Finally, water is pumped at a rate of 0.006 cubic meters per hour until failure point.
- *Photographic records:* The failure location was photographed and the initiation point of failure was identified. The initiation site was determined based on localized necking through the wall thickness, bulging of the pipe material and the fracture surface. Some selected photos are attached in Appendix D.

4.4 Instrumentation

The main devices used to record the data and to monitor the test samples during burst testing are the strain gauges, pressure transducers, thermocouples and CCTV cameras. The objective of each device and the device setup are briefly discussed in the following sections.

4.4.1 Strain gauges

In each burst test sample six strain gauges were attached and a multiple channel data acquisition (data logger) to record the strain at different locations along the test sample. The pictorial representation of the strain gauges layout in reference to the simulated flat-bottomed defect is shown in Figure 4.3. The symmetry of the simulated defects on the test samples was exploited to limit the number of strain gauges to six. Details of dimensional description of the placement of strain gauges are shown in Appendix B within the burst test samples' drawings.

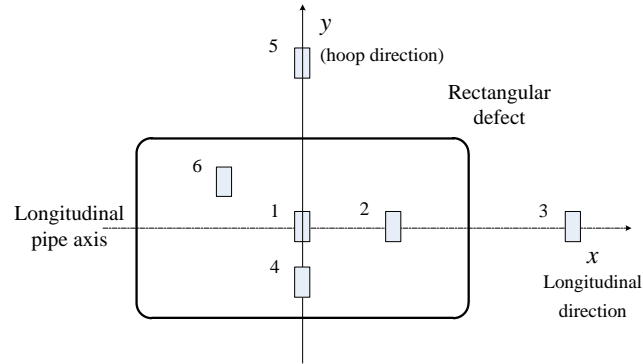


Figure 4.3 Strain gauges placement

Strain gauges, SG 1, SG 2, SG 4 and SG 6 were used to record the deformation within the defect. SG 1 was placed at the center of the defect where theoretically the maximum strain is expected. SG 2 and SG 4 were placed offset from the center of the defect towards longitudinal and circumferential directions, respectively. These strain gauges were placed in order to compare the strain propagation along transversal and circumferential direction. SG 6 is placed offset circumferentially and longitudinal in opposite quadrant to SG 2 and SG 4. In addition, SG 3 and SG 5 are attached farther from the defect in order to record the strain at intact (defect free) pipe section, which were later used for comparison purposes.

All the strain gauges used for these test were type YFLA-2 post yield single filament cross gauges allowing for large strains from Tokyo Sokki Kenkyujo co., LTD. Knowing that the maximum deformation and stress are along the hoop direction for these tests; the gauges were attached in such a way that they can record the strain in hoop direction. The strain gauges were attached using standard cement glue on a slightly grinded and polished pipe surface.

4.4.2 Pressure gauges

Two pressure gauges were used during the test. One of the gauges was installed on the burst test sample and monitored by a CCTV camera. The second pressure gauge was installed at the outlet of the water pump and the pressure increment was controlled by the use of special data logger with digital display. The display was used to monitor the injected water pressure during the test.

4.4.3 Thermocouple

A thermocouple was attached at the defect in order to record any abnormal temperature rise during yielding before rupture or burst. The display was recorded by the data logger combined within the injected water pressure gauge.

4.4.4 CCTV Cameras

While the burst test is on progress, especially when it approaches the burst point, it is not recommended for workers to cross the barrier wall. At an elevated pressure, the sample can rupture at any instant, so that pressurized water or some flying fractured metal pieces can cause harm. Therefore, CCTV cameras were used to monitor the test sample located behind the barrier wall.

4.4.5 Safety Precaution

The test samples were anchored by means of U-bolt on to saddle support. The saddle support itself was fixed to the ground by cable for further safety. Furthermore, the burst test assembly was placed behind strong barrier wall. As a result, data recording and pumping of the water were done from remote. While when test was progressing safety precaution signs were posted by the nearby vicinity of the lab. Plate 4.1 shows one of the test setup.



Plate 4.1 Sample prepared for test

4.5 Material Characterization

Since most failure prediction methods are based on stress criterion, correct material properties are required for accurate prediction of the failure pressure. The present accepted codes for failure assessment are based on the SMYS of the material, although the proposed techniques require the actual yield strength or ultimate tensile strength to predict the failure pressure of a defect [45]. The FE analysis discussed in Section 5.1 makes use of actual material properties obtained from stress-strain data of flattened circumferential tensile specimens. Fracture toughness is another material property that is generally quoted since earlier pipeline steels could experience brittle fracture [74]. Today, minimum fracture toughness limits are placed on pipeline steels based on fracture initiation and propagations considerations. Since all pipes in AGA database failed in a ductile manner, it was concluded that all of the failure criteria considered were based on a critical stress so that only the plastic material properties were required [37]. The fracture toughness was not measured for these materials.

The pipe material used in this research was a retired seamless pipe made of API 5L X52 steel. The chemical composition of the retired metal has not changed from its original form. The nominal outside diameter and the nominal wall thickness of the

pipe were, respectively, 273.1mm and 11.1mm. Eight tensile test specimens were cut and machined according to ASTM E 8M-04 standard [75]. These specimens were tested to determine the stress-strain curve, the yield strength, the ultimate tensile strength and the total strain corresponding to the ultimate tensile strength of the pipe material.

A summary of the tension test results for the transverse tensile specimens is presented in Table 4.1. The mean yield strength and the mean ultimate tensile strength were 377.7MPa and 513.4MPa, respectively. The mean yield strength is 5.5% greater than the SMYS of API 5L X52 steel ($SMYS = 358MPa$). The mean ultimate strength is 12.8% greater than the SMTS of API 5L X52 steel ($SMTS = 455MPa$). The mean value of the ratio $\sigma_U/\sigma_y = 1.36$ is greater than the ratio $SMTS/SMYS = 1.27$. The conservatism of σ_{flow} expression based on the yield strength is a function of the σ_U/σ_y ratio the greater the value of σ_U/σ_y , the greater the conservatism of σ_{flow} expression [68].

Table 4.1 Summary of tensile test results

Tensile Specimen	σ_y (MPa)	σ_U (MPa)	ε_U (%)	ε_f (%)	σ_U/σ_y
1	410.0	530.6	8.0	16.6	1.29
2	304.5	472.1	9.0	16.2	1.55
3	402.5	536.5	10.0	19.7	1.33
4	381.6	512.3	10.6	17.9	1.34
5	360.2	507.5	10.6	16.0	1.41
6	375.0	519.5	10.0	18.5	1.39
7	440.0	546.7	7.0	13.0	1.24
8	347.5	481.9	7.5	14.0	1.39
Mean	377.7	513.4	9.1	16.5	1.36

The true strain and true stress can be calculated from the engineering strain and engineering stress respectively. Assuming constant volume theory, the expression for true strain is given by Eq. (4.1) and the true stress is expressed as in Eq. (4.2). These

equations are only valid up to the point of necking where the deformation becomes localized in the tensile specimen.

$$\varepsilon_{true} = \ln(1 + \varepsilon_{eng}) \quad (4.1)$$

$$\sigma_{true} = \sigma_{eng}(1 + \varepsilon_{eng}) \quad (4.2)$$

In order to accurately predict the behavior of a corrosion defect, the material behavior, in particular the plastic behavior must be modeled appropriately. The FE method allows the material behavior to be modeled with uniaxial true stress-strain curve. The use of true stress versus true strain data allows an incremental plasticity scheme to be used which can account for strain hardening and subsequent unloading despite a significant increase in computing resources [4]. If the stresses increase monotonically and significant unloading does not occur, the stress-strain behavior of typical pipeline materials can be modeled with deformation plasticity theory using Ramberg-Osgood equation to represent the true stress-strain curve [63].

The Ramberg-Osgood equation can express the total strain as the sum of the elastic and plastic strain in terms of three parameters α , n and σ_y . The yield stress, σ_y was determined from the engineering stress and engineering strain curve using the 0.2% offset method and the constants α and n are calculated from a nonlinear regression based on the true stress-strain tensile test data. This is useful since it provides a simple means for describing the true material behavior as shown in Eq. (4.3) and Eq. (4.4).

$$\varepsilon_{total} = \varepsilon_{elastic} + \varepsilon_{plastic} \quad (4.3)$$

$$\varepsilon_{total} = \frac{\sigma}{E} + \frac{\alpha}{E} \left(\frac{|\sigma|}{\sigma_y} \right)^{n-1} \sigma \quad (4.4)$$

The stress strain curve obtained from the experiment and Ramberg-Osgood curve fitting in Eq. (4.4) is shown in Figure 4.4.

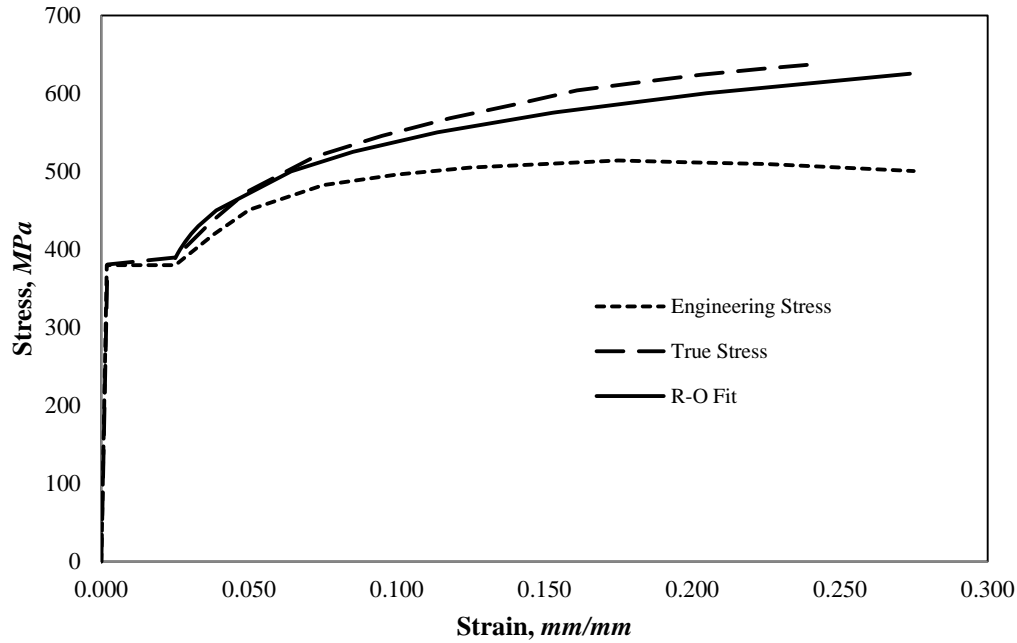


Figure 4.4 Tensile properties of the API X52 grade steel pipe material

Stress is uniquely related to strain when both increase monotonically in a simple situations such as uniaxial loading. But this relationship is not always valid in the more general three-dimensional case. A proportional increase in the deviatoric stress components with respect to the effective stress is also required for this material model to be equivalent to incremental plasticity. It was shown that the deformation plasticity is valid for simple defect shapes through experimental validation of the FE results [4].

Pipeline steels typically display anisotropic yield behavior as a result of the rolling process used to create the steel plate from which the pipe is manufactured. For the analysis of corroded pipe, it is recommended to use the material properties in the circumferential direction since this is the direction of maximum principal stress in plain pipe [38, 76]. It should be noted that at the location of failure, the stresses are found to be triaxial in nature and so the use of circumferential properties may be questioned [4]. However, the ultimate tensile strength of the material and hardening behavior are not similar in both longitudinal and circumferential directions. But, since a large degree of plasticity occurs within a corrosion defect near failure, the use of the circumferential properties is reasonable.

4.6 Burst Test Results and Discussions

Burst tests were successfully conducted for test samples T1, T2, T3 and T4. Test sample, T5 failed during machining of deep defect due to imbedded pinhole defect on the internal wall of the pipeline. The burst test results are presented in Table 4.2. When the pressure was increased, crack initiated and propagated through the ligament at the defect. Finally, the pipes exploded and the internal pressure drastically dropped to zero. The pressure increment versus the test time for the test samples are shown in Figure 4.5 and Appendix C.

Table 4.2 Summary of Burst Test Results

Test No	Average wall thickness, (<i>mm</i>)	Defect Dimensions, (<i>mm</i>)			Burst Pressure (<i>bar</i>)		
		Depth, <i>d</i>	Length, <i>L</i>	Width, <i>w</i>	Burst Test	FE Simulation	Error (%)
T1	10.87	4	200	100	326.5	316.8	3.0
T2	10.58	N.A.	N.A.	N.A.	385	368	4.4
T3	12.11	6	200	100	294.9	285.6	3.2
T4	11.94	9	200	100	Leak at 158.2	196.6	N.A
T5	11.79	10	200	100	N.A.*	143.9	N.A

*Sample failed while machining of 85% defect depth

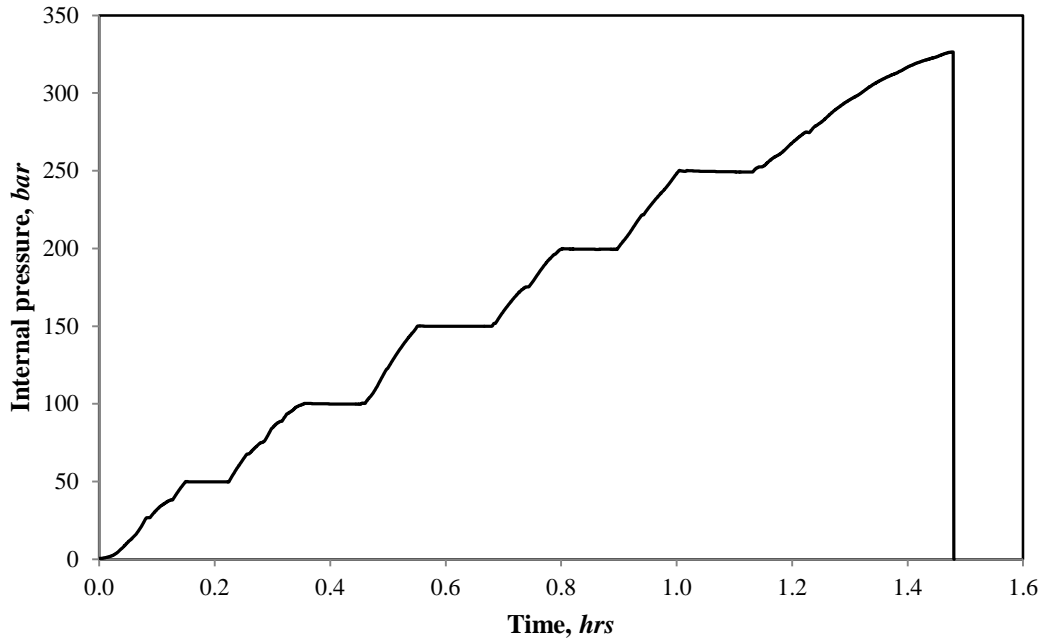


Figure 4.5 Burst test, T1

The corresponding FE burst pressure predictions for the test samples with simulated defects were also performed and the results are shown in Table 4.2. The detail of the FE approach is discussed in Section 5.5. The FE simulation results agreed with the experimental results within acceptable accuracy. Therefore, the experimental results and burst test database available in published literatures were used to validate the FE approach which is discussed in Section 6.3.

Figure 4.6 shows the total strain distribution recorded by the strain gauges for test sample T2. This sample was with general corrosion, and thus the strain was distributed over the shell with no localization. The total strain reading by all gauges increases drastically near the failure pressure. The readings keep on increasing to infinity as we can see for SG 1, SG 2, SG 4 and SG 5 or start to decline as we can see for SG 3 and SG 6. Practically, the total strain can't exceed beyond the maximum allowable strain at failure of the material. The abrupt increment of the strain gauge reading implies that the gauge itself was broken (cut), therefore, only the reading up to the allowable critical strain shall be considered. On the other hand, the readings start to decline due to failure of strain gauge bonding cement.

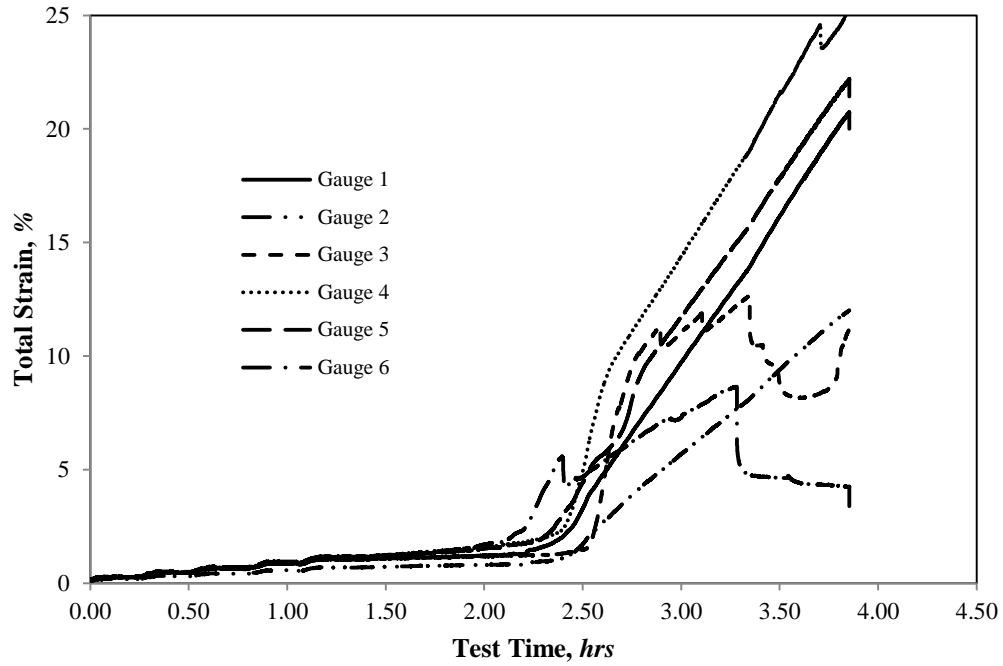


Figure 4.6 Total strain distribution, T2

Figure 4.7 show the total strain distribution recorded by the strain gauges for the test samples T1. Additional results for the remaining samples are shown in Appendix C. In all tests large strain was recorded at the defect zone. But, away from the defect zone, the strain was insignificant (very small elastic deformation). The total strain reading by the strain gauges within the defect zone (SG 1, SG 2, SG 4 and SG 6) in the vicinity of the failures showed significant amount of plastic deformation. The reading from strain gauge away from the defect (SG 3 and SG 5) showed very small (negligible) reading. As a result, it justified that stress is localized in the defect.

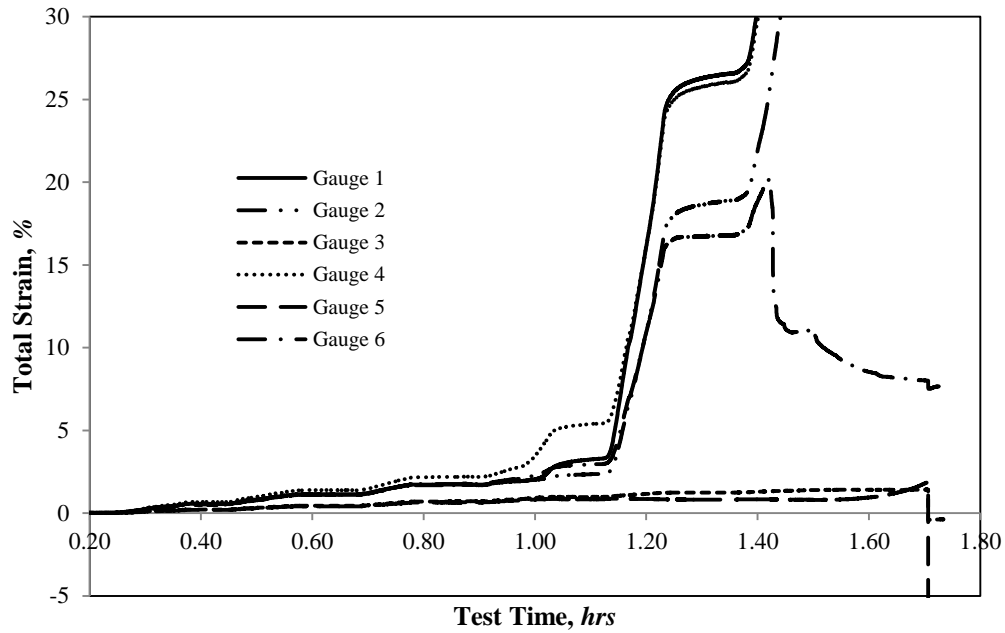


Figure 4.7 Total strain distribution, T1

When the pressure increases, bulging deformation around the defect area occurs and which is followed by a crack-like penetration in the longitudinal direction. As a result, a local wall thinning occurs in the remaining net section. This local wall thinning could continue, leading to necking of the wall and failure due to void nucleation, growth and coalescence in a manner comparable to that of a tensile test specimen.

As shown in Plate 4.2, observations of ruptured corroded pipe sections in the vicinity of the failures showed significant amount of plastic deformation and localized necking which is an indication that the initial failure occurred by plastic collapse. The contours of the grain structure in the vicinity of the failure showed a significant localization of the deformations at the failure location.



(a) T2



(b) T3

Plate 4.2 Ductile failures of corroded pipe sections

4.7 Conclusion

The following conclusions are made based on the lab experiments conducted during this research work.

- Based on visual inspection of the abandoned pipes, corrosion was found to be distributed between 3 O'clock to 9 O'clock (bottom half) of the pipeline. Corrosion debris, solid precipitates and scale like deposits were also deposited along the bottom surface. Theoretically, periodic rotation of pipelines can prolong the useful life of operating pipelines. However, practically rotation of pipe sections is not easy due to attached auxiliary pipes and weld jointed segments.
- The corrosion on the external surface of the pipeline at service can be kept at minimum by a protective rubber coating and by means of sacrificial anode. However due to imperfect wrapping of new laminations after maintenance or inspection activities, the pipeline surface can be exposed to rusting by the sea water infiltration under the laminations.
- IP inspection results show the relative thickness loss of the pipeline. Thus for a reliable result, accurate nominal thickness value should be introduced into the system during the launching of the IP. According to the comparison of the IP results with UT scan, IP inspection results can be

used for integrity assessment of corroded pipelines with about 85% confidence level. The summary of our comparison showed that the minimum wall thicknesses measured by IP in these sections is only about 12.5% and the average wall thickness is about 10% less than the P-Scan measurements.

- The FE simulation results agreed with the experimental results within acceptable accuracy. Therefore, the FE simulation can be used as a complement to the burst test database in order to develop new corrosion assessment method.
- The experimental results and burst test database available in published literatures were used to validate the new method for corrosion assessment.
- The total strain reading by the strain gauges within the defect zone in the vicinity of the failures showed significant amount of plastic deformation and localized necking which is an indication that the initial failure occurred by plastic collapse. The contours of the grain structure in the vicinity of the failure showed a significant localization of the deformations at the failure location. Whereas, the reading from strain gauge away from the defect showed very small (negligible) reading. It justified that stress is localized in the defect.
- As the pressure increases, bulging deformation around the defect area occurred and was followed by a crack-like penetration in the longitudinal direction. As a result, a local wall thinning will occur in the remaining net section. This local wall thinning could continue leading to necking of the wall and failure due to void nucleation, growth and coalescence in a manner comparable to that of a tensile test specimen.
- Failure of corroded pipeline occurs due to plastic collapse as it is seen that the contours of the grain structure in the vicinity of the failure showed a significant localization of the deformations at the failure location.

CHAPTER 5

FINITE ELEMENT ANALYSIS

Modern numerical methods have enabled the modeling of realistic defect shapes and nonlinear material behavior [24]. Conventional procedures used to assess the integrity of corroded piping systems with axial defects generally employ simplified failure criteria based upon a plastic collapse failure mechanism incorporating the tensile properties of the pipe material [9]. The FE approach for simulation of various corrosion defects is presented in this chapter. A central focus is to gain insight into the effects of defect depth, defect extent and defect width on the burst strength of the pipeline. Stress-based criterion based on plastic instability analysis was used to predict the failure pressure [77]. During the simulation, nonlinearities due to plastic-deformation and large-deformation were considered.

The results of the FE analyses were used to determine the relationship between the failure pressures and characterize the defect parameters. It also forms the basis for the development of the new guideline for corroded pipelines assessment.

5.1 Nonlinear FE Analyses

A nonlinear elastic-plastic stress criterion typically provides a better prediction of safe load carrying capacity of a component. Traditional linear elastic stress classification and allowable stress criteria give only a rough estimate of failure loads because they ignore nonlinear phenomenon that occurs in components at failure. Nonlinear elastic plastic analysis accounts for the nonlinearities due to large deformation, material or combination of these in the analyses of plastic collapse load. Plastic collapse loads are defined as the maximum load where the material response is elastic-plastic which

includes the strain hardening and large displacement effects. Closed form solutions for plastic collapse loads are not readily available, so numerical techniques such as FE analyses may be used to obtain a solution. The calculated stress intensity for limit or plastic collapse loads can be compared to allowable stress intensities to determine the structural integrity of the component.

During failure simulation the pipeline materials are subjected to irreversible structural deformation due to loading beyond yielding point of the material. Therefore, the nonlinear stress-strain relationship and the changes in geometry due to large displacements require a nonlinear structural analysis. These structural nonlinearities can be classified as material nonlinearities and geometric nonlinearities.

5.1.1 Geometrical nonlinearities

Small deflection and small strain analyses assume that displacements are small enough that the resulting stiffness changes are insignificant. In contrast, large strain analyses account for the stiffness changes result from the changes in elements' shape and orientation. Large deformations are associated with the necessity to update the coordinates of the node locations. Therefore, during the simulation the large strain effects were activated. The large strain procedure places no theoretical limit on the total rotation or strain experienced by an element. Certain ANSYS® element types will be subjected to practical limitation on total strain [78]. However, the procedure requires that strain increments must be restricted to maintain accuracy. Thus, the total load should be divided into smaller steps and to be applied incrementally step-by-step up to the failure point.

5.1.2 Material Nonlinearities

Material nonlinearities arise from the presence of time-independent behavior, such as plasticity in the case of pipelines. To predict the behavior of a corrosion defect, the material behavior, in particular the plastic behavior must be modeled accurately. The FE model allows the material behavior to be modeled with a uniaxial true stress-strain

curve as shown in Figure 4.4 (refer section 4.5). The use of true-stress versus true-strain data allows an incremental plasticity scheme to be used which can account for strain hardening and subsequent unloading, but requires a significant increase in computing resources [79]. If the stresses increase monotonically and significant unloading doesn't occur, the stress-strain behavior of typical pipeline materials can be modeled with deformation plasticity theory using the Ramberg-Osgood equation.

ANSYS® offers a wide variety of nonlinear material behavior models, including nonlinear elasticity, hyperelasticity, viscoelasticity, plasticity, viscoplasticity, creep, swelling, and shape memory alloys. Several of these nonlinear material models can be specified in a combined fashion (an exhaustive list of models that can be combined is given in the ANSYS® Structural Analysis Guide). In this research, the material properties for the simulation are assumed as *multilinear kinematic hardening material model* from the ANSYS® materials list.

5.2 FE Analysis Procedures

The solution to the nonlinear governing equations can be achieved through an incremental approach. The solution is constructed by taking a series of linear steps in the appropriate direction in order to closely approximate the exact solution. The nonlinear problems were solved by using the Newton-Raphson (N-R) method, which involves an iterative procedure. The incremental form of the governing equations can be written as shown in Eq. (5.1) [80].

$$K(u)\Delta u = \Delta P \quad (5.1)$$

This method starts with assumed solution (Eq. (5.2)) to determine the magnitude of the increment (Eq. (5.3)) and the corresponding out-of-balance load vector (Eq. (5.4)), which is the difference between the applied loads and the loads evaluated based on the assumed solution.

$$\mathbf{u} = \mathbf{u}_i \quad (5.2)$$

$$\Delta \mathbf{u}_i = \mathbf{K}^{-1}(\mathbf{u}_i)\Delta \mathbf{P} \quad (5.3)$$

$$\Delta R_i = \Delta P - K(u_i)\Delta u_i \quad (5.4)$$

In order to satisfy the equilibrium conditions exactly, the out-of-balance load vector must be zero. However, as the nonlinear equilibrium conditions are solved approximately, a tolerance is introduced for the out-of-balance load vector in order to terminate the solution procedure. In each iteration, the N-R method computes the out-of-balance load vector and checks for convergence based on the specified tolerance. If the convergence criterion is not satisfied, the trial solution is updated and based on the calculated incremental displacements, and the next incremental solution vector is determined as shown in Eq. (5.5) and Eq. (5.6) leading to the computation of the new out-of-balance load vector as shown in Eq. (5.7).

$$u_{i+1} = u_i + \Delta u_i \quad (5.5)$$

$$\Delta u_{i+1} = K^{-1}(u_{i+1})\Delta P \quad (5.6)$$

$$\Delta R_{i+1} = \Delta P - K(u_{i+1})\Delta u_{i+1} \quad (5.7)$$

This procedure is repeated until convergence is accomplished. There are also options like time stepping, a bisection method and line search algorithm methods for improving the convergence.

5.3 FE Modeling

5.3.1 Coupled Degrees of Freedom

In certain engineering problems, the behavior of some of the unknown degrees of freedoms may be known. For example, certain points (nodes) may be expected to have the same displacement in a certain direction. One can take advantage of this behavior and enforce it in order to achieve an accurate solution with minimum computational resources. If a particular degree of freedom at several nodes is

expected to have the same unknown value, these degrees of freedoms can be coupled. Depending on the different forms of corrosion defects, axisymmetric idealization, plane strain idealization or 3D approaches were used to analyze the FE models.

5.3.2 Plane Strain Modeling

In a structural problem, if one of the dimensions is significantly longer than the other dimensions defining a uniform cross-sectional area, and if the structure is subjected to only uniform lateral loads, then plane strain idealization is valid. Plane strain idealization drastically reduces the number of elements to be used in the model. Therefore, utilization of plane strain idealization leads to significant savings in computational cost without loss of accuracy in the quantities of interest. Stresses in a bi-material cylindrical pressure vessel are used to demonstrate plane strain idealization.

The effect of the corrosion width on failure behavior was studied using 2D plane strain FE models as shown in Figure 5.1. Practically, such longitudinally extended groove like defects exist due to many reasons like accumulation of water in bottom part of the inner wall of the pipeline, due to sand erosion or due to fluid level mark of stratified flow at inner side walls of the pipeline. Such idealization can be reasonable for an infinite length of corrosion along the pipeline axis [38]. The corrosion widths considered range from $w/t = 1.0$ to $w/t = 25.0$. The basic dimensions and FE model are shown in Figure 5.2(a).

For this model one half of the cross-section was considered and PLANE182 elements were used for the analyses. This element is used for 2D modeling of solid structures. The element can be used as either a plane element (plane stress, plane strain or generalized plane strain) or an axisymmetric element. The element has plasticity, hyperelasticity, stress stiffening, and large strain capabilities [78]. As it is shown in Figure 5.2(b), the symmetric ends are constrained and pressure is applied to the internal surface according to the specified Substeps until failure point.

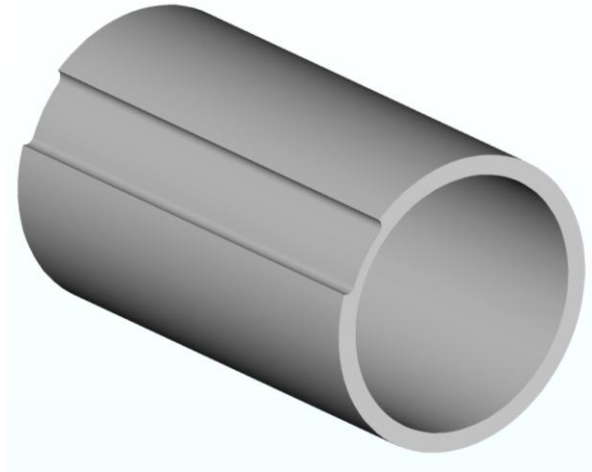
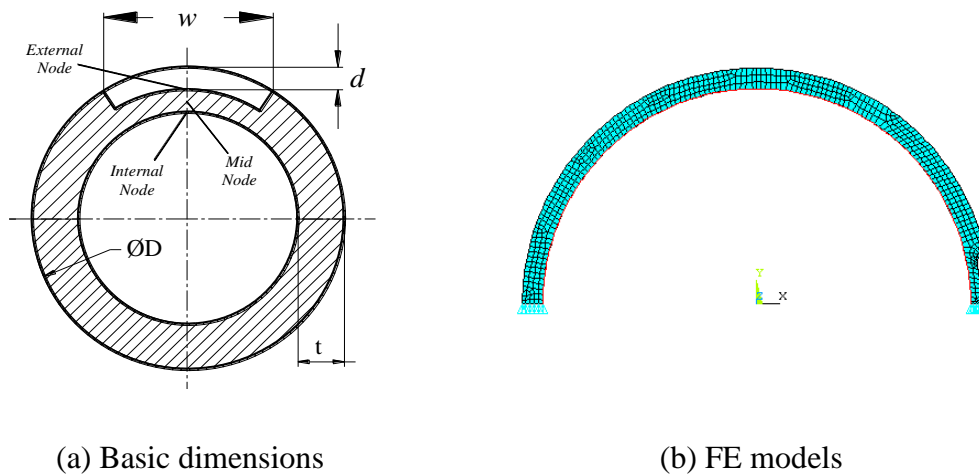


Figure 5.1 Idealized longitudinally extended slot



(a) Basic dimensions

(b) FE models

Figure 5.2 Plane strain idealization

5.3.3 Axisymmetric Modeling

In a solid of revolution, location of a point in the body can conveniently be identified by cylindrical coordinates, r , θ and z , with z being the axis of rotation. When a solid of revolution is subjected to loading that can also be obtained by revolution about the z -axis, the results become independent of θ which is called an *axisymmetric condition*. Circumferentially extended defects in pipelines as shown in Figure 5.3 can be idealized by an axisymmetric model. Practically, such defects can be present on the pipeline due to cases like girth weld defect.

In order to utilize axisymmetry, the mesh is generated on the x - z plane, as shown in Figure 5.4(a) and Figure 5.4(b). Along the left vertical boundary, the inner pressure is specified while the right vertical boundary is traction free. Based on the problem definition (long in the z -direction), it is known that the z -displacement on the x - y plane is uniform but its value is unknown. This condition is enforced by constraining the z -displacements along the bottom boundary and coupling of the z -displacements of the nodes along the top surface. Similar to plane strain model, PLANE182 elements were used for the analyses.

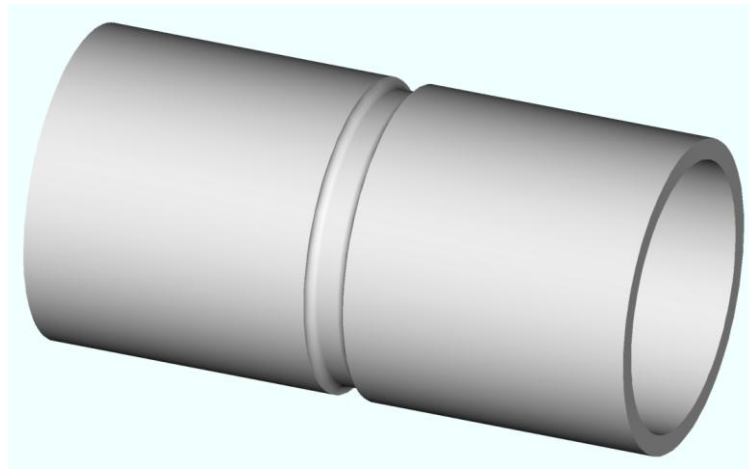
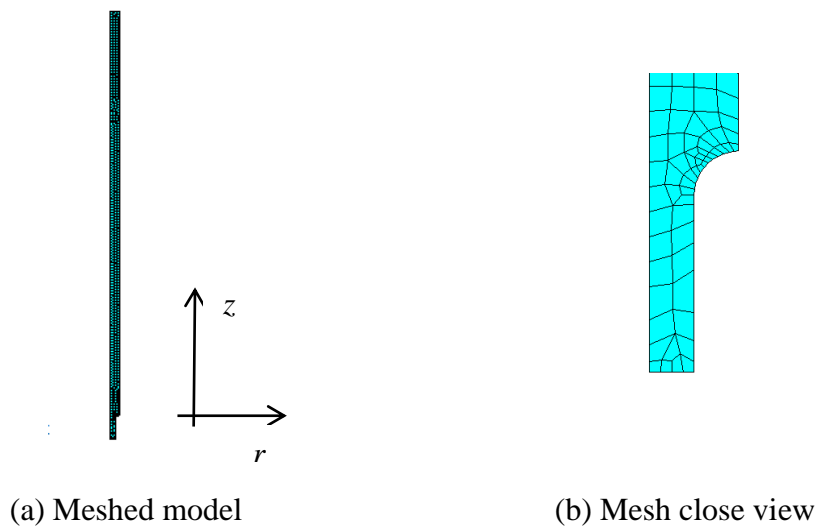


Figure 5.3 Idealized circumferentially extended groove



(a) Meshed model

(b) Mesh close view

Figure 5.4 Axisymmetric FE model

5.3.4 Flat-bottomed Rectangular Defect Modeling

An accurate application of the FE method involves two important things. These are the use of a large number of 3D solid elements in order to correctly model the corrosion geometry and the use of large displacement elastic-plastic analysis to model the material response. A patch like corrosion defects can be represented by a 3D model as shown in Figure 5.5. Taking symmetry into consideration, only one quarter of the pipe section was modeled for FE analysis as shown in Figure 5.6. At least two layers of elements were used through the remaining ligament of each corrosion defect. A higher order 8-node solid element (SOLID45) was used for analyses. This element has plasticity, creep, swelling, stress stiffening, large deflection, and large strain capabilities.

Symmetry boundary conditions were used at the cut sections and additional restraints were also applied to the models to eliminate rigid body motion. The model was extended far enough from the region of interest to ensure that end effects due to the application of the boundary conditions did not affect the results of the analyses. Internal pressure loading was applied to each model and automatically increased during the FE analysis. Pressure loads were also applied to the ends of the pipe in order to simulate the effects of end caps during the burst testing.

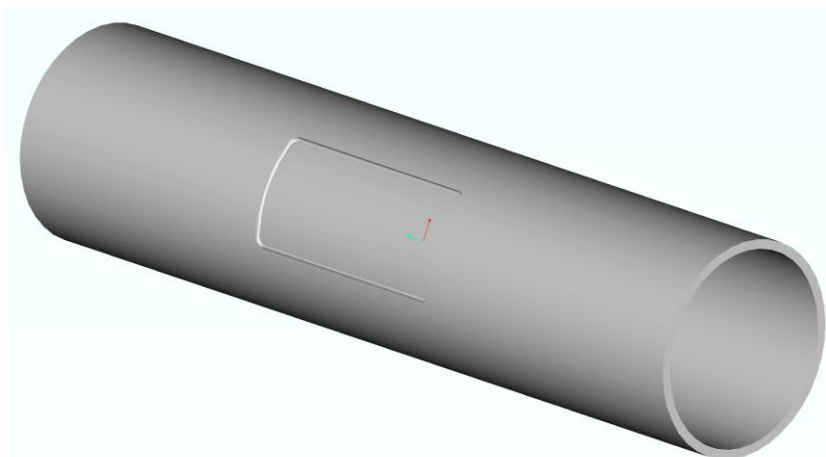


Figure 5.5 Idealized flat-bottomed rectangular defect

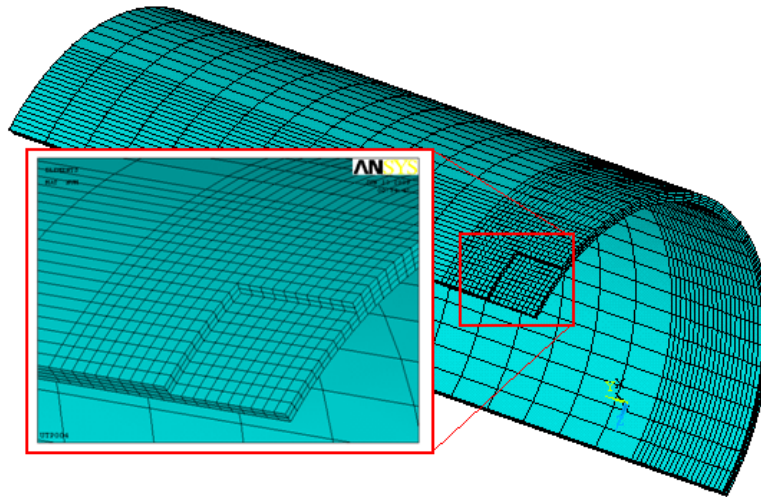


Figure 5.6 FE quarter model and mesh close view at the defect

5.4 Computational Tools for Modeling and Automatic Analysis of Defects

Even though the FE method is one of the most efficient tools to quantify reliably, FE modeling of the defects requires specific knowledge and training that are not familiarized by all pipeline engineers. Good computational models of the defect include precise representation of the geometry and generation of an appropriate mesh. This process demand an intense manual labor from the engineer and it is also slow and extremely repetitive. Therefore, it is very error prone. Normally, this process is repeated from the very beginning for each new defect to be analyzed. Thus it is a clear waste of qualified human resources if automated analyses are not used.

5.4.1 Use of Log Files

This section discusses about the computational tools developed for automatically modeling of pipes with defects, ready to be analyzed with ANSYS[®], starting from a few parameters that locate and provide the defect dimensions. This ANSYS[®] Parametric Design Language (APDL) script file is prepared based on the ANSYS[®] *Log File*. The *Log File* is an ASCII file, which is resumed immediately upon entering ANSYS[®]. Every action taken by the user is stored sequentially in this file in APDL command format. Further, the *Log File* can be utilized to understand how an analysis

was performed by another user and learn the command equivalents of the actions taken within ANSYS®. In Figure 5.7 few command lines of the script file for automatic modeling of flat-bottomed rectangular defect are shown.

```
/FILNAME, Rectangular_Defect, 0
/TITLE, 3D Model for a Flat-Bottomed Rectangular Defect

/PREP7                                ! Inter pre-processing mode

*ASK,De, Nominal Diameter of the Pipeline (mm), 274 ! Prompts for an input parameter
*ASK,t, Nominal Wall Thickness of the Pipeline (mm), 12
...
ET, 1, SOLID45                        ! Define element type and material properties
...
/SOL                                  ! Inter Solver mode
...
NSUBST, 100, 1000, 10                ! Declare loadsteps, substeps, etc
...
/POST26                              ! Inter post processing mode read and store results
...
```

Figure 5.7 Automatic defect modeling and analyses command lines

5.4.2 Solution Algorithms

There are three basic phases in order to obtain the required FE solutions. These are pre-processing phase, the solution phase and post-processing phases. The computational tools were useful while going through the phases step by step.

5.4.2.1 Pre-processing Phase

At this phase, the FE model is developed step by step according to the input pipe dimensions and defect details. The material properties are also declared at this stage and finally meshing and when necessary, refinements of the mesh were done.

5.4.2.2 Solution Phase

First at this phase, all the boundary conditions (constraints) and loads are applied. Before solving such nonlinear problems, some techniques must be employed to

improve the convergence of the solution, so that the computational time can be reduced. There are several methods used for improving the convergence (or convergence rate). For example, in ANSYS[®], there are automatic time stepping, a bisection method, and line search algorithms. The user may choose to have full control or let ANSYS[®] choose the options.

The nonlinear solution phase has three distinct levels. These are *Load Steps*, *Substeps*, and *Equilibrium Iterations*. The number of *Load Steps* is specified by the user. Different *Load Steps* must be used if the loading on the structure changes abruptly. The use of *Load Steps* also becomes necessary as we need the progressive reading at specific points in time. A solution within each load step is obtained by applying the load incrementally in *Substeps*. Within each substep, several equilibrium iterations are performed until convergence is accomplished. As the number of *Substeps* used increases, the accuracy of the solution improves. However, this also means that more computational time is being used. ANSYS[®] offers the *Automatic Time Stepping* feature to optimize the task of obtaining a solution with acceptable accuracy in a reasonable amount of time. The automatic time stepping feature decides on the number and size of *Substeps* within *Load Steps*. When using automatic time stepping, if a solution fails to converge within a sub-step, the *bisection* method is activated, which restarts the solution from the last converged sub-step.

The ANSYS[®] program has default values for all of the nonlinear *solution controls*, including the convergence options. The *SOLCONTROL* command is used to turn these defaults *on* or *off*. The help page for the *SOLCONTROL* command provides a comprehensive list of the default values of nonlinear analysis settings when solution controls are on (*SOLCONTROL, ON*), which is the default setting. It is also possible to modify specific controls while leaving the rest for ANSYS[®] to assign. To summarize, some of the commonly used commands for modifying/specifying nonlinear analysis settings with brief descriptions are:

- *AUTOTS* Command: Turns automatic time stepping *on* or *off*.
- *DELTIM* Command: Specifies time step size and/or minimum and maximum time step sizes to be used within a load step.

- *NSUBST* Command: Specifies number of Substeps and/or minimum and maximum number of Substeps to be used within a load step.
- *NEQIT* Command: Specifies maximum number of equilibrium iterations within a sub-step. If this number is reached with no converged solution, and if automatic time stepping is on, then ANSYS® employs the *bisection* method to achieve convergence. Otherwise, the solution is terminated.
- *CNVTOL* Command: Specifies convergence tolerance values for the nonlinear analyses.
- *NROPT* Command: Specifies which type of Newton-Raphson method is used in the solution.
- *LNSRCH* Command: Specifies whether a line search is to be used with the Newton-Raphson method in the solution.
- *OUTRES* Command: Specifies the amount and frequency of the data saved in the results file. By default, results associated with the last sub-step of each load step are written in the results file.

5.4.2.3 Post-processing Phase

Once the analyses results are found from the solution phase, the reading of the critical stress and strain values at the critical sections will be automatically displayed. Then interpretation of the results and their significance is investigated.

5.5 Mesh Convergence Study

The most critical and sensitive location of the mesh is at the corrosion ligament. Therefore, mesh convergence was studied by taking various numbers of elements at the ligament. The convergence versus different number of elements is shown in Figure 5.8. When the number of elements through the ligament increased, the convergence was decreased but the computing time was increased tremendously.

Therefore, it is essential to use the minimum number of elements with an acceptable accuracy. However, the relative error for just two elements along the ligament was $\pm 0.20\%$, which is precise enough for our calculation. Thus, the number of elements in the ligament is limited to two in our modeling afterwards. For some exceptional cases, where the defect is small, up to four elements were used along the ligament.

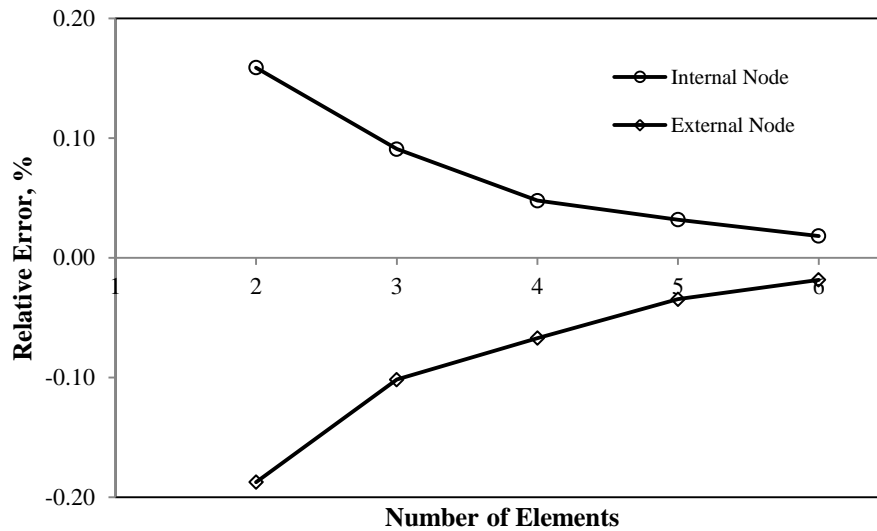


Figure 5.8 Convergence of mesh number in the ligament

5.6 Failure Analyses

Failure may be defined as a certain limit above which material fails. It may occur as a fracture, excessive deformation or when an arbitrary set value of stress, strain or energy is reached. Corrosion defects are relatively smooth and pipe materials are generally tough. Therefore, the failure of the corrosion defect is usually by plastic collapse of the defect ligament as opposed to low ductile fracture [4]. Observations of the corroded material in the vicinity of the failures showed a significant amount of plastic deformation and localized necking indicating that the initial failure occurred by plastic collapse. The contours of the grain structure in the vicinity of the failure show a significant localization of the deformations at the failure location (Refer section 4.6).

5.6.1 Failure Criteria

FE analysis of the pipe with corrosion defects does not predict the failure pressure of the pipe by itself. Because the FE model used to date does not predict local instabilities, such as necking, which are usually factors for ultimate failure. Thus, there should be a defined criterion to decide the failure point during simulation. Two criteria have been proposed and are commonly in use to assess the plastic collapse of a corrosion defect using the FE method. These are strain-based criterion and two criterion approach (stress-based or instability-based).

5.6.1.1 Strain-based Criterion

This criterion was proposed by Mok *et al.* [38] and the criterion predicts plastic collapse to occur when the gradient of plastic strain through the entire ligament becomes constant and the plastic strain increases asymptotically. It has been found that this occurs at the deepest point in the corrosion defect for simple corrosion geometries. Failure initiates on the outside surface of the pipe when the corrosion defect is located on the outside of the pipe [21].

5.6.1.2 Stress-based or Instability-based Criterion

This second criterion for predicting plastic collapse and necking is actually a two criterion approach which is stress-based or instability-based [4]. These approaches involve the determination of a critical stress or strain value from stress-strain relationship of the material. The critical stress is defined as the ultimate tensile strength on the true stress-strain curve. Plastic collapse is predicted to occur when the equivalent stress exceeded the critical stress through the entire thickness of the ligament. Among the different failure theories ANSYS[®] uses the von Mises (distortion energy) theory. Therefore, for pipe calculation it is more convenient to use this theory with cylindrical coordinates, where stress components are combined into one effective stress as shown in Eq. (5.8).

$$\sigma_e = \frac{1}{2} \sqrt{(\sigma_\theta - \sigma_r)^2 + (\sigma_\theta - \sigma_L)^2 + (\sigma_r - \sigma_L)^2} \quad (5.8)$$

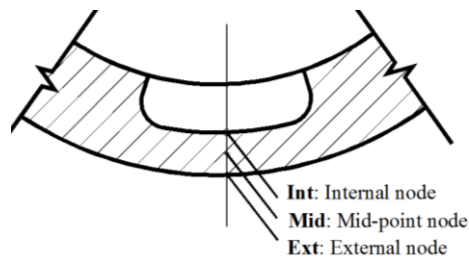
A similar approach was taken for the critical strain criterion which used the strain at necking. It was found that a great deal of scatter existed for the strain-based approach [4]. An investigation by BG concluded that the strain-based approach typically overestimates the failure pressure. A critical stress is based on the true von Mises stress at the point of necking increase the accuracy of the results [21].

5.6.2 Failure Prediction

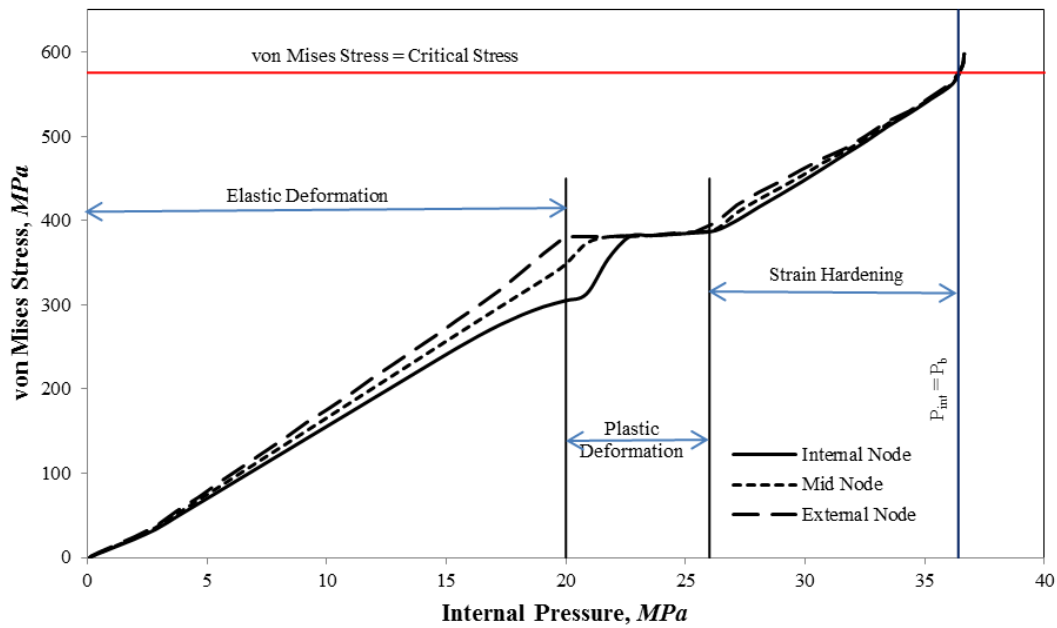
In order to demonstrate the theories discussed in Section 5.5.1, a step-by-step FE analysis for three different types of corrosion models are shown in the following sections. In all cases, variation of local von Mises stress through the corrosion ligament exhibits three distinct stages as the internal pressure increases before a numerical instability occurs as shown in Figure 5.9 (a) and (b). These are identified as the elastic deformation, the plastic deformation and the material hardening stage.

- *The elastic deformation stage:* a linear response progressing throughout the ligament until the plastic limit is reached
- *The plastic deformation stage:* after the stress state at the corrosion bottom exceeds the materials yield strength, the plasticity spreads through the remaining ligament until the plasticity reaches the opposite wall surface. In this stage, as shown in Figure 5.9 (b), when the external surface started to yield, the external surface still deformed elastically. Once the plasticity spread to propagate to the opposite surface, the material hardening stage will continue. In this stage, the von Mises equivalent stress increases slowly because of the constraint of the surrounding pipe wall. During the burst test, this phenomenon was manifested in the form of permanent deformation in the form of bulging at the defect (refer section 4.6).
- *The material hardening stage:* the whole of the ligament deforms plastically but failure does not occur because of material work hardening.

Finally failure occurred when the minimum von Mises equivalent stress in the ligament was equal to the true ultimate tensile strength of the material. At this stage, as shown in Figure 5.10, the plastic strain increases drastically by which it confirms structural instability.



(a) Node locations along the defect ligament



(b) Stages of deformations

Figure 5.9 von Mises stress distribution through the ligament

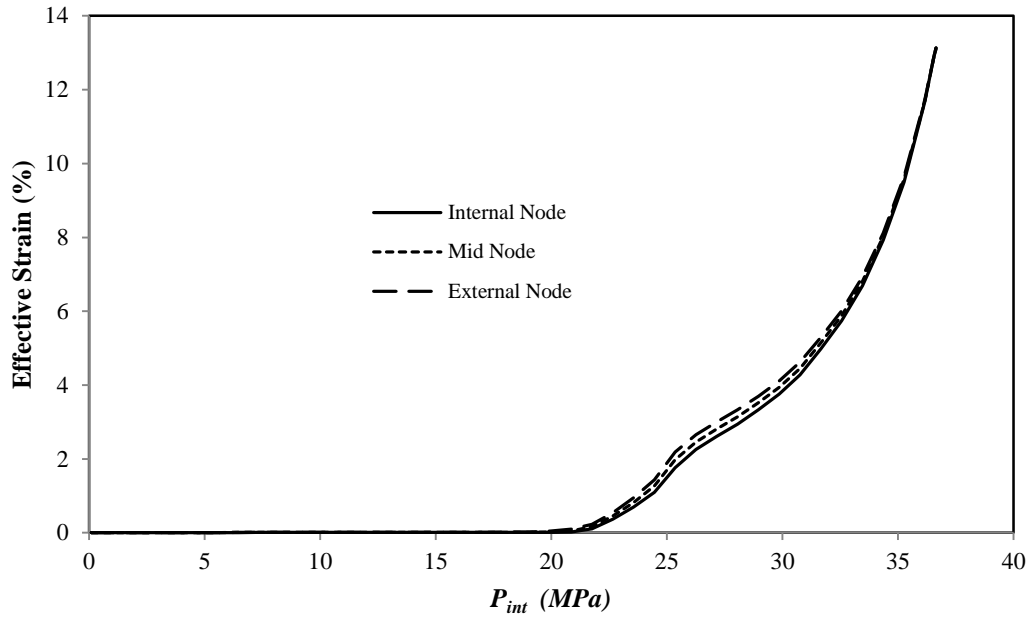


Figure 5.10 von Mises plastic strain distribution through the ligament

5.6.3 Sample of FE Analyses

The von Mises total strain distribution at three points through the remaining thickness of the plane strain defect, axisymmetric defect and flat-bottomed rectangular defect models are shown in Figure 5.11, Figure 5.12 and Figure 5.13, respectively. Similar to the effective stress distribution, the strain has the same three distinct stages. During the elastic deformation stage, the strain level remains at minimum due to small amount of elastic deformation. Once the elastic point is exceeded, plastic deformation starts and the total von Mises strain keeps on increasing faster with small increment in the internal pressure.

Finally, in the material hardening stage the whole ligament deforms plastically and the strain increases in an asymptotic manner. By the strain based criteria, this asymptotic pressure value is considered as the burst pressure. But, obviously the strain value is limited to some finite value. As verified by the tensile test in section 4.5, at the burst point, the strain value was recorded on average about 11%. Therefore, as the strain-based criteria gives over prediction, we chose the stress-based or instability-based criteria to decide the failure pressure.

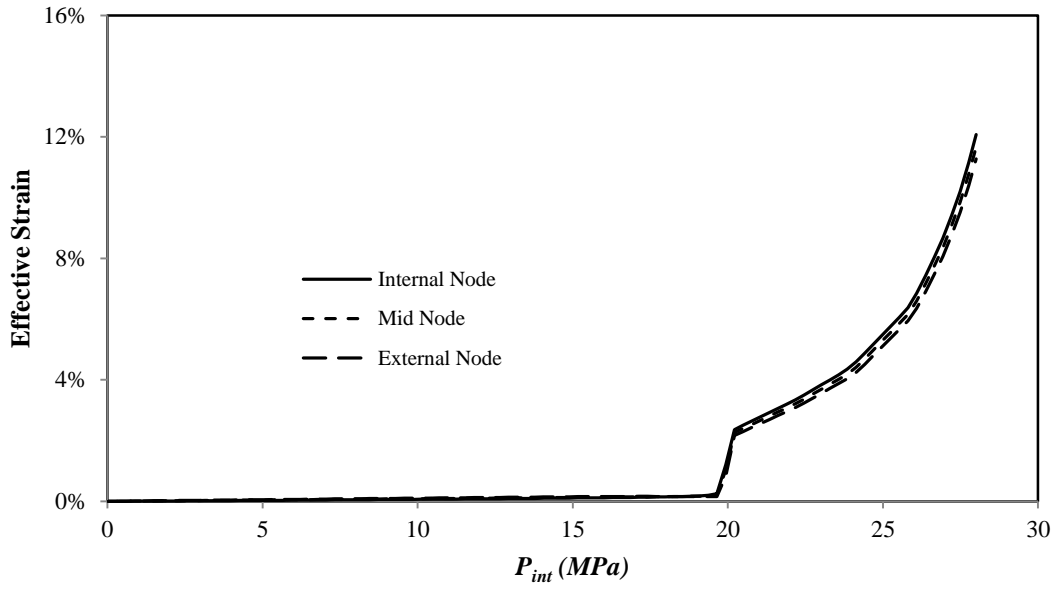


Figure 5.11 von Mises plastic strain distribution through the longitudinal slot

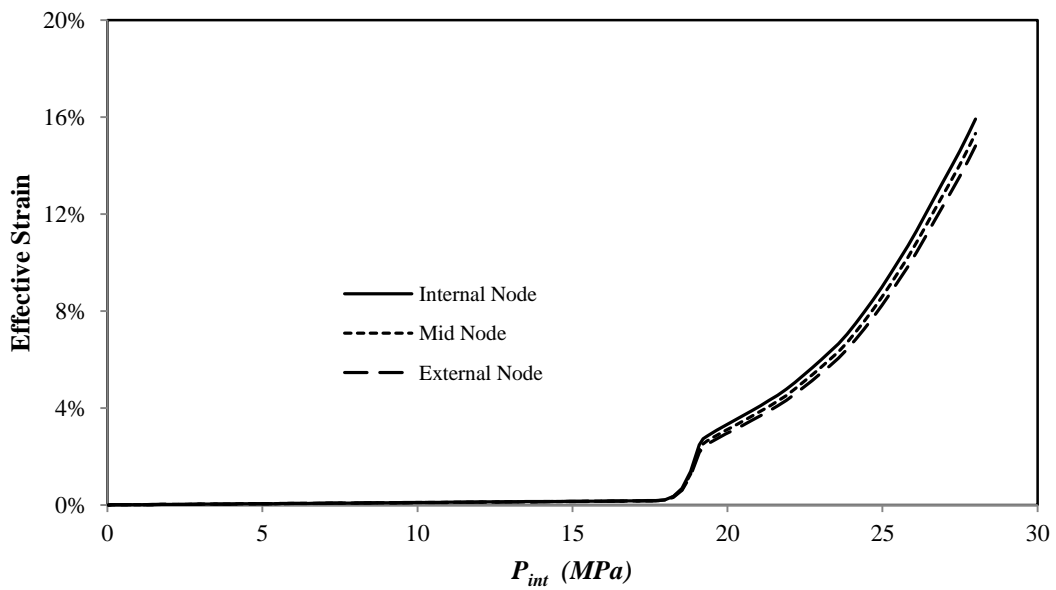


Figure 5.12 von Mises plastic strain distribution through the circumferential groove

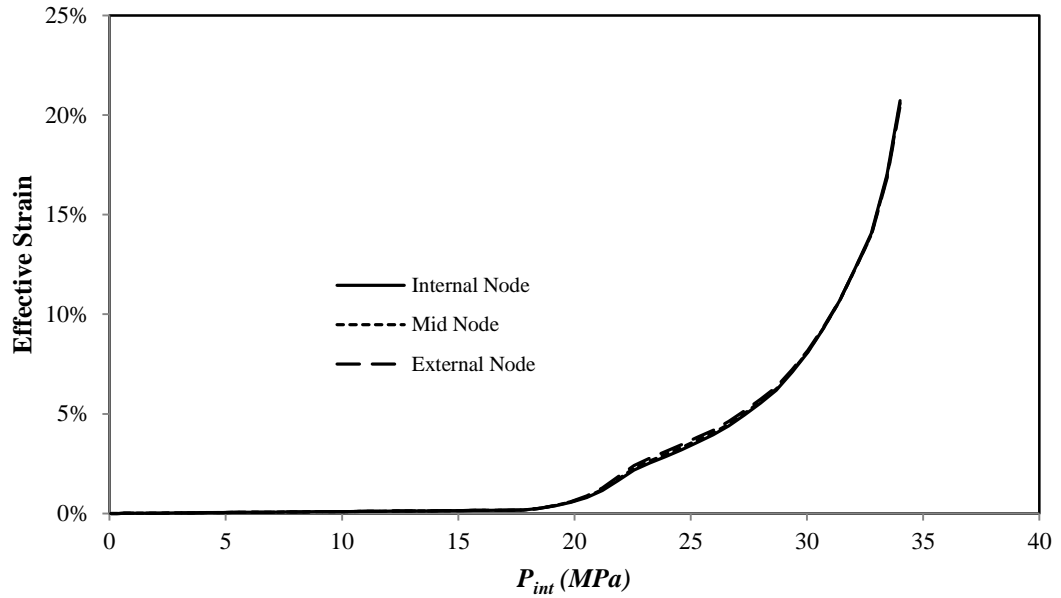


Figure 5.13 von Mises plastic strain distribution through the rectangular defect

The von Mises total stress distribution at three points through the remaining thickness of plane strain defect model, axisymmetric defect model and flat-bottomed rectangular defect models are also shown in Figure 5.14, Figure 5.15 and Figure 5.16, respectively. As discussed in section 5.5.2, the stress distribution showed the three distinctive stages for all types of models. Unlike the flat-bottomed rectangular defect, the plastic stage in the case of plane strain and axisymmetric models were very short plastic deformation stage (short transition). This was basically due to the resistance of surrounding material to plasticity spreading in the ligament. Once plastic stage is reached at corrosion bottom, it will spread faster to the opposite wall as seen for the axisymmetric and plane strain models.

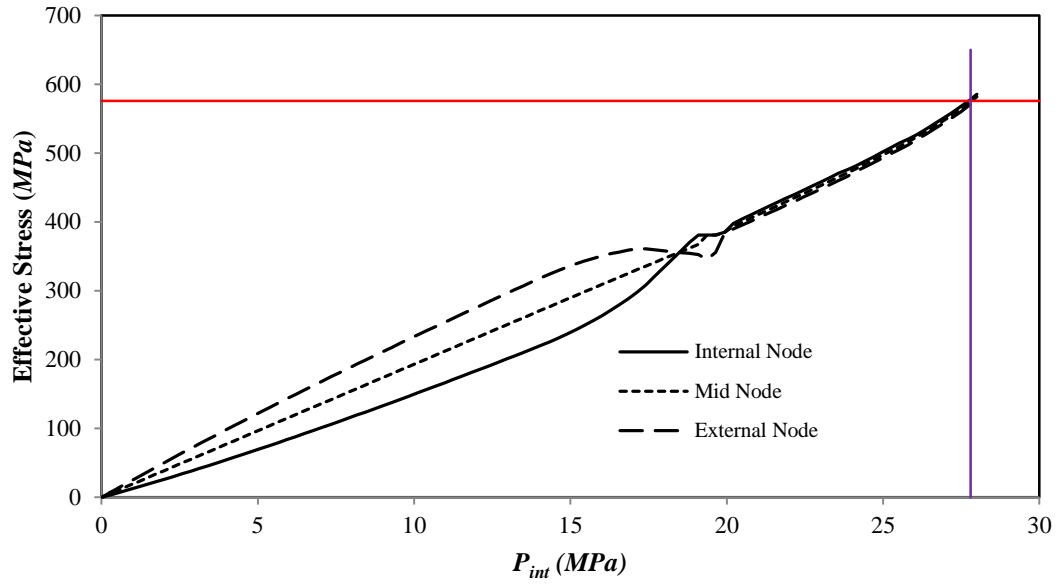


Figure 5.14 von Mises stress distribution through the longitudinal slot

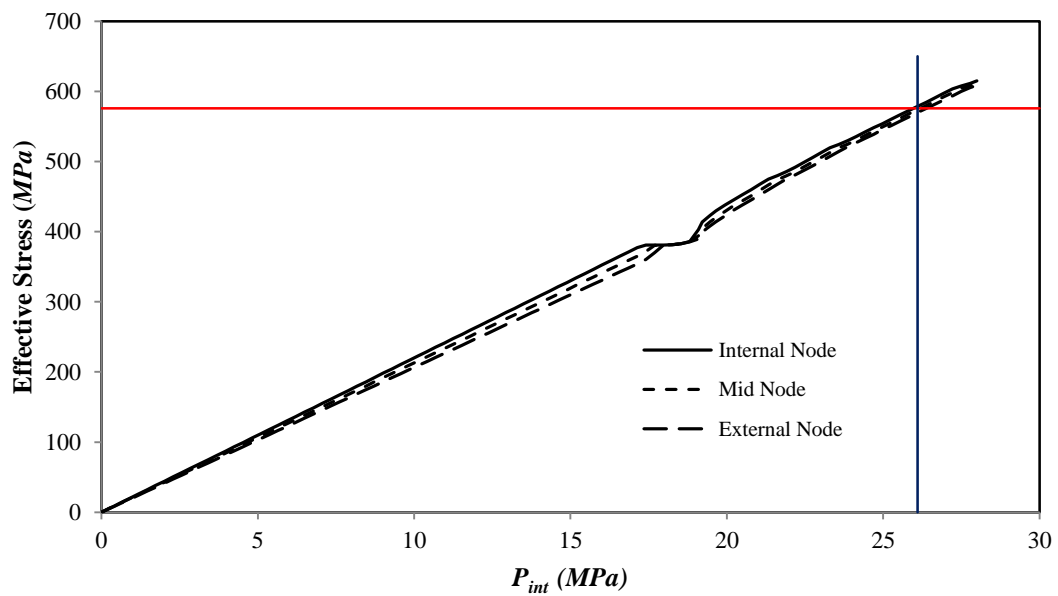


Figure 5.15 von Mises stress distribution through the circumferential groove

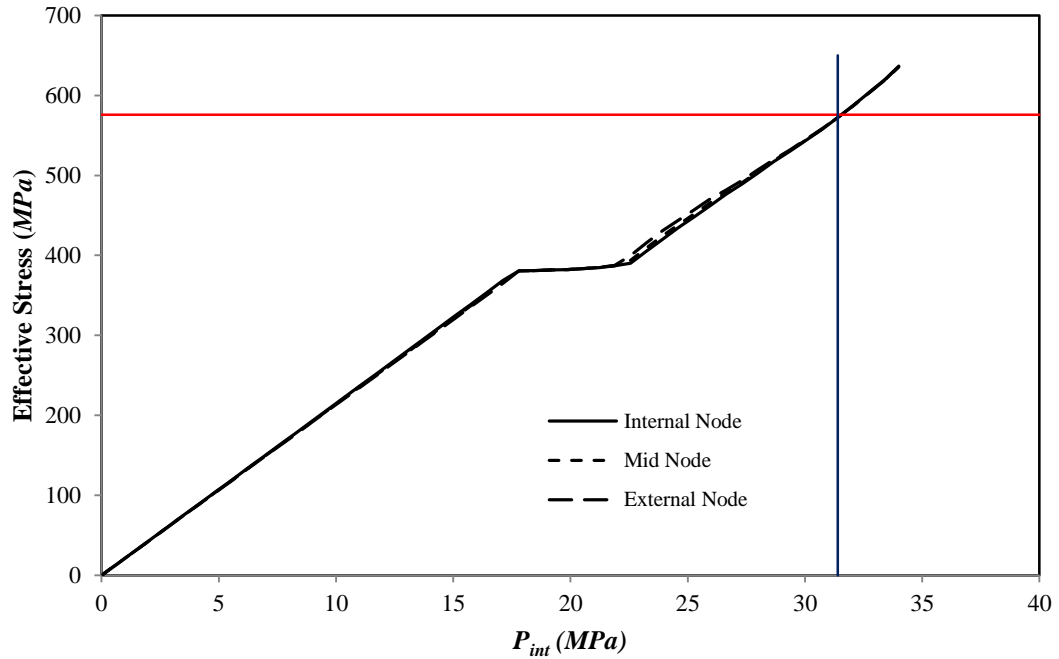


Figure 5.16 von Mises stress distribution through the rectangular defect

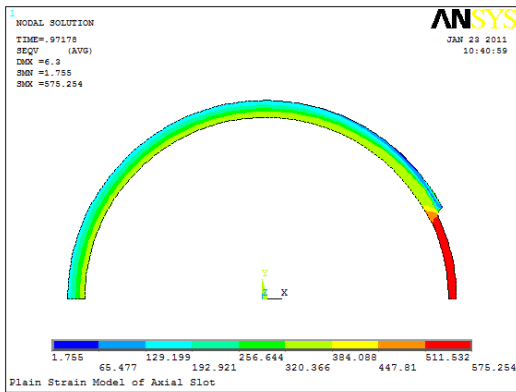
The von Mises stress fields at the defect area with increasing internal pressure near the failure point for the three models are shown in Figure 5.17, Figure 5.18 and Figure 5.19, respectively. The stress values corresponding to these figures are shown in Table 5.1, Table 5.2 and Table 5.3, respectively. The complete lists are given in Appendix E. The von Mises stress became high at the midway of the defect along the longitudinal axis and as the pressure increases, the stress zone propagated in all direction. The internal pressure, at which the von Mises stress reached the critical stress along the entire ligament, is said to be burst pressure.

For example, in Table 5.1 at substep (c) the stress distribution in the internal node just reached the critical stress and further propagating to the external node. But in substep (d), the stress through the whole ligament exceeded the critical stress. This shows that the pressure that can cause burst is between these substeps. Therefore, the failure pressure point can be determined by linear interpolation between upper and lower load steps (shown in italic shade font in Table 5.1).

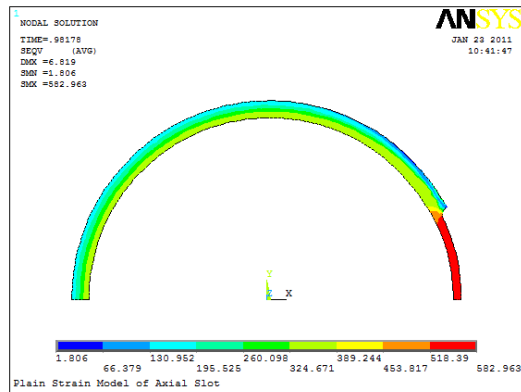
Table 5.1 von Mises stress near burst point in axial groove

Load Substeps	P_{int} (MPa)	Internal Node		Mid Node		External Node	
		ϵ_{int}	σ_{int} (MPa)	ϵ_{mid}	σ_{mid} (MPa)	ϵ_{ext}	σ_{ext} (MPa)

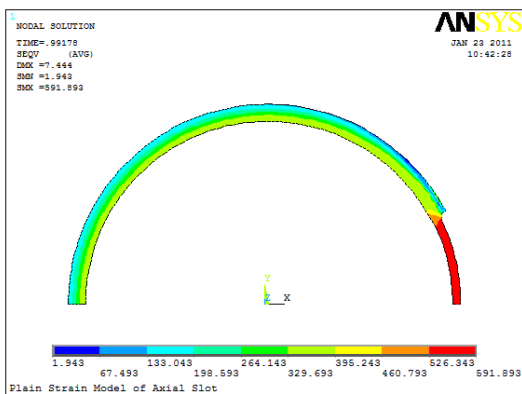
a	27.21	0.094018	558.82	0.090752	555.13	0.087565	551.53
b	27.49	0.101970	567.79	0.098517	563.89	0.095149	560.09
c	27.77	0.111596	576.83	0.107755	573.24	0.104013	569.75
d	28.00	0.120732	585.36	0.116666	581.56	0.112721	577.88



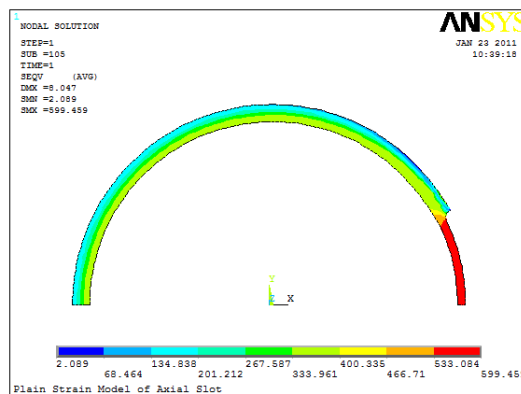
(a) $P_{int} = 27.21$ MPa



(b) $P_{int} = 27.49$ MPa



(c) $P_{int} = 27.77$ MPa



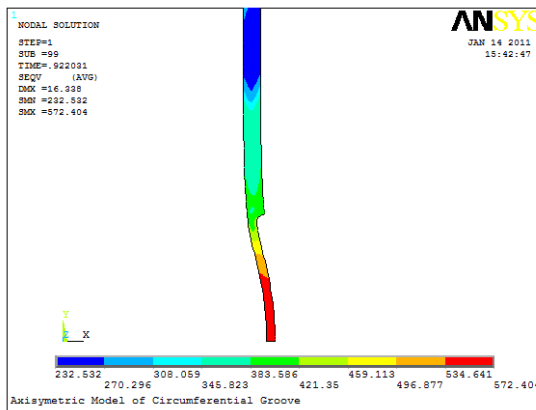
(d) $P_{int} = 28.00$ MPa

Figure 5.17 The variation of von Mises stress through the slot near failure pressure

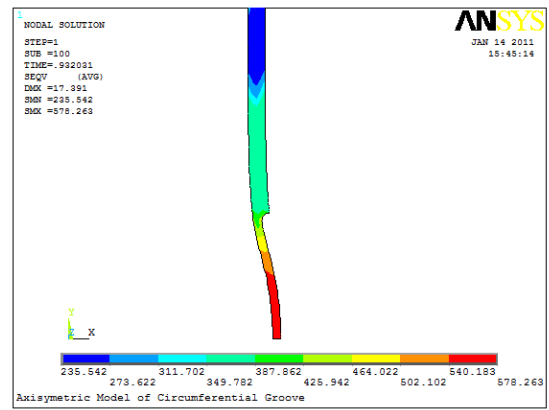
Table 5.2 von Mises stress near burst point in circumferential slot

Load Substeps	P_{int} (MPa)	Internal Node		Mid Node		External Node	
		ϵ_{int}	σ_{int} (MPa)	ϵ_{mid}	σ_{mid} (MPa)	ϵ_{ext}	σ_{ext} (MPa)

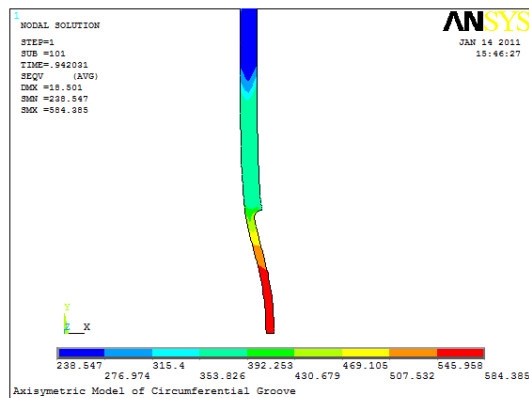
a	26.10	0.113127	578.26	0.108279	573.67	0.104224	569.95
b	26.38	0.119685	584.38	0.114664	579.63	0.110446	575.76
c	26.66	0.126298	590.84	0.121113	585.67	0.116737	581.63



(a) $P_{int} = 26.10$ MPa



(b) $P_{int} = 26.38$ MPa



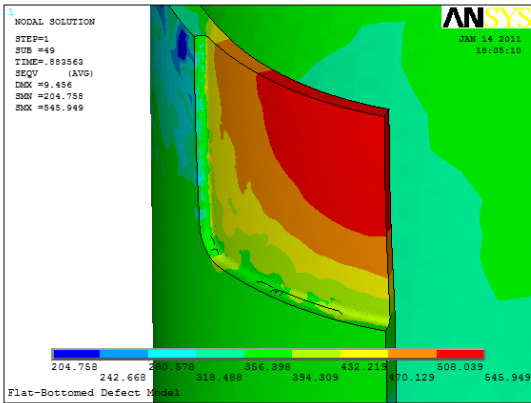
(c) $P_{int} = 26.66$ MPa

Figure 5.18 The variation of von Mises stress through the groove near failure pressure

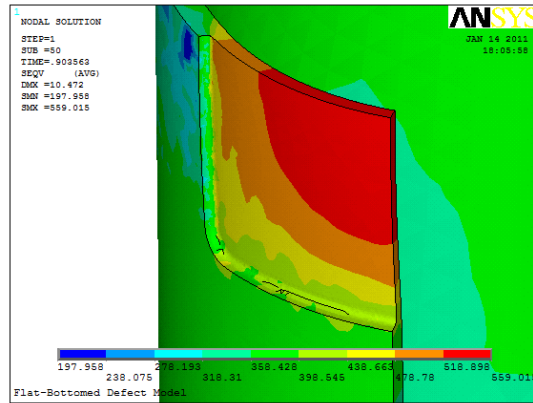
Table 5.3 von Mises stress near burst point in flat bottomed defect

Load Substeps	P_{int} (MPa)	Internal Node		Mid Node		External Node	
		ϵ_{int}	σ_{int} (MPa)	ϵ_{mid}	σ_{mid} (MPa)	ϵ_{ext}	σ_{ext} (MPa)

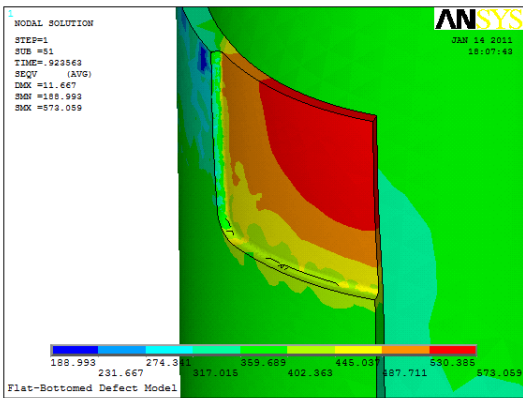
a	30.04	0.080893	543.62	0.081216	544.06	0.081905	544.93
b	30.72	0.092945	557.55	0.093084	557.71	0.093579	558.21
c	<u>31.40</u>	0.106795	572.30	0.106713	572.23	0.106973	<u>572.42</u>
d	<u>32.08</u>	0.123164	587.69	0.122814	587.35	0.122800	<u>587.28</u>



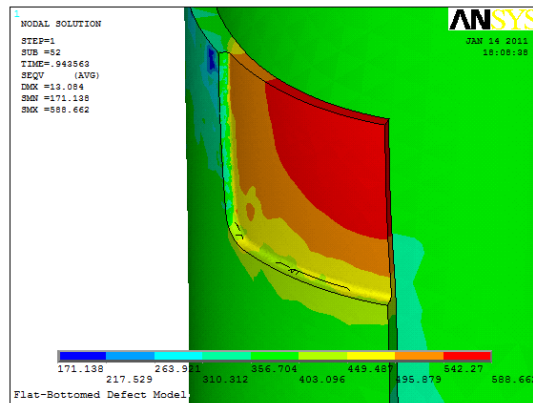
(a) $P_{int} = 30.04$ MPa



(b) $P_{int} = 30.72$ MPa



(c) $P_{int} = 31.40$ MPa



(d) $P_{int} = 32.08$ MPa

Figure 5.19 The variation of von Mises stress through the defect near failure pressure

CHAPTER 6

PARAMETRIC STUDY

The discussions in this chapter are based on a comprehensive FE analyses results from the previous chapter. First, explicit studies on the influence of each defect parameters are systematically investigated by means of parametric study. Then, the mathematical modeling for the new defect assessment method is discussed. Finally, the validation and benchmarking of the new method against the burst test database and currently available defect assessment methods are presented.

6.1 Geometric Parameters

The simulated flat-bottomed corrosion defect models were used to conduct an extensive parametric study on the influence of geometric parameters of the pipe and defects on the burst pressure on pipelines made of API X52 grade steel. The material and ranges of geometric parameters used in the analyses are given in Table 6.1.

The parameters marked in bold face in Table 6.1 were adopted as the base case. For example, in one series of analyses, D , t , d/t , and w/t were assigned to the bold values while changing L/D from 0.25 to 2.0. Similarly for another series, D , t , L/D and w/t were kept constant, and d/t was varied from 0.1 to 0.9. For the full matrix of the pipe and defect dimensions, a total of 150 FE models (51 plane strain, 45 axisymmetric and 54 flat-bottomed rectangular defect) were analyzed. Summary of the simulation results are given in Appendix F. For convenience, all the predicted values were normalized by the failure pressure of defect free according to maximum hoop stress theory as discussed in section 3.3. This normalized factor indicates the Remaining Strength Factor (RSF) of the defected pipeline and is given by Eq. (6.1).

Table 6.1 Material and geometric parameters analyzed

Material	API X52
D (mm)	274.0
t (mm)	12.0
d/t	0.1, 0.2, 0.3, 0.4, 0.5 , 0.6, 0.7, 0.8, 0.9
L/D	0.25, 0.5, 0.75, 1.0 , 1.25, 1.5, 1.75, 2.0
w/t	1, 2, 3, 4, 6 , 10, 15

$$RSF = \frac{P_b}{P_o} \text{ where, } P_o = \varphi SMTS \frac{2t}{D-t} \quad (6.1)$$

The effect of corrosion width on predicting critical pressure levels was studied using 2D plane strain FE models. The predicted RSF values versus normalized defect depth at different values of w/t for plane strain corrosion defected models are shown in Figure 6.1. The predicted RSF values are almost equal for all values of the corrosion defect for $w/t \geq 2$ and are inversely proportional with d/t . For example, the RSF value for $w/t = 15$ at $d/t = 0.6$ is only less by 0.45% from the RSF values for $w/t = 5$ at $d/t = 0.6$. For narrow defects like in the case of $w/t \leq 1$, stress concentrations develop at the corrosion bottom and the plasticity spreading stage and the post yielding hardening stage are mixed. When the highest von Mises stress value at the bottom of the defect exceeds the true stress level, the shallow corrosion models still deforms elastically. Such stress level may cause cracking. In order to establish a relevant failure criterion for such narrow defects, a fracture mechanics study is required.

Further studies on the analyses of shallow ($d/t = 0.3$), intermediate ($d/t = 0.5$) and deep ($d/t = 0.7$) plane strain corrosion defect models versus w/t are shown in Figure 6.2. As the corrosion width increases from $w/t = 2$ to $w/t = 15$, the gradient of the through thickness stress distribution at the corrosion center becomes approximately uniform and the stage of plasticity spreading reduces. Therefore, the predicted RSF values are slightly sensitive to the corrosion width when the $w/t \geq 2$.

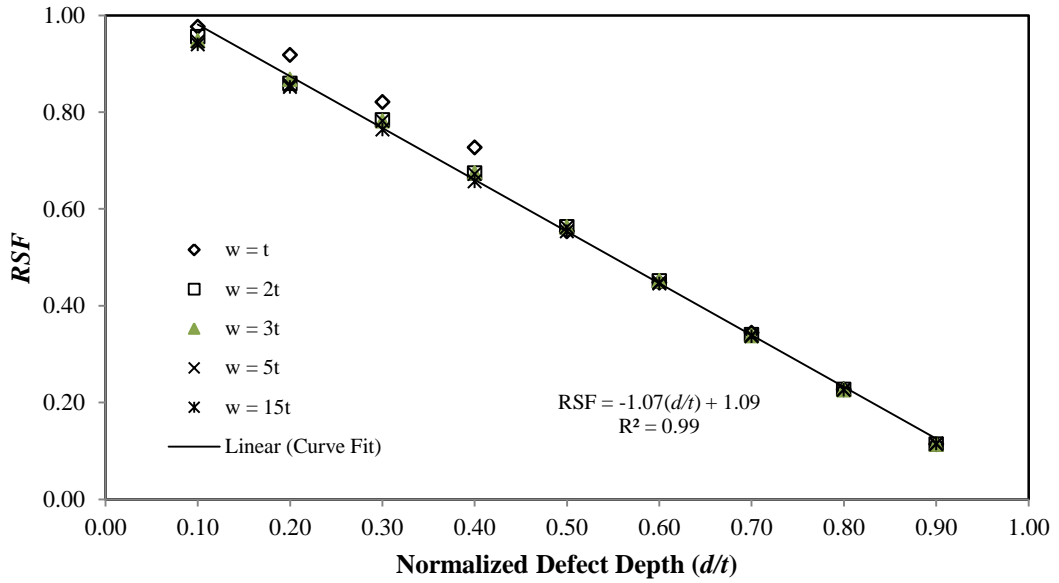


Figure 6.1 *RSF* versus defect depth for longitudinal defects

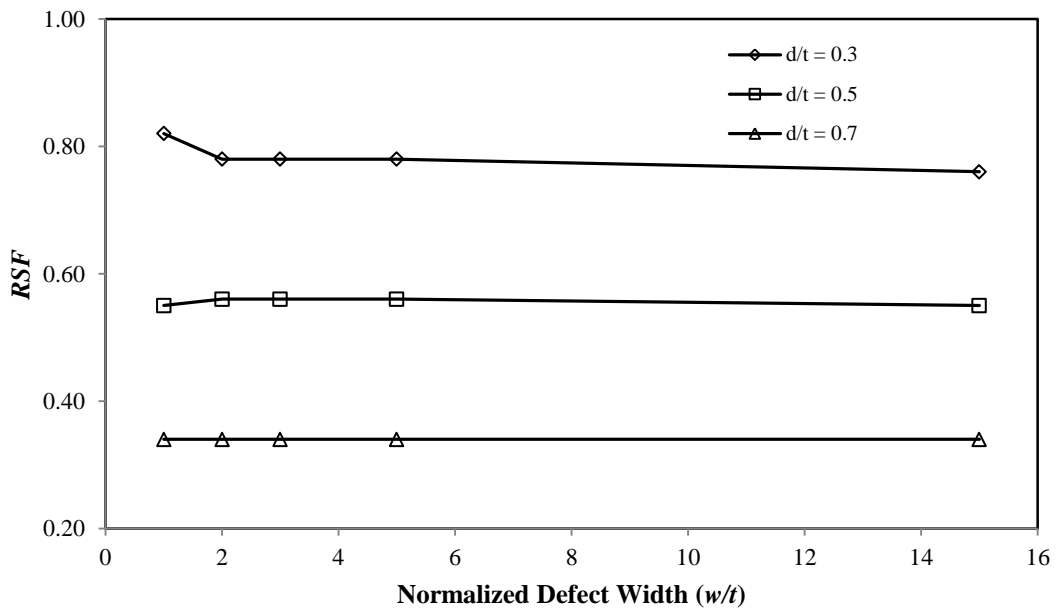


Figure 6.2 *RSF* versus defect width for longitudinal defects

Figure 6.3 and Figure 6.7 show the *RSF* values for various L/D values of axisymmetric and flat-bottomed defect models, respectively. For longer corrosion defects ($L/D > 1.0$), approximately linear, *RSF* distributions were obtained for both the axisymmetric and the flat-bottomed rectangular corrosion defect models. This type of stress distribution indicates that the local stress states are controlled by a membrane

stress and a bending moment, instead of a stress concentration. Both the membrane stress and the bending stress in the hoop direction increase. The nonlinear stress analyses shows that such stress states results in a localized bulging deformation. This implies that failure would occur in the manner of plastic collapse as the pressure load exceeds a critical level.

For shorter corrosion defects ($L/D \leq 1.0$), the RSF is no more linear with d/t values because of the stress concentration due to small localized defect. Therefore, the effects of shorter defects must be incorporated by appropriate exponential factor while developing the new method.

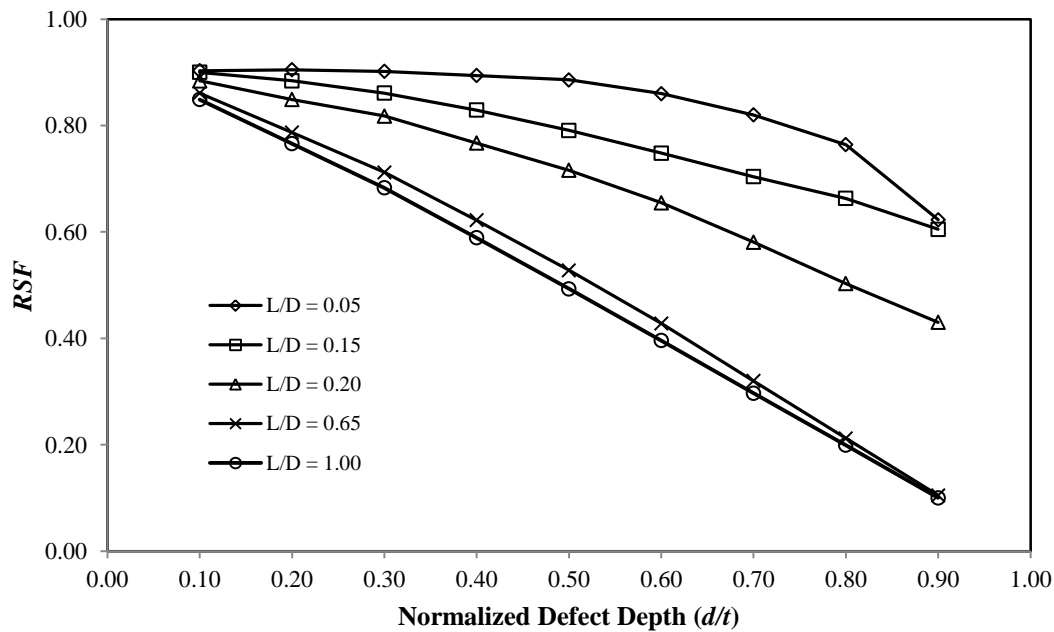


Figure 6.3 RSF versus defect depth for circumferential defects

The RSF values versus the defect length are shown in Figure 6.4 and Figure 6.6, for axisymmetric and flat-bottomed defect models, respectively. As the corrosion length decreases, the predicted critical pressure values for the shallow, intermediate and deep corrosion models increase and converge to a certain limit value. At specific values of d/t , as corrosion length increases, the predicted critical pressure values reduce to constant values. This indicates that critical pressure levels remain constant when a corrosion length exceeds a certain value, $L/D \geq 2$. Again, one can see that the depth of the defect has the strongest detrimental effect on the RSF values, but with

varied severity depending on the d/t range. For $d/t < 0.1$, the loss in the burst capacity is fairly small (within 5%). As the defect grows deeper, this effect gets much more pronounced.

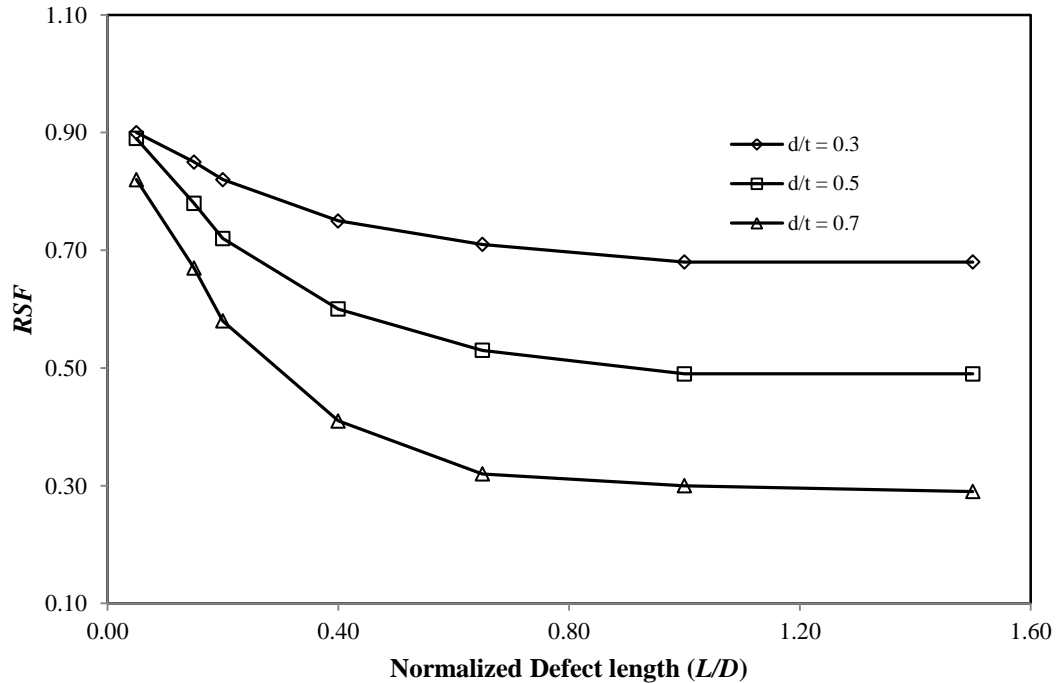


Figure 6.4 RSF versus defect length for circumferential defects

The predicted RSF values versus normalized defect depths at different values of w/t for flat-bottomed rectangular defect models are shown in Figure 6.5. Shorter defect ($L/D = 0.75$) and longer defect ($L/D = 1.50$) of the same defect depth ($d/t = 0.5$) were considered to investigate the effect of corrosion width on the RSF value. In similar manner for the plane strain models shown in Figure 6.2, as the corrosion width increases from $w/t = 2$ to $w/t = 15$, the gradient of the through thickness stress distribution at the corrosion center becomes approximately uniform and the stage of plasticity spreading reduces. Once again, it was observed that the predicted RSF values are slightly sensitive to the corrosion width when $w/t \geq 2$. Therefore, it is concluded that the corrosion width has no influence on the RSF for $w/t > 2$.

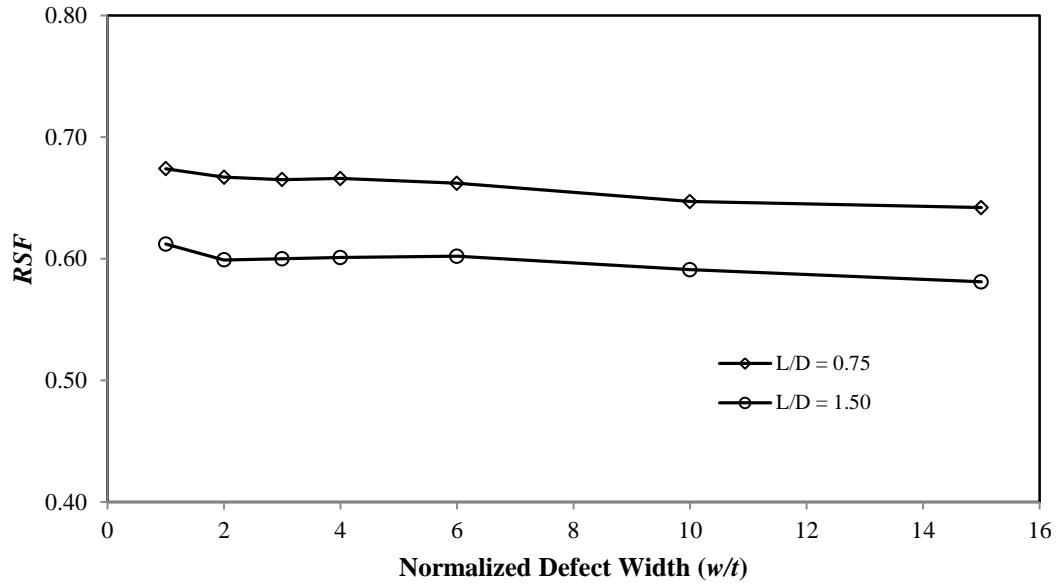


Figure 6.5 RSF versus defect width for flat-bottomed rectangular defects

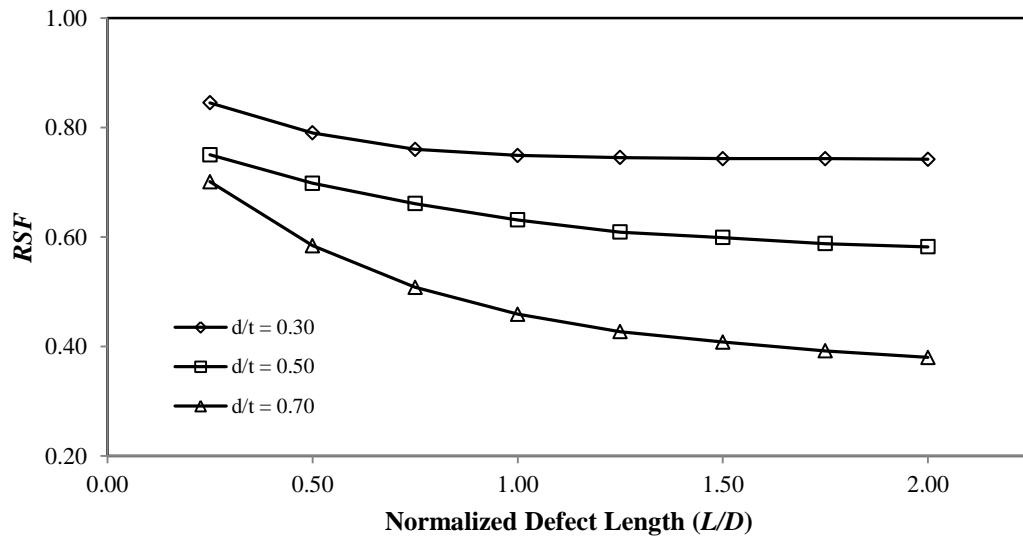


Figure 6.6 RSF versus defect length for flat-bottomed rectangular defects

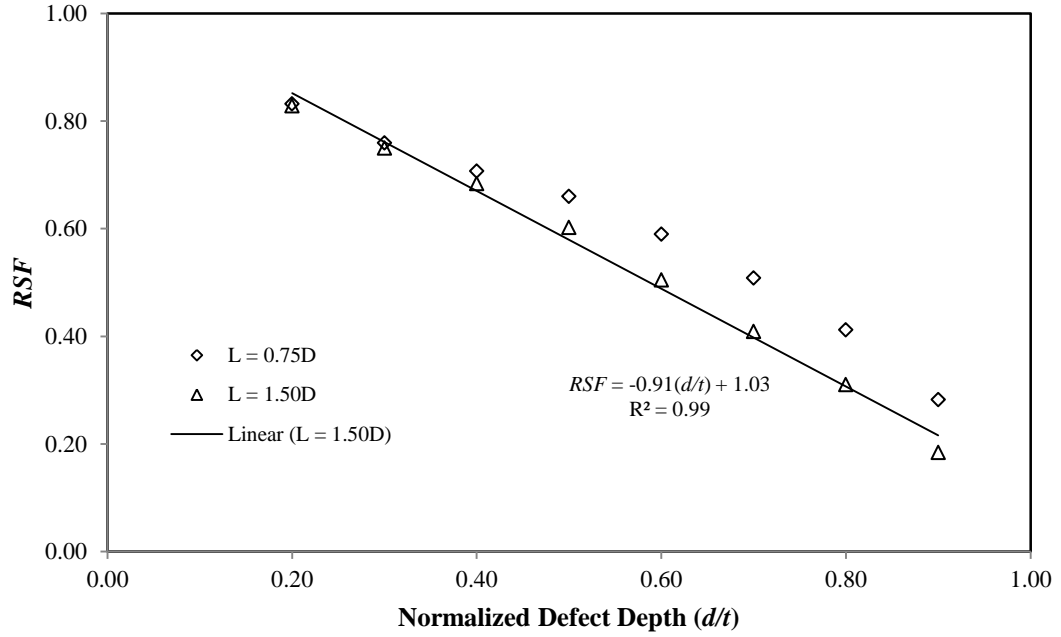


Figure 6.7 RSF versus defect depth for flat-bottomed rectangular defects

6.2 Mathematical Model

The new corrosion defect assessment code was developed based on the dimensional analysis of variables describing the defect. Dimensional analysis can provide a means of consolidating experimental, analytical, and computational results into a compact form and are an aid in designing both experiments and techniques for obtaining analytical results. Using Buckingham's Π theorem the model is formulated which states that "If there are n dependent and independent variables in a dimensionally homogeneous equation and if these variables contain m fundamental dimensions, then the variables are arranged into $(n - m)$ dimensionless terms, which are called as Π -terms" [81].

The variables which can influence the failure pressure of the defected pipe P_b , for a given defect dimensions are given in Eq. (6.2).

$$P_b = f(D, t, d, L, w, P_o) \quad (6.2)$$

Eq. (6.2) can be rewritten as:

$$f_1(P_b, D, t, d, L, w, P_o) = 0 \quad (6.3)$$

The units for each parameters described in Eq. (6.3) are given in Eq. (6.4).

$$P_b = P_o = \mathbf{M} \times \mathbf{L}^{-1} \times \mathbf{T}^{-2} \text{ and } D = t = d = L = w = \mathbf{L} \quad (6.4)$$

In Eq. (6.4), the total numbers of variables is 7 and the total number of fundamental dimensions is 3. According to Buckingham's Π theorem, the number of Π terms that can be formed is 4 ($7 - 3 = 4$). Therefore, using Buckingham's Π theorem, Eq. (6.3) can be reduced to a relationship between non-dimensional variables as shown in Eq. (6.5).

$$\frac{P_b}{P_o} = F\left(\frac{t}{D}, \frac{L}{D}, \frac{d}{D}, \frac{w}{D}\right) \quad (6.5)$$

Eq. (6.5) is simplified to the power series as shown in Eq. (6.6).

$$\frac{P_b}{P_o} = \sum_{n=0}^{\infty} A_n \left[\left(\frac{t}{D}\right)^{\alpha_1}, \left(\frac{L}{D}\right)^{\alpha_2}, \left(\frac{d}{D}\right)^{\alpha_3}, \left(\frac{w}{D}\right)^{\alpha_4} \right]^n \quad (6.6)$$

We can further simplify the expression by neglecting higher order terms ($n > 1$). On setting $A_0 = 1$, Eq. (6.6) can be simplified as shown in Eq. (6.7).

$$\frac{P_b}{P_o} \approx 1 + A_1 \left(\frac{t}{D}\right)^{\alpha_1} \left(\frac{L}{D}\right)^{\alpha_2} \left(\frac{d}{D}\right)^{\alpha_3} \left(\frac{w}{D}\right)^{\alpha_4} \quad (6.7)$$

In Eq. (6.7) can be further simplified by considering the following three points:

- The parametric factor t/D is constant and is independent of the corrosion

defect: $\left(\frac{t}{D}\right)^{\alpha_1} = k_1$, we may rearrange this expression as $D = k_1^{-\frac{1}{\alpha_1}} t = k_2 t$

- The defect depth is usually expressed as a percentage loss of the wall thickness, thus the parametric factor d/D can be expressed as:

$$\left(\frac{d}{D}\right)^{\alpha_3} = \left(\frac{d}{k_2 t}\right)^{\alpha_3} = k_3 \left(\frac{d}{t}\right)^{\alpha_3}$$

- Since the parametric study indicated little influence of the parameter w/D on P_b for $w/D \geq 2.0$, the exponent α_4 was assigned to zero. Therefore, Eq. (6.7) can be simplified and rewritten as follows.

$$RSF = \frac{P_b}{P_o} = 1 - k \left(\frac{d}{t} \right)^m \left(\frac{L}{D} \right)^n \quad (6.8)$$

The parameters in the right hand side of Eq. (6.8) are related to the defect geometry. For smaller sizes of defect depths or lengths, the RSF value is approaching 1. Therefore, as this factor is indicating the lost strength due to the defect, we may call it the Lost Strength Factor (LSF). The constants (k , m and n) in Eq. (6.8) can be determined from the curve fitting of the simulation result based on the least-squares error method. We may rearrange Eq. (6.8) to suite the iterative scheme as shown in Eq. (6.9).

$$1 - \frac{P_b}{P_o} = 1 - RSF \text{ is proportional to } \left(\frac{d}{t} \right)^m \left(\frac{L}{D} \right)^n = LSF \quad (6.9)$$

Figure 6.8 and 6.9 show the FE result plotted versus the LSF for $L/D \leq 1$ and for $1 < L/D \leq 2$, respectively. The best fits as proposed by Eq. (6.10) are best fit with correlation coefficients of 0.97 and 0.99, respectively. Therefore, the newly proposed method has the form depicted by Eq. (6.10).

If $w \geq 2t$, and $0.2 \leq d/t \leq 0.8$:

$$P_b = P_o \left[1 - 0.8 \left(\frac{d}{t} \right) \left(\frac{L}{D} \right)^{0.4} \right] \text{ for } L/D \leq 1.0, \quad (6.10a)$$

$$P_b = P_o \left[1 - 0.8 \left(\frac{d}{t} \right) \left(\frac{L}{D} \right)^{0.1} \right] \text{ for } 1.0 < L/D \leq 2.0, \quad (6.10b)$$

$$P_b = P_o \left[1 - 0.85 \left(\frac{d}{t} \right) \right] \text{ for } L/D \geq 2.0 \quad (6.10c)$$

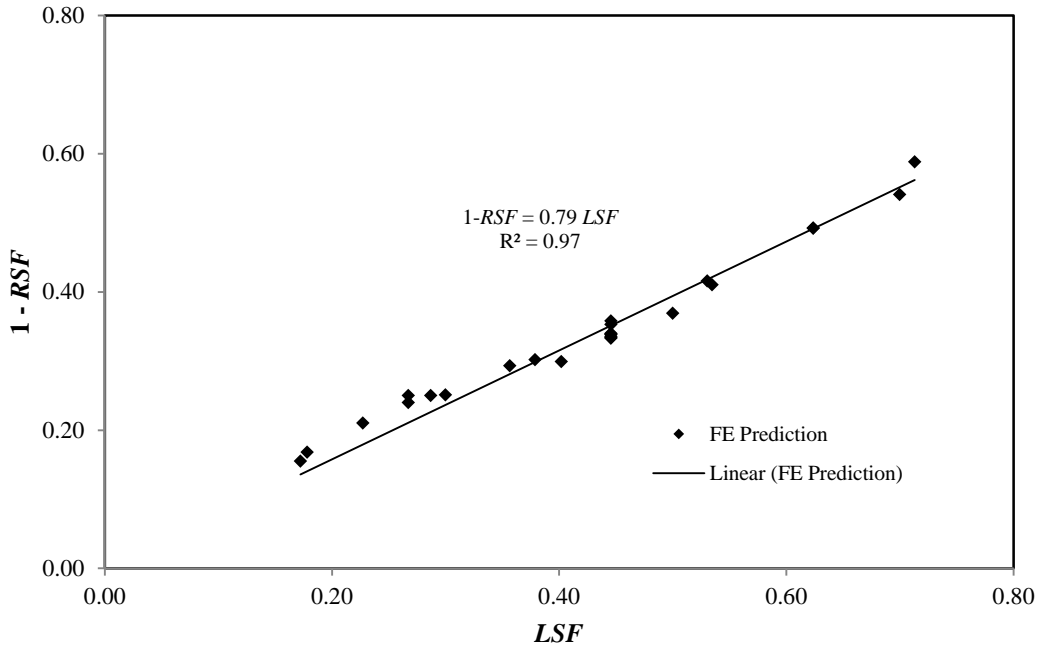


Figure 6.8 FE results versus the LSF for $L/D \leq 1$

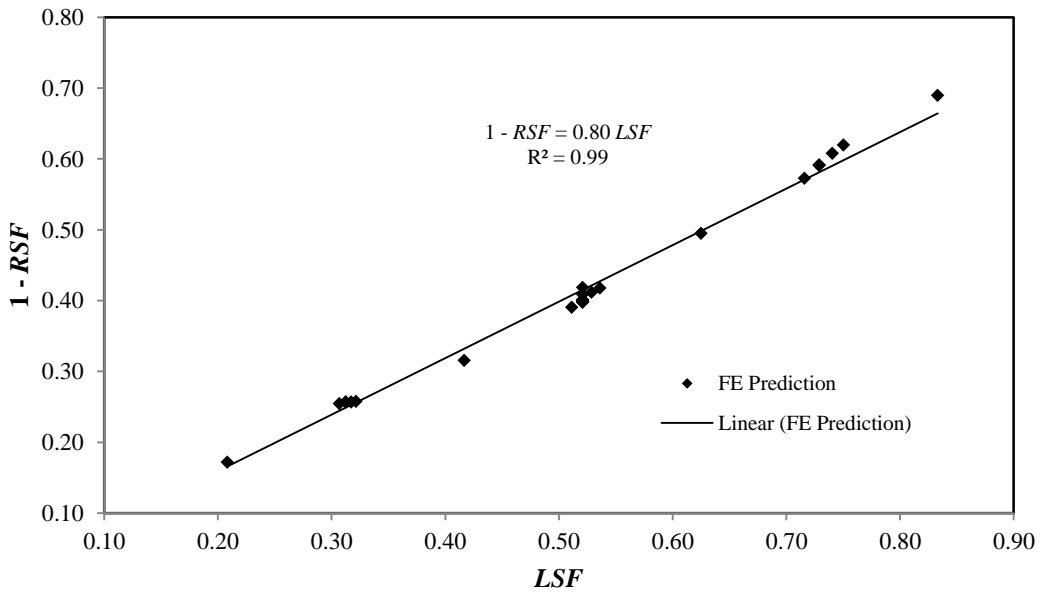


Figure 6.9 FE results versus the LSF for $1 < L/D \leq 2$

6.3 Benchmarking of the Findings

6.3.1 Comparison with the Available Methods

The comparison of *RSF* predictions by the new method (Eq. (6.10)), B31G, Modified B31G and DNV methods with the FE results are shown in Figure 6.10. This plot is helpful to see if the predictions agree with the FE simulation results. Since the new method was developed based on the curve fitting of the FE simulations, it showed excellent agreement with an average error of less than 1.0%, and standard deviation of the error less than 3%. The predictions were slightly scattered within only $\pm 5\%$ along the 1:1 line. But the comparison of the remaining three methods with the FE results provided conservative estimates and showed big scatters. The comparison of predictions by B31G code with the FE result showed an overall mean error of greater than 33% and standard deviation of the error of about 12% with some of the predictions were lower up to 56% from the FE predictions. Similarly the predictions by Modified B31G criteria showed an average error of 21% and standard deviation of the error is 3.5% with relatively minimum scatter of about 28%. The by DNV method showed mean error of 28% and standard deviation of the error of 6% with scatters of up to 43% were observed.

Figure 6.11, Figure 6.12 and Figure 6.13 show the predicted *RSF* values versus normalized defect length for a shallow ($d/t = 0.3$), an intermediate ($d/t = 0.5$) and a deep ($d/t = 0.7$) corrosion defects, respectively. The comparisons of predictions by the new method and by the three most common commercial codes (B31G, Modified B31G and DNV) were made. The variations of the predicted *RSF* are generally similar to that predicted by the codes, except that the codes gave consistently conservative estimation.

When the corrosion length reduces, the predicted *RSF* values for all defect models increases and converge to a limit value. In the case of the new model, for defect free pipe, the *RSF* converge to the ideal case, 1.0. In all cases, as the corrosion length increases, the predicted pressure values reduce to constant values. This indicates that critical pressure levels remain constant when a corrosion length exceeds a certain

value. It was observed that for L/D greater than 1.0, the gradient of the predicted RSF values are very small and as L/D is greater than 2.0, the difference in the predictions is insignificant. Therefore, increasing the pit depth or increasing the groove length of shallow defect does not significantly reduce the remaining strength of pipe.

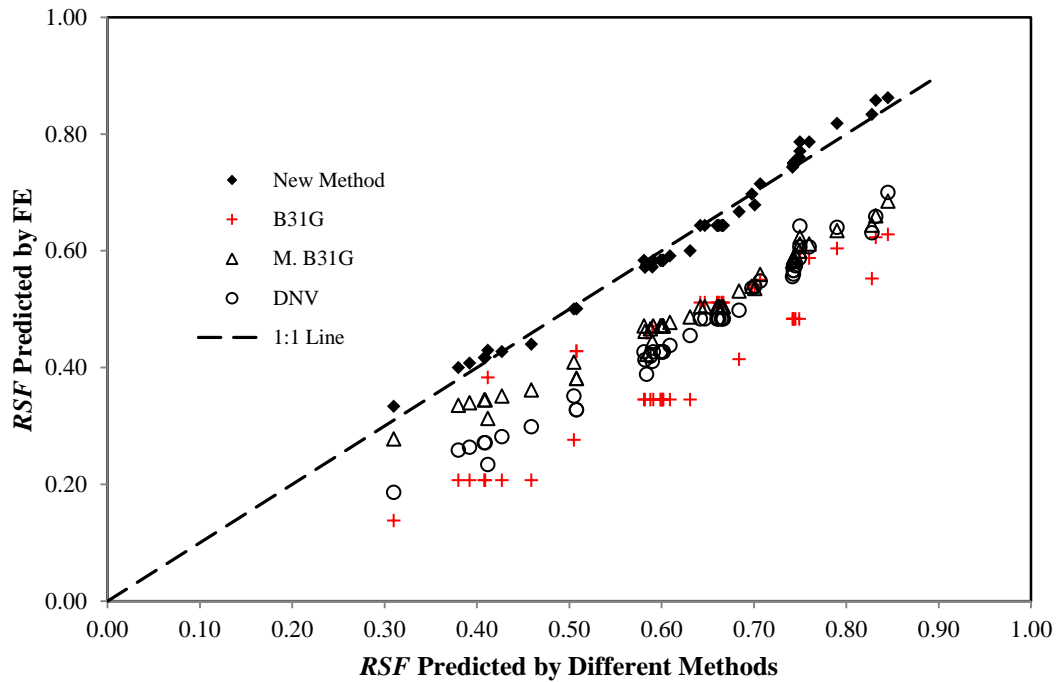


Figure 6.10 Comparison of RSF predictions with the FE results

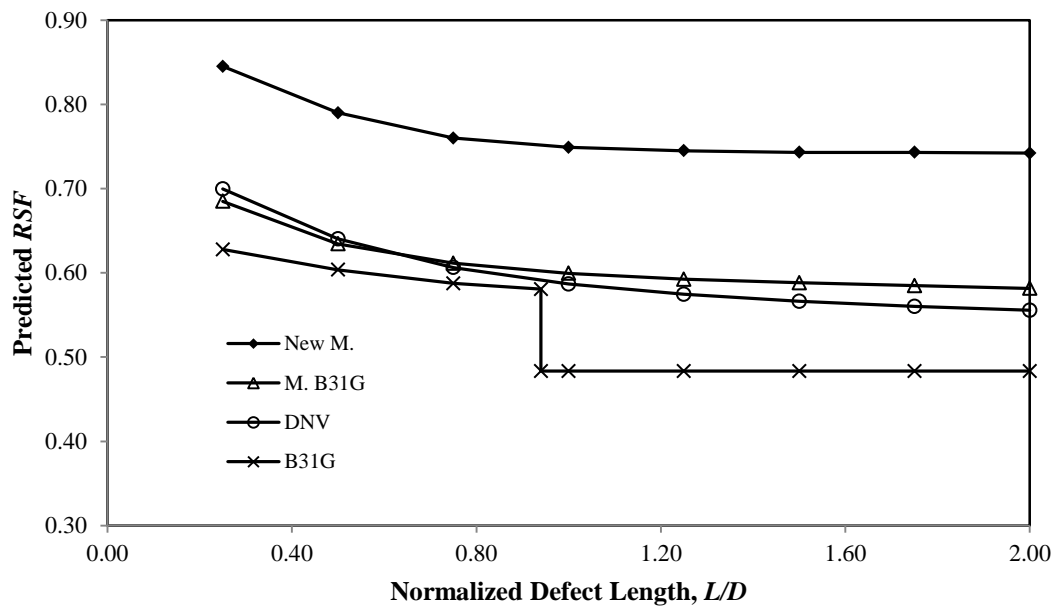


Figure 6.11 Comparison of RSF predictions by different methods ($d/t = 0.3$)

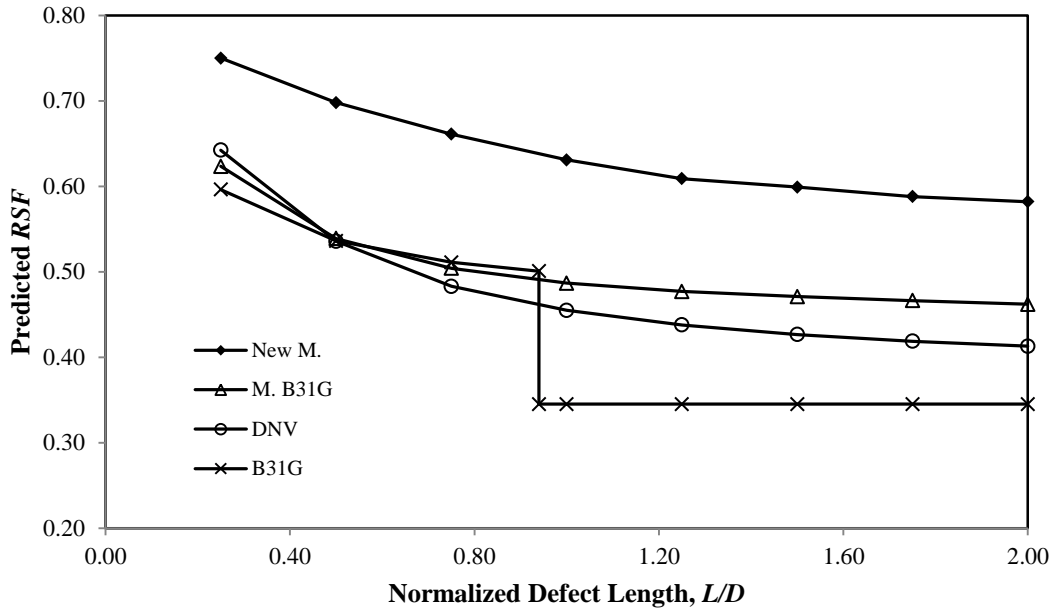


Figure 6.12 Comparison of RSF predictions by different methods ($d/t = 0.5$)

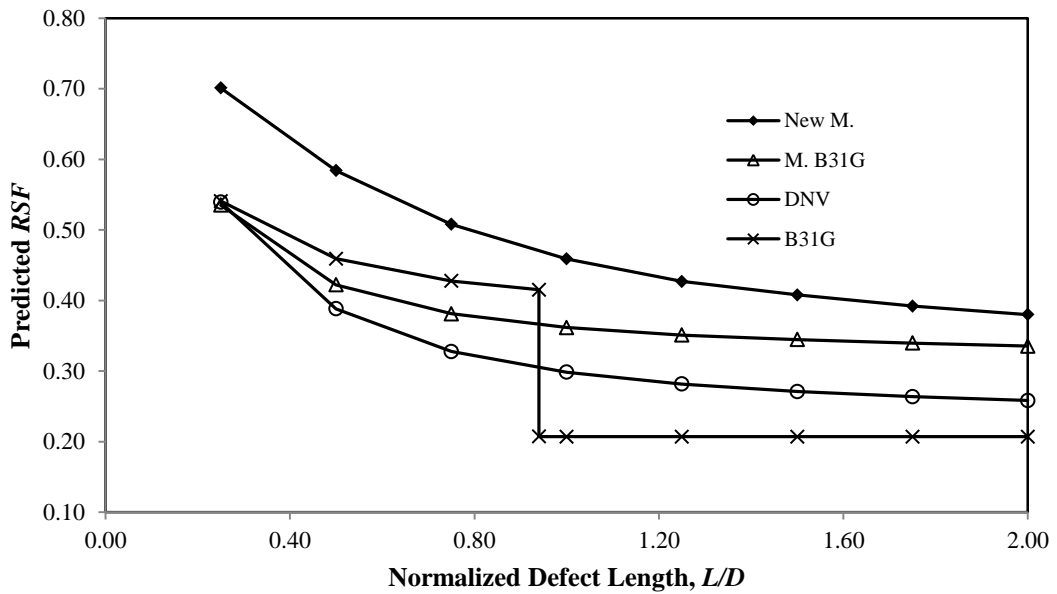


Figure 6.13 Comparison of RSF predictions by different methods ($d/t = 0.7$)

Figure 6.14 and Figure 6.15 show the predicted RSF values versus normalized defect depth for shorter ($L/D = 0.75$) and longer ($L/D = 1.50$) corrosion defects, respectively. Once again, the comparisons of predictions by the New Method and by the three codes were made. The trends of the variation of the predicted RSF are generally similar, as the corrosion depth increases, the RSF value decreases. More

specifically, for longer corrosion defects, the *RSF* values decrease linearly with the increase of the corrosion depth. Generally, the predictions by codes are more conservative for shallower and shorter defects and less conservative for longer and deeper defects.

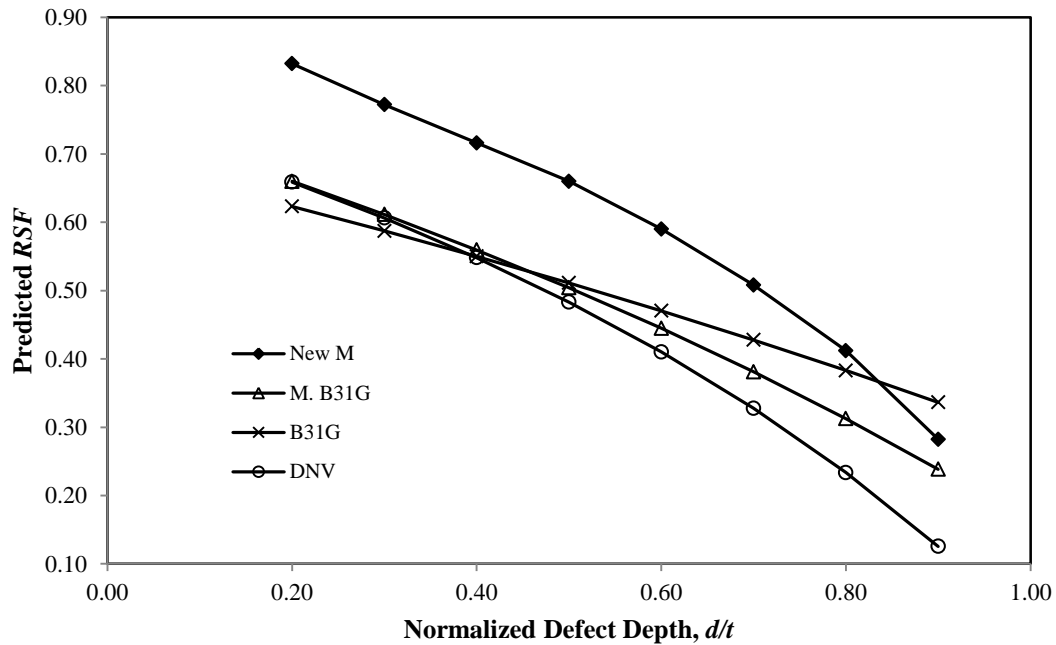


Figure 6.14 Comparison of *RSF* predictions by different methods ($L/D = 0.75$)

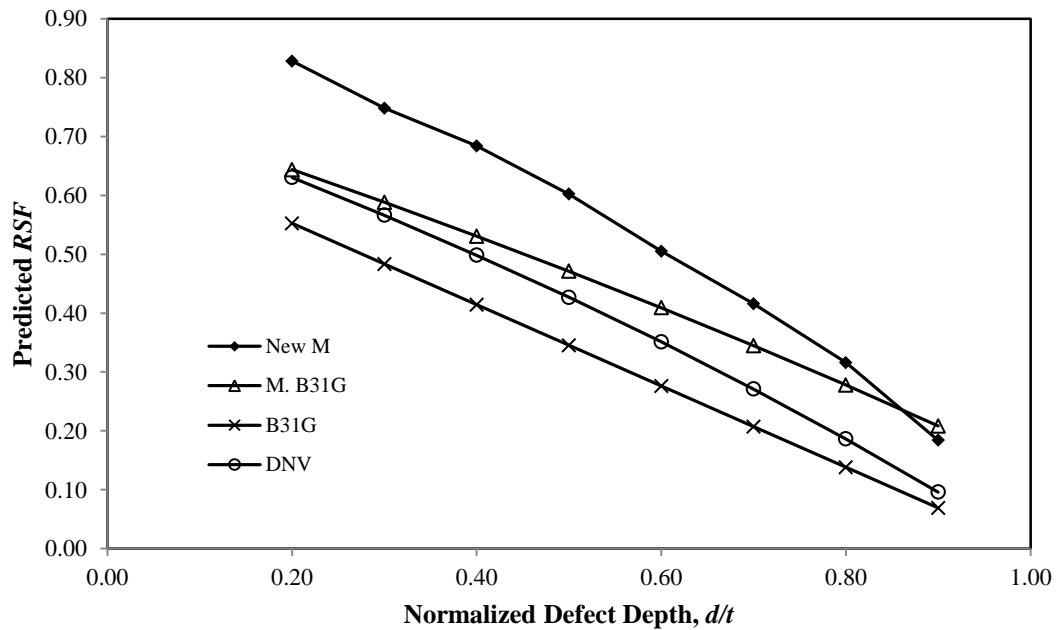


Figure 6.15 Comparison of *RSF* predictions by different methods ($L/D = 1.50$)

6.3.2 Comparison with Burst Test Database

Since the new method was developed based on the API X52 steel, it is necessary to check the applicability of the method to lower or higher grade pipe materials. As a result, benchmarking of the method with burst test database consisting of more than 100 tests with different grade of steel had been done. The comparison of the available methods with the burst test database has been conducted as discussed in section 3.7. Therefore, in this section only modified B31G code was considered for further discussion and comparison. Detail descriptions of the burst test database are shown in Table A.2 (Appendix A).

The comparison of *RSF* values predicted by the new method and the *RSF* obtained from burst test database is shown in Figure 6.16. For a reference purpose, the predictions by Modified B31G code are plotted in the same graph. A prediction coincides with the 1:1 line is an exact prediction (non-conservative). A prediction which lies below the 1:1 line is an under-prediction (conservative) and that which lies above the 1:1 line is an over-predicted (unsafe). Therefore, the best pipeline assessment method shall predict *RSF* values which lie in the close proximity of the 1:1 line with minimum scatters.

As shown in Figure 6.16, the *RSF* predicted by the new method shows excellent agreement with the burst test database. The predictions are evenly distributed within about $\pm 7.0\%$ from the burst test database result and a standard deviation of mean error of about 3%. For the Modified B31G shown in the same plot, the predictions were all conservative with a mean error of about 21% and with up to 28% of underestimation. The most conservative prediction was observed for B31G code, the predictions were all conservative with mean error of 34%. Moreover, the most scattered predictions of up to 56% under-estimation were seen.

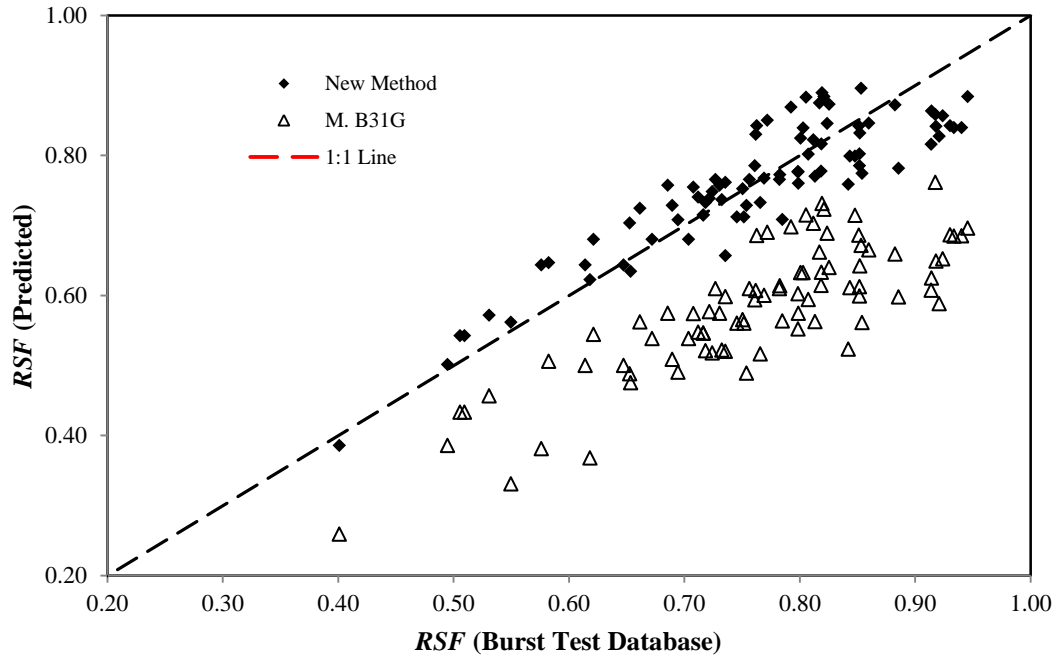


Figure 6.16 Benchmarking of the new method with the actual *RSF* values

To conclude, this new method can predict the burst pressure of corroded pipelines with better accuracy and minimum scatters. Therefore, it can be used to predict the capacity of corroded pipelines. The MAOP can be estimated based on the specified safety factors by individual pipeline operators.

6.4 Chapter Summary

A new method for corrosion defect assessment is developed based on the FE simulation results. The new approach is benchmarked with contemporary defect assessment methods and against burst test database. The new method predicted the burst pressure with better accuracy and less scatters. It is concluded that pipeline operators may use this method according there safety class to estimate the MAOP.

CHAPTER 7

CONCLUSIONS AND RECOMMENDATIONS

7.1 Conclusions

The main objective of this research is achieved by developing a new and more reliable defect assessment method. Moreover, all details under the scope of the research have been properly addressed. In the following sections conclusive discussions and remarks are given.

- The ASME, DNV-RP-F101 and PCORRC methods are conservative (bias) and inconsistent for the burst prediction. For example, the burst capacity prediction made by B31G criteria was on average less by about 31% than the burst test database with as low as 72% under predictions. Similarly, the Modified B31G, the RSTRENG and the DNV underestimated the capacity by an average of about 24%, 27% and 26%, respectively. The extreme under estimations were also up to 52% for Modified B31G and up to 62% for RSTRENG and DNV methods. The Modified PCORRC method predicted the burst capacity with an error limited to about 13% under estimation, while some values were scattered as low as 58% from the actual.
- Corrosion is found to be distributed at the bottom half of the pipe section. Corrosion debris, solid precipitates and scale like deposits are accumulated along the bottom line. Most of the external surfaces of the pipeline were free from corrosion because of the protective rubber coating. In few locations where the lamination was broken, there was rusting on the pipe surface due to sea water permeation.

- The comparison of IP tally to the UCS/P-Scan inspection confirmed that IP inspection measured the minimum wall thicknesses only by 12.5% and the average wall thickness by 10% less than the P-Scan measurements. Therefore, the IP records were acceptable as compared to the 80% confidence level given by the vendors.
- Based on the burst test result it was observed that as the pressure increased, bulging deformation around the defect area occurred and is followed by a crack-like penetration in the longitudinal direction. Once the crack grows and propagates to the opposite wall of the defect surface, the pipe explodes. Therefore, the initial failure of corroded pipes was observed to occur by plastic collapse due to localized stress at the defect.
- The FE simulations corresponding to the test samples well matched with the burst test results with error less than 5%. Therefore, the FE simulation would be used as a complement to the burst test database in order to develop a new corrosion assessment method.
- Results of these burst tests combined with burst test database in published literatures into a wider database were used to validate the new residual strength assessment method.
- Based on the FE modelling of various types of practical corrosion defects:
 - Longitudinally extended groove like defects can be simulated by plane strain analyses.
 - Circumferentially extended slot like defects can be simulated by axisymmetric analyses.
 - A patch like corrosion defects were modeled as flat-bottomed rectangular defects with round corners. The explicit study on the influence of defect width, defect length and defect depth on the burst pressure were conducted by using these models.

- The following conclusions were drawn based on the study of various corrosion defect sizes:
 - If the defect depth is greater than 20% of the wall thickness, the failure pressure due to an infinite length of uniform depth defect is a linear function of the defect depth.
 - Shallower defects (defect depth less than 20% of the wall thickness) fail at pressure close to the failure pressure of plain pipe.
 - Short defects (typically less than $2t$ in length) of any depth record high burst pressures, typically above the pressure required to yield the uncorroded pipe.
 - As defects get longer, end effect die away and no further reduction in burst pressure was observed. Therefore, the effect of an infinitely long defect on the burst pressure is equivalent to the effect of a defect having length equal to twice of the diameter.
 - Circumferentially extended defects by more than two times the nominal wall thickness of the pipe have the same effect as finite defect of width equal to twice the nominal wall thickness, on the burst pressure.
 - Generally, the longitudinal extent of a corroded area is the most important length parameter for the burst strength under internal pressure loading. Corrosion depth followed by the length is the main defect geometric parameters affecting the residual strength of corroded pipe. The circumferential extent has a small influence on the burst strength and hence not considered. However, the circumferential extent must be considered if external axial and/or bending loads are present.
 - The failure of a part-wall defect in a pipeline subjected to internal pressure has two limits, namely a defect with a length and depth approaching to zero (i.e. defect-free pipe) and an infinitely long defect of finite depth.

- The following points are concluded based on validation of the new method:
 - The new defect assessment method was best fitted to the FE simulation results within average error of less than 1% and the scatterings of $\pm 5\%$ from the mean value.
 - The predictions by the new method agreed with the burst test database within about $\pm 7.0\%$ from the actual value.

7.2 Contributions of the Research

This research contributed to the development of an alternative corrosion defect assessment method. This new method can predict the burst pressure of corroded pipelines with better accuracy than the currently corrosion assessment codes and norms. Therefore, pipeline operators and engineers will benefit from this research.

Along the course of the research, there were some valuable experiences and contributions which might be useful for pipeline operators and researchers in this area. Some of these contributions are briefly mentioned as follows:

- i. *Appraisal of current defect assessment methods:* Appraisal of five currently most applicable corrosion defect assessment methods were conducted based on quantitative study by comparing with burst test database. The average biases of the predictions by the codes were demonstrated for precaution. Furthermore, modification was suggested on the PCORRC method. The modified PCORRC method is capable of making better predictions, but, the inconsistency of prediction is similar with other conventional methods.
- ii. *Validation of IP data:* Investigation of the accuracy and credibility of an IP data with advanced scanning techniques like C-Scan and P-Scan boost the confidence level of pipeline operators and engineers to rely on the IP data. This is very useful for engineers to conduct any maintenance or FFS assessment based on any available code.

- iii. Burst test setup established:* The burst test facilities and procedures are established in UTP. The establishment of such facilities in the university will drive and facilitate further research from the industry. Furthermore, the burst test results are an additional resource to the burst test database.

7.3 Recommendations for Future Work

Some of the limitations of this research are portrayed and recommendations for future work are given in the following section:

- i.* This research has presented a new defect assessment method based on a series of nonlinear FE simulation of idealized flat-bottomed rectangular (patch-like) defects. In reality, corrosion defects are irregular in shape and most of the time multiple corrosion defects are interacting. More accurate and reliable prediction can be achieved by FE analyses if the corrosion area is modeled similar to the real corrosion. Therefore, it is recommended that future research shall deal with an actual corrosion area modeling for betterment of defect assessment methods.
- ii.* The new method can be utilized by manipulating the proposed equations according to the defect size measured by MFL tool or any advanced scanning. These empirical equations were developed based on most practical corrosion defect dimensions. Such equations can give good estimations at the data points but the predictions of any arbitrary points are obtained by linear interpolation. In the future, software shall allow pipeline engineers to directly map the inspection records to FE model. Therefore, the remaining strength prediction can be calculated instantly for any specific defects without using the empirical equations.

REFERENCES

1. Seleznev, V., V. Aleshin, and V. Kobayakov. *Analysis of the Corroded Pipeline Segments Using In-Line Inspection Data*. in *The 8th International Conference of the Slovenian Society for Non-Destructive Testing*. 2005. Portoroz, Slovenia.
2. Cosham, A. and M. Kirkwood. *Best practice in pipeline defect assessment*. in *International pipeline conference, IPC 2000*. 2000. Calgary, Alberta, Canada: Penspen Integrity.
3. Cosham, A., *The Assessment of Corrosion in Pipelines-Guidance in the Pipeline*, in *Pipeline Pigging and Integrity Management Conference*. 2004: Amsterdam, the Netherlands.
4. Chouchaoui, B., *Evaluating the Remaining Strength of Corroded Pipelines*, in *Mechanical Engineering*. 1993, University of Waterloo: Ontario, Canada.
5. Cronin, D.S., *Assessment of Corrosion Defect in Pipelines*, in *Mechanical Engineering*. 2000, University of Waterloo: Ontario, Canada.
6. PHMSA. *Data and Statistics: Pipeline and Hazardous Materials safety Administration*. 2010 [cited; Available from: <http://ops.dot.gov/stats.htm>].
7. BP. *Gulf of Mexico Response*. 2010 [cited; Available from: <http://www.bp.com/extendedsectiongenericarticle.do?categoryId=40&contentId=7061813>].
8. Brown, B., S. Reddy, and P. Nestic, *CO₂ corrosion in the presence of trace amounts of H₂S*, in *NACE Corrosion 2004 Conference and Expo*. 2004.
9. Chiodo, M.S.G. and C. Ruggieri, *Failure assessments of corroded pipelines with axial defects using stress-based criteria: Numerical studies and verification analyses*. *International Journal of Pressure Vessels and Piping*, 2009. **86**(2-3): p. 164-176.
10. Netto, T.A., U.S. Ferraz, and A. Botto, *On the effect of corrosion defects on the collapse pressure of pipelines*. *International Journal of Solids and Structures*, 2007. **44**(22-23): p. 7597-7614.
11. Netto, T.A., U.S. Ferraz, and S.F. Estefen, *The effect of corrosion defects on the burst pressure of pipelines*. *Journal of Constructional Steel Research*, 2005. **61**(8): p. 1185-1204.

12. ASME, *Manual for determining the remaining strength of corroded pipelines. A supplement to ANSI/ASME B31 code for pressure piping*, in *ASME B31G 1991*. 1991.
13. Kiefner, J.F. and P.H. Vieth, *A Modified Criterion for Evaluating the Remaining Strength of Corroded Pipe*. 1989, Pipeline Research Committee.
14. Vieth, P.H. and J.F. Kiefner, *RSTRENG User's Manual and Software*. 1993, Pipeline Research Supervisory Committee, A.G.A.
15. DNV, *Recommended practice DNV-RP-F101. Corroded pipelines*, in *DET NORSE VERITAS*, DNV, Editor. 2004.
16. Cosham, A. and P. Hopkins, *An Overview of the Pipeline Defect Assessment Manual (PDAM)*, in *4th International Pipeline Technology Conference*. 2004: Ostende, Belgium.
17. Batte, A.D., F.B. Kirkwood, and D. Vu, *New Methods for Determining the Remaining Strength of Corroded Pipelines*, in *OMAE V Pipeline Technology*, B.G. plc, Editor. 1997, ASME.
18. Belachew, C.T., M.C. Ismail, and S. Karuppanan, *Capacity Assessment of Corroded Pipelines Using Available Codes*, in *National Post Graduate Conference on Engineering, Science and Technology (NPC)*. 2009a: Universiti Teknologi PETRONAS, Tronoh, Malaysia.
19. MSL, *Appraisal and development of pipeline defect assessment methodologies*, M.e. limited, Editor. 2000, MSL house: Ascot, Berkshire.
20. Stephens, D.R., et al., *Development of an Alternative Failure Criterion for Residual Strength of Corrosion Defects in Moderate- to High- Toughness Pipe*. 1999, Battelle reports to PRC International.
21. Fu, B. and M.G. Kirkwood, *Predicting Failure Pressure of Internally Corroded Linepipe using the Finite Element Method*, in *OMAE V Pipeline Technology*. 1995, ASME.
22. Andrade, E.Q.d., et al. *Finite Element Modeling of the Failure Behavior of Pipelines Containing Interacting Corrosion Defects*. in *Proceedings of OMAE2006, 25th International Conference on Offshore Mechanics and Arctic Engineering*. 2006. Hamburg, Germany.

23. Teitsma, A., *Technology assessment for Delivery Reliability for Natural Gas-Inspection Technologies: RFEC*. 2004, Pipeline Inspection Technology Des Plaines, Illinois
24. Lee, O.S. and H.J. Kim, *Effect of external corrosion in pipeline on failure prediction*. International Journal of the Korean society of precision engineering, 2000. **1**(2): p. 48-54.
25. Benjamin, A.C., et al. *Burst Tests on Pipeline Containing Closely Spaced Corrosion Defects*. in *Proceedings of OMAE2006, 25th International conference on offshore Mechanics and Arctic Engineering* 2006. Hamburg, Germany.
26. Cosham, A., P. Hopkins, and K.A. Macdonald, *Best practice for the assessment of defects in pipelines - Corrosion*. Engineering Failure Analysis, 2007. **14**(7): p. 1245-1265.
27. Bickerstaff, R., et al., *Review of Sensor Technologies for In-line Inspection of Natural Gas Pipelines*, Sandia National Laboratories.
28. Nestleroth, J.B. and T.A. Bubenik. *Magnetic Flux Leakage (MFL) Technology For Natural Gas Pipeline Inspection* 1999 [cited; Available from: <http://www.battelle.org/pipetechnology/mfl/mfl98main.html>].
29. UKOPA, *UKOPA Recommendations for Pipeline Maintenance and Inspection*, in *Pipeline Insection and Maintenance Strategies*. 2006, United Kingdom Onshore Pipeline Operators' Association
30. API, *API Recommended Practice 579, Fitness for Service*, ed. API. 2000, Washington, D. C. 971.
31. Choi, J.B., et al., *Development of limit load solutions for corroded gas pipelines*. International Journal of Pressure Vessels and Piping, 2003. **80**(2): p. 121-128.
32. Choi, H.S. and J.G. Bomba, *Acceptance Criteria of Defects in Undersea Pipeline Using Internal Inspection*. Ocean Engineering, 2003. **30**: p. 1613-1624.
33. Silva, R.C.C., J.N.C. Guerreiro, and P.R.C. Drach, *Automatic finite element solid modeling, burst and error analyses of corroded pipelines*. International Journal of Mechanics, 2008. **2**(3): p. 77-86.

34. Wilkowski, G., et al., *Progress in development of acceptance criteria for local thinned areas in pipe and piping components*. Nuclear Engineering and Design, 2000. **195**(2): p. 149-169.
35. Adib-Ramezani, H., J. Jeong, and G. Pluvinage, *Structural integrity evaluation of X52 gas pipes subjected to external corrosion defects using the SINTAP procedure*. International Journal of Pressure Vessels and Piping, 2006. **83**(6): p. 420-432.
36. API, *API Recommended Practice 579, Fitness for Service*. 2000, American Petroleum Institute: 1220 L Street, Northwest, Washington D.C. p. 971.
37. Vieth, P.H. and J.K. Kiefner, *Database for Corroded Pipe Tests*. 1994, AGA Catalog No. L51689.
38. Mok, D.H.B., et al., *Bursting of Line Pipe with Long External Corrosion*. International Journal of Pressure Vessel & Piping, 1991. **46**: p. 159-216.
39. Wiesner, C.S., et al., *Engineering critical analyses to BS 7910 -- the UK guide on methods for assessing the acceptability of flaws in metallic structures*. International Journal of Pressure Vessels and Piping, 2000. **77**(14-15): p. 883-893.
40. Bjornoy, O.H., G. Sigurdsson, and E. Cramer, *Recommended practice DNV-RP-F101. Corroded pipelines*. 2004, DET NORSKE VERITAS N-1322 Høvik, Norway.
41. Chen, H.F. and D. Shu, *Simplified Limit Analysis of Pipelines with Multi-defects*. Engineering Structures, 2001. **23**: p. 207-213.
42. KAPA, *A Modified Criterion for Evaluating the Remaining Strength of Corroded Pipe*. 2000, Kiefner and Associates, Inc.
43. Bjornoy, O.H., G. Sigurdsson, and E. Cramer. *Residual Strength of Corroded Pipelines, DNV Test Results*. in *Proceedings of the Tenth (2000) International offshore and polar engineering conference*. 2000. Seattle, USA: The International Society of offshore and polar engineering.
44. Bai, Y. and O.H. Bjornoy, *Reliability-Based Residual Strength Criteria for Corroded Pipes: Residual Strength of Corroded and Dented Pipes*, in *Joint Industry Project*. 1995, DET NORSKE VERITAS: N-1322 Høvik, Norway.

45. Bjornoy, O.H. and M.J. Marley. *Assessment of Corroded Pipelines: Past, Present and Future*. in *Proceedings of the eleventh (2001) International offshore and polar engineering conference*. 2001. Stavanger, Norway: The International Society of offshore and polar engineering.
46. Chouchaoui, B.A. and R.J. Pick, *Behaviour of longitudinally aligned corrosion pits*. International Journal of Pressure Vessels and Piping, 1996. **67**(1): p. 17-35.
47. Diniz, J.L.C., et al., *Stress and strain analysis of pipelines with localized metal loss*. Society of Experimental Mechanics, 2006. **46**: p. 765-775.
48. Valenta, F., et al., *Theoretical and experimental evaluation of the limit state of transit gas pipelines having corrosion defects*. international journal of pressure vessels and piping, 1996. **66**: p. 187-198.
49. Ahammed, M. and R.E. Melchers, *probabilistic analysis of pipelines subjected to pitting corrosion leaks*. Journal of engineering structures, 1995. **17**(2): p. 74-80.
50. Ahammed, M., *Prediction of remaining strength of corroded pressurised pipelines*. International Journal of Pressure Vessels and Piping, 1997. **71**(3): p. 213-217.
51. Ahammed, M. and R.E. Melchers, *Reliability of underground pipelines subjected to corrosion*. journal of transportation engineering, 1994. **120**(6): p. 989-1002.
52. Ahammed, M. and R.E. Melchers, *probabilistic analysis of underground pipelines subjected to combined stress and corrosion*. international journal of Engineering structures, 1996. **19**(12): p. 988-994.
53. Ahammed, M., *Probabilistic estimation of remaining life of a pipeline in the presence of active corrosion defects*. International Journal of Pressure Vessels and Piping, 1998. **75**(4): p. 321-329.
54. Ahammed, M. and R.E. Melchers, *Reliability estimation of pressurised pipelines subject to localised corrosion defects*. International Journal of Pressure Vessels and Piping, 1996. **69**(3): p. 267-272.
55. Pandey, M.D., *Probabilistic Models for Condition Assessment of Oil and Gas Pipelines*. international journal of Engineering structures, 1997: p. 349-358.

56. Kale, A., et al., *A Probabilistic Model for Internal Corrosion of Gas Pipelines*. ASME Conference Proceedings, 2004. **2004**(41766): p. 2437-2445.
57. Sadiq, R., B. Rajani, and Y. Kleiner, *Probabilistic risk analysis of corrosion associated failures in cast iron water mains*. Reliability Engineering & System Safety, 2004. **86**(1): p. 1-10.
58. Cronin, D.S. and R.J. Pick, *Prediction of the failure pressure for complex corrosion defects*. International Journal of Pressure Vessels and Piping, 2002. **79**(4): p. 279-287.
59. Cabral, H.L.D., et al., *Development of Computational Tools for Automatic Modeling and FE Analysis of Corroded Pipelines*. International Journal of Modeling and Simulation for the Petroleum Industry, 2007. **1**.
60. Leis, B. and X. Zhu, *Corrosion Assessment Criteria: Rationalizing Their Use for Vintage vs. Modern Pipelines*. 2005, Battelle: Columbus, OH. p. 96.
61. Andueza, A. and T. Pontual. *Structural Integrity evaluation for the analysis of corroded pipelines with multiple corrosion defects*. in *Proceedings of IPC2006, 6th International Pipeline Conference*. 2006.
62. Lee, O.S. and H.J. Kim, *Effect of External Corrosion in Pipeline on Failure Prediction*. International Journal of the Korean Society of Precision Engineering, 2000. **1**(2): p. 48-54.
63. Ramberg, W. and W.R. Osgood, *Description of Stress-Strain Curves by Three Parameters*. 1943: Washington. p. 29.
64. Chouchaoui, B.A. and R.J. Pick, *Behaviour of circumferentially aligned corrosion pits*. International Journal of Pressure Vessels and Piping, 1994. **57**(2): p. 187-200.
65. Klever, F.J., G. Stewart, and C.A.C.v.d. Valk. *New Developments in Burst Predictions for Locally Corroded Pipelines*. in *OMAE 1995*. 1995.
66. Bjornoy, O.H., G. Sigurdsson, and E. Cramer, *Assessment of Corrosion in Linepipe*, in *Joint Industry Project*, B. Technology, Editor. 1998, Det Norske Veritas AS: N-1322 Høvik, Norway.
67. Leis, B.N. and D.R. Stephens. *An alternative approach to assess the integrity of corroded line pipe – part II: alternative criterion*. in *Proceedings of the seventh international offshore and polar engineering conference 1997*. Honolulu, USA.

68. Bjornoy, O.H., G. Sigurdsson, and E. Cramer, *Reliability of Corroded Pipes Assessment of Capacity and Acceptance Criteria*, in *Joint Industry Project*. 1997, DET NORSKE VERITAS (DNV): N-1322 Høvik, Norway.
69. Coulson, K.E.W. and R.G. Worthingham, *New guidelines promise more accurate damage assessment*. *Oil Gas Journal*, 1990. **16**: p. 41–44.
70. Keifner, J.F., P.H. Vieth, and I. Roytman, *Continuing validation of RSTRENG*. 1996, Pipeline Research Supervisory Committee, A.G.A.
71. Kiefner, *A Modified Criterion for Evaluating the Remaining Strength of Corroded Pipe*. 2000, Kiefner and Associates, Inc.
72. Bjornoy, O.H., G. Sigurdsson, and E. Cramer, *Unified Guidance Document: Guidance for the Assessment of Corrosion in Linepipe*. 1998, DNV and BG: N-1322 Høvik, Norway.
73. Kiefner, *KAPA 2006*. 2006, Kiefner and Associates, Inc.
74. Keifner, J.F. and A.R. Duffy, *Summary of Research to Determine the Strength of Corroded Areas in Line Pipe*. 1971, Battelle Interim Report to Texas Eastern Transmission Corporation.
75. ASTM, *ASTM E8M-04 Standard Test Methods for Tension Testing of Metallic Materials*, in *ASTM E8M-04*. 2008.
76. Chouchaoui, B.A. and R.J. Pick. *Residual Burst Strength of Pipe with Internal Corrosion Pits*. in *Proc. International Conference on Pipeline Reliability*. 1992. Calgary, Canada.
77. Belachew, C.T., M.C. Ismaiel, and S. Karuppanan, *Effect of Corrosion Defect on Burst Pressure of Pipelines: Numerical Studies and Validation* in *NACE East Asian & Pacific Regional Conference & Exposition*. 2009: Kuala Lumpur, Malaysia.
78. ANSYS, *ANSYS Release 12.0 Documentation*. 2009.
79. Chouchaoui, B., *Evaluating the Remaining Strength of Corroded Pipelines*, in *Mechanical Engineering*. 1993, University of Waterloo: Ontario, Canada.
80. Zienkiewicz, O.C., *The finite element method in engineering science*. 1971: McGraw-Hill.
81. Graebel, W.I., *Dimensional Analysis*, in *Engineering Fluid Mechanics*. 2001, Taylor & Francis.

APPENDIX A
BURST TEST DATABASE

Table A.1 Actual and theoretical burst pressure of defect-free pipelines

ID	Material	D (mm)	t (mm)	$SMYS$ (MPa)	$SMTS$ (MPa)	Burst Pressure (bar)	
						Actual	Theoretical
SOL-1	X46	323.7	8.51	317.2	434.4	250.9	234.6
SOL-2	X46	323.7	8.64	317.2	434.4	244.7	238.2
SOL-5	X46	324.2	8.54	317.2	434.4	250.3	235.0
SOL-7	X46	321.7	8.33	317.2	434.4	224.8	231.1
SOL-8	X46	323.7	8.74	317.2	434.4	239.4	241.1
SOL-9	X46	324.2	8.44	317.2	434.4	232.9	232.1
SOL-14	X46	324.0	8.64	317.2	434.4	245.4	238.0
NOR-3	X52	273.2	5.29	358.9	455.1	172.6	179.6
SOL-1	X46	323.7	8.51	317.2	434.4	250.9	234.6
SOL-2	X46	323.7	8.64	317.2	434.1	244.7	238.1

Table A.1 Actual and theoretical burst pressure of defect-free pipelines (continued)

ID	Material	D (mm)	t (mm)	$SMYS$ (MPa)	$SMTS$ (MPa)	Burst Pressure (bar)	
						Actual	Theoretical
NOVA 08	X60	508.0	6.35	414.0	517.1	130.5	130.9
NOVA 09	X60	508.0	6.35	414.0	517.1	130.5	130.9
NOVA 13	X60	508.0	6.35	414.0	517.1	154.5	130.9
NOVA 14	X60	508.0	6.40	414.0	517.1	152.5	132.0
BG Ring 1-1	X52	610.0	12.34	359.0	471.0	213.0	194.5
BG Ring 2-1	X52	610.0	12.34	359.0	471.0	212.0	194.5
BG 1	X60	914.0	22.00	414.0	517.1	263.0	255.1
BG 2	X60	914.0	22.00	414.0	517.1	264.0	255.1
T002	X52	273.1	10.58	414.0	455.1	385.0	366.8

Table A.2 Actual and predicted burst pressure of corroded pipeline

No	Test ID	Material	D (mm)	t (mm)	d/t	L (mm)	Material Strength (MPa)		Burst Pressure (bar)					
							SMYS	SMTS	Test	B31G	M. B31G	RSTRENG	DNV	M. PCORRC
1	AGA 1	X52	762.0	9.40	0.39	64.0	358.3	454.7	111.9	88.4	98.5	100.7	97.4	115.1
2	AGA 2	X52	762.0	9.40	0.39	57.0	358.3	454.7	111.7	88.4	99.7	101.2	98.2	115.9
3	AGA 3	X52	762.0	9.40	0.42	108.0	358.3	454.7	117.2	85.9	90.6	98.8	90.2	108.9
4	AGA 4	X52	762.0	9.53	0.64	140.0	358.3	454.7	115.2	74.4	73.1	95.9	70.7	92.0
5	AGA 5	X52	762.0	9.53	0.56	121.0	358.3	454.7	105.2	80.4	82.1	91.4	81.3	101.2
6	AGA 27	X52	762.0	9.53	0.39	140.0	358.3	454.7	126.9	85.5	89.7	99.8	88.8	108.7
7	AGA 28	X52	762.0	9.53	0.31	114.0	358.3	454.7	130.7	89.6	96.2	99.7	95.2	114.6
8	AGA 29	X52	762.0	9.53	0.61	102.0	358.3	454.7	122.4	81.0	82.7	96.7	82.1	101.3
9	AGA 30	X52	762.0	9.53	0.56	41.0	358.3	454.7	147.6	89.6	100.9	104.0	99.4	115.9
10	AGA 31	X52	762.0	9.53	0.56	51.0	358.3	454.7	137.8	89.6	98.3	103.1	97.3	113.8
11	AGA 68	X52	762.0	9.45	0.35	914.0	358.3	454.7	127.2	63.5	77.8	93.9	70.9	83.8
12	AGA 69	X52	762.0	9.55	0.61	305.0	358.3	454.7	104.5	66.7	62.8	73.2	55.8	73.9
13	AGA 70	X52	762.0	9.53	0.37	305.0	358.3	454.7	125.2	80.2	82.2	86.4	78.3	98.0
14	AGA 71	X52	762.0	9.70	0.38	508.0	358.3	454.7	131.2	62.2	79.6	94.9	73.6	90.1
15	AGA 72	X52	762.0	9.55	0.35	508.0	358.3	454.7	123.1	64.2	80.8	89.7	75.1	91.9

Table A.2 Actual and predicted burst pressure of corroded pipeline (Continued)

No	Test ID	Material	D (mm)	t (mm)	d/t	L (mm)	Material Strength (MPa)		Burst Pressure (bar)					
							SMYS	SMTS	Test	B31G	M. B31G	RSTRENG	DNV	M. PCORRC
16	AGA 73	X52	762.0	9.60	0.29	838.0	358.3	454.7	132.1	70.5	84.4	96.3	78.2	93.3
17	AGA 74	X52	762.0	9.63	0.45	356.0	358.3	454.7	122.4	75.6	75.5	92.1	70.1	88.6
18	AGA 75	X52	762.0	9.68	0.79	305.0	358.3	454.7	77.2	56.3	46.5	31.4	34.4	48.8
19	AGA 76	X52	762.0	9.60	0.42	203.0	358.3	454.7	118.6	81.2	83.4	93.5	81.1	101.9
20	AGA 77	X52	762.0	9.58	0.42	305.0	358.3	454.7	123.4	77.9	78.8	90.3	74.5	94.1
21	AGA 78	X52	762.0	9.47	0.29	229.0	358.3	454.7	126.9	85.4	89.6	92.8	87.1	107.6
22	AGA 80	X52	762.0	9.27	0.63	406.0	358.3	454.7	68.1	35.5	56.5	46.4	47.8	61.3
23	AGA 81	X52	762.0	9.53	0.65	686.0	358.3	454.7	68.4	34.5	53.3	53.3	42.3	49.5
24	AGA 83	X52	508.0	6.60	0.84	406.0	358.3	454.7	57.6	16.4	37.2	50.5	21.8	24.4
25	AGA 86	X52	558.8	5.03	0.75	152.0	358.3	454.7	57.1	43.4	37.8	54.5	30.9	44.6
26	AGA 82	X56	762.0	9.53	0.40	191.0	385.8	489.2	135.9	88.4	90.4	101.6	89.2	111.4
27	AGA 84	X65	914.4	8.38	0.66	406.0	447.9	530.5	53.4	30.7	49.3	39.5	39.4	51.3
28	NOVA 5	X60	508.0	6.35	0.40	381.0	413.4	516.8	112.5	68.2	85.8	79.1	78.8	95.8
29	NOVA 6	X60	508.0	6.35	0.40	1016.0	413.4	516.8	115.5	68.2	81.7	74.6	73.6	85.9
30	NOVA 7	X60	508.0	6.35	0.40	381.0	413.4	516.8	130.5	68.2	85.8	79.1	78.8	95.8

Table A.2 Actual and predicted burst pressure of corroded pipeline (Continued)

No	Test ID	Material	D (mm)	t (mm)	d/t	L (mm)	Material Strength (MPa)		Burst Pressure (bar)					
							SMYS	SMTS	Test	B31G	M. B31G	RSTRENG	DNV	M. PCORRC
31	NOVA 11	X60	508.0	6.35	0.40	508.0	413.4	516.8	110.5	68.2	84.5	77.7	76.7	91.2
32	NOVA 12	X60	508.0	6.35	0.40	508.0	413.4	516.8	105.5	68.2	84.5	77.7	76.7	91.2
33	NOVA 15	X60	508.0	6.40	0.54	900.0	413.4	516.8	80.0	52.7	68.6	58.7	58.2	66.7
34	NOVA 16	X60	508.0	6.40	0.34	900.0	413.4	516.8	118.0	75.6	88.7	82.7	81.5	95.6
35	NOVA 19	X60	508.0	6.40	0.53	205.0	413.4	516.8	84.5	82.8	79.0	69.8	73.1	94.6
36	NOVA 20	X60	508.0	6.40	0.50	1000.0	413.4	516.8	84.0	57.3	72.2	63.2	62.5	72.2
37	BG Ves 1-1	X52	610.0	12.34	0.40	304.8	358.3	454.7	144.4	127.2	129.5	120.6	124.0	154.8
38	BG Ves 2-1	X52	610.0	12.34	0.40	610.0	358.3	454.7	140.0	95.7	122.7	113.0	112.5	135.2
39	BG Ves 2-2	X52	610.0	12.34	0.40	305.0	358.3	454.7	154.5	127.2	129.5	120.6	124.0	154.8
40	BG Ves 2-3	X52	610.0	12.34	0.40	305.0	358.3	454.7	164.6	127.2	129.5	120.6	124.0	154.8
41	BG Ves 2-4	X52	610.0	12.34	0.40	152.0	358.3	454.7	184.5	136.6	142.7	135.7	142.1	173.5
42	F1	X46	324.0	5.93	0.79	47.0	316.9	434.1	134.9	97.5	95.3	74.8	95.1	124.2
43	F4	X46	324.0	6.07	0.66	59.0	316.9	434.1	142.9	102.1	103.7	90.4	108.0	136.5
44	F5	X46	324.0	5.84	0.67	33.0	316.9	434.1	162.9	110.3	117.1	108.0	123.6	145.9
45	F7	X46	324.0	5.99	0.78	26.0	316.9	434.1	153.6	114.6	120.5	107.1	125.0	146.6

Table A.2 Actual and predicted burst pressure of corroded pipeline (Continued)

No	Test ID	Material	D (mm)	t (mm)	d/t	L (mm)	Material Strength (MPa)		Burst Pressure (bar)					
							SMYS	SMTS	Test	B31G	M. B31G	RSTRENG	DNV	M. PCORRC
46	F14A	X46	324.0	6.00	0.73	29.0	316.9	434.1	160.9	114.2	120.7	109.6	126.6	148.6
47	F17	X46	324.0	6.07	0.48	41.0	316.9	434.1	169.5	117.9	127.7	122.8	135.3	159.9
48	F18	X46	324.0	5.58	0.79	35.0	316.9	434.1	130.0	98.7	100.0	82.7	102.0	126.1
49	F20	X46	324.0	6.14	0.39	29.0	316.9	434.1	157.8	120.1	138.7	136.6	145.4	170.4
50	F25	X46	324.0	6.16	0.73	37.0	316.9	434.1	142.9	111.8	115.9	101.9	121.3	146.1
51	F29	X46	324.0	5.95	0.70	39.0	316.9	434.1	155.7	107.6	112.0	99.6	117.7	142.1
52	F32B	X46	324.0	6.02	0.33	50.0	316.9	434.1	161.2	117.8	130.5	127.5	137.5	163.6
53	S1C0	X46	324.0	6.40	0.50	20.0	316.9	434.1	166.4	125.2	146.5	144.5	153.1	177.9
54	S2C0	X46	324.0	6.01	0.60	19.0	316.9	434.1	162.2	117.6	135.7	132.6	141.8	163.9
55	S3C0	X46	324.0	6.30	0.57	20.0	316.9	434.1	159.5	123.2	142.6	139.7	149.2	172.6
56	S4C0	X46	323.0	6.31	0.59	20.0	316.9	434.1	141.6	123.8	142.7	139.5	149.4	172.7
57	S1CC	X46	324.0	6.16	0.61	20.0	316.9	434.1	188.5	120.5	138.2	134.7	144.7	167.1
58	S2CC	X46	324.0	6.27	0.60	20.0	316.9	434.1	191.3	122.7	141.1	137.8	147.7	170.6
59	S3CC	X46	324.0	6.25	0.61	20.0	316.9	434.1	192.7	122.3	140.4	136.8	147.0	169.7
60	S4CC	X46	324.0	6.18	0.61	20.0	316.9	434.1	194.4	120.9	138.7	135.2	145.2	167.7

Table A.2 Actual and predicted burst pressure of corroded pipeline (Continued)

No	Test ID	Material	D (mm)	t (mm)	d/t	L (mm)	Material Strength (MPa)		Burst Pressure (bar)					
							$SMYS$	$SMTS$	Test	B31G	M. B31G	RSTRENG	DNV	M. PCORRC
61	S110	X46	325.0	6.45	0.47	21.0	316.9	434.1	158.1	125.8	147.3	145.5	154.0	179.2
62	S210	X46	324.0	6.40	0.58	39.0	316.9	434.1	138.7	121.9	130.7	123.3	138.8	163.8
63	S310	X46	325.0	6.45	0.59	20.0	316.9	434.1	148.4	125.8	145.2	142.0	152.0	175.6
64	S410	X46	324.0	6.35	0.59	20.0	316.9	434.1	153.3	124.2	143.3	140.1	150.0	173.3
65	S11C	X46	322.0	6.27	0.60	20.0	316.9	434.1	176.1	123.4	142.0	138.5	148.6	171.6
66	S21C	X46	324.0	6.29	0.60	72.0	316.9	434.1	151.1	105.5	107.7	95.8	112.2	142.2
67	S31C	X46	324.0	6.24	0.61	72.0	316.9	434.1	156.7	103.9	105.7	93.5	109.9	139.8
68	S41C	X46	324.0	6.10	0.60	20.0	316.9	434.1	152.5	119.3	137.1	133.8	143.5	165.8
69	1	X52	324.0	10.30	0.50	243.0	358.3	454.7	232.0	182.7	179.2	160.0	167.2	208.8
70	8	X52	324.0	10.30	0.50	243.0	358.3	454.7	220.0	182.7	179.2	160.0	167.2	208.8
71	DA	X65	762.0	17.50	0.25	200.0	447.9	530.5	241.1	205.7	214.0	209.1	205.3	246.4
72	DB	X65	762.0	17.50	0.50	200.0	447.9	530.5	217.6	184.2	182.5	168.7	175.3	217.1
73	DC	X65	762.0	17.50	0.75	200.0	447.9	530.5	171.5	155.3	138.4	106.9	122.0	169.3
74	LA	X65	762.0	17.50	0.50	100.0	447.9	530.5	243.0	204.9	210.3	202.2	204.2	239.5
75	LC	X65	762.0	17.50	0.50	300.0	447.9	530.5	198.0	173.8	168.3	152.6	156.8	199.4

Table A.2 Actual and predicted burst pressure of corroded pipeline (Continued)

No	Test ID	Material	D (mm)	t (mm)	d/t	L (mm)	Material Strength (MPa)		Burst Pressure (bar)					
							SMYS	SMTS	Test	B31G	M. B31G	RSTRENG	DNV	M. PCORRC
76	CB	X65	762.0	17.50	0.50	200.0	447.9	530.5	234.2	184.2	182.5	168.7	175.3	217.1
77	CC	X65	762.0	17.50	0.50	200.0	447.9	530.5	226.4	184.2	182.5	168.7	175.3	217.1
78	IDTS 8	X80	459.4	8.00	0.47	40.1	551.2	620.1	242.0	192.0	200.9	196.3	187.6	219.4
79	T12	X60	508.0	6.35	0.54	900.0	413.4	516.8	80.0	52.3	68.0	58.3	57.7	66.2
80	T14	X60	508.0	6.35	0.34	900.0	413.4	516.8	118.0	75.0	88.0	82.1	80.8	94.9
81	T10	X60	508.0	6.35	0.40	381.0	413.4	516.8	112.5	68.2	85.8	79.1	78.8	95.8
82	F01	X46	304.8	5.93	0.79	46.0	316.9	434.1	134.9	103.3	100.9	79.1	100.7	131.6
83	F05	X46	304.8	5.84	0.67	34.0	316.9	434.1	162.5	116.0	122.6	112.3	129.6	153.6
84	F07	X46	304.8	5.99	0.78	27.5	316.9	434.1	153.6	119.8	125.0	109.5	129.7	153.3
85	F14	X46	304.8	6.00	0.73	30.5	316.9	434.1	160.9	119.5	125.5	112.7	131.8	155.7
86	F17	X46	304.8	6.07	0.48	43.0	316.9	434.1	169.5	124.0	133.9	128.3	142.2	168.5
87	F25	X46	304.8	6.16	0.73	36.5	316.9	434.1	142.9	118.4	122.5	107.4	128.3	154.8
88	F29	X46	304.8	5.95	0.70	39.6	316.9	434.1	155.7	113.2	117.3	103.8	123.4	149.6
89	IDTS 2	X80	458.8	8.10	0.67	39.6	551.2	620.1	226.8	193.1	191.1	178.9	178.9	208.9
90	SOL-2	X46	323.5	8.64	0.25	63.5	316.9	434.1	244.0	169.3	192.0	188.9	203.0	239.9

Table A.2 Actual and predicted burst pressure of corroded pipeline (Continued)

No	Test ID	Material	D (mm)	t (mm)	d/t	L (mm)	Material Strength (MPa)		Burst Pressure (bar)					
							SMYS	SMTS	Test	B31G	M. B31G	RSTRENG	DNV	M. PCORRC
91	SOL-4	X46	323.2	8.59	0.35	203.3	316.9	434.1	231.3	152.3	160.0	151.0	163.3	200.5
92	SOL-6	X46	323.2	8.64	0.31	61.0	316.9	434.1	252.5	169.4	188.7	184.6	200.2	236.4
93	SOL-10	X46	323.7	8.49	0.39	144.8	316.9	434.1	239.5	150.0	157.5	148.0	163.1	201.8
94	SOL-11	X46	323.7	8.64	0.31	127.1	316.9	434.1	217.7	161.8	173.4	166.7	181.7	220.9
95	SOL-12	X46	323.2	8.54	0.26	50.8	316.9	434.1	215.8	167.4	192.9	190.5	203.6	239.6
96	NOR-1	X52	273.2	5.23	0.35	409.1	358.3	454.7	167.2	98.1	120.0	111.9	110.2	129.4
97	NOR-2	X52	273.2	5.26	0.33	139.8	358.3	454.7	180.7	126.6	130.9	124.2	126.0	155.6
98	TNG-1	X46	273.2	8.26	0.48	241.4	316.7	434.1	212.3	109.5	154.4	138.5	150.8	185.2
99	RLK-1	X52	611.6	6.56	0.50	902.1	358.3	454.7	94.5	41.9	54.8	47.9	47.0	54.2
100	RLK-2	X52	612.8	6.43	0.55	1433.1	358.3	454.7	78.9	36.9	48.6	41.2	40.5	46.9
101	RLK-3	X52	611.7	6.40	0.40	1372.1	358.3	454.7	98.2	49.4	60.1	54.8	53.6	62.9
102	BCG-1	X42	273.4	4.95	0.67	183.0	289.4	413.4	137.6	38.5	66.2	52.5	59.2	75.4
103	BCG-2	X42	273.1	4.68	0.56	48.3	289.4	413.4	138.0	89.7	95.5	87.7	103.3	127.1
104	BCG-3	X42	273.6	4.78	0.34	30.5	289.4	413.4	137.2	101.0	117.2	115.2	126.0	148.9
105	BCG-4	X42	273.2	4.88	0.45	101.6	289.4	413.4	151.9	89.7	94.4	87.1	98.7	124.7

Table A.2 Actual and predicted burst pressure of corroded pipeline (Continued)

No	Test ID	Material	D (mm)	t (mm)	d/t	L (mm)	Material Strength (MPa)		Burst Pressure (bar)					
							SMYS	SMTS	Test	B31G	M. B31G	RSTRENG	DNV	M. PCORRC
106	BCG-5	X42	274.0	4.93	0.32	45.7	289.4	413.4	150.0	104.1	116.3	113.4	125.6	150.0
107	BCG-6	X42	274.3	5.01	0.43	124.5	289.4	413.4	133.6	91.1	95.6	88.2	98.7	124.4
108	BCG-7	X42	274.6	4.57	0.60	66.1	289.4	413.4	126.7	80.2	82.2	72.3	86.4	111.7
109	BCG-8	X42	274.2	4.98	0.55	38.1	289.4	413.4	148.2	100.4	109.1	102.6	118.7	141.9
110	BCG-9	X42	274.6	4.98	0.42	157.5	289.4	413.4	126.4	89.3	93.2	85.8	94.8	118.5
111	ESS-01	X46	324.0	4.83	0.76	99.1	316.9	434.1	97.4	64.8	58.0	42.6	51.2	74.4
112	TCP-01	X46	863.9	9.63	0.38	213.4	316.9	434.1	108.1	65.3	69.1	65.5	71.2	88.8
113	TCP-02	X46	863.9	9.48	0.32	185.5	316.9	434.1	105.7	67.1	72.2	69.5	74.9	92.1
114	TCP-03	X46	863.9	9.38	0.49	91.5	316.9	434.1	91.8	67.1	72.3	69.0	76.1	91.2
115	T001	X52	273.1	10.87	0.37	200.0	358.3	454.7	326.5	254.7	260.9	244.9	255.3	310.6
116	T003	X52	273.1	12.11	0.50	200.0	358.3	454.7	294.9	259.5	256.3	230.0	246.4	306.7

APPENDIX B

BURST TEST SAMPLES DRAWING

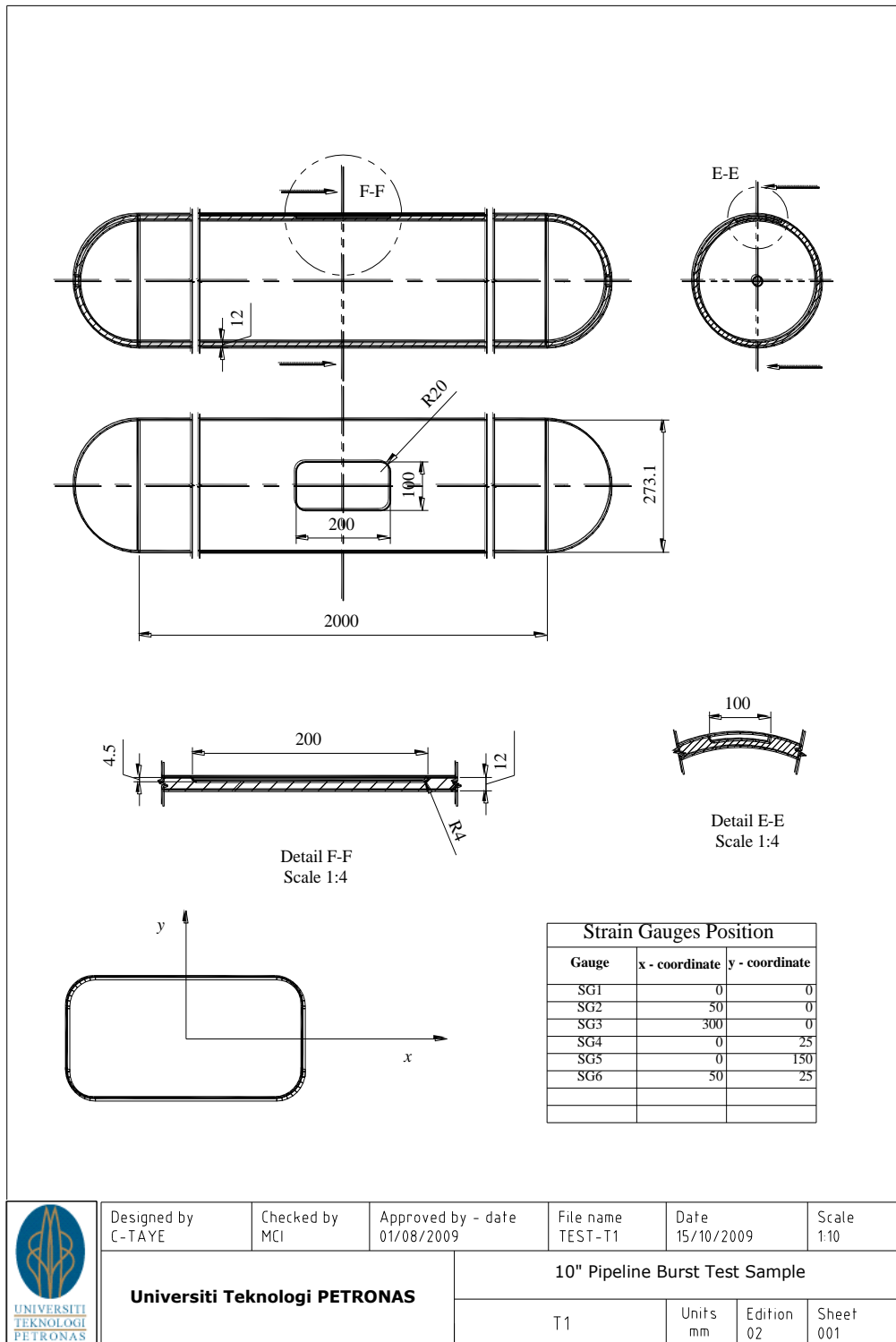


Figure B.1 Burst test sample drawing, T1

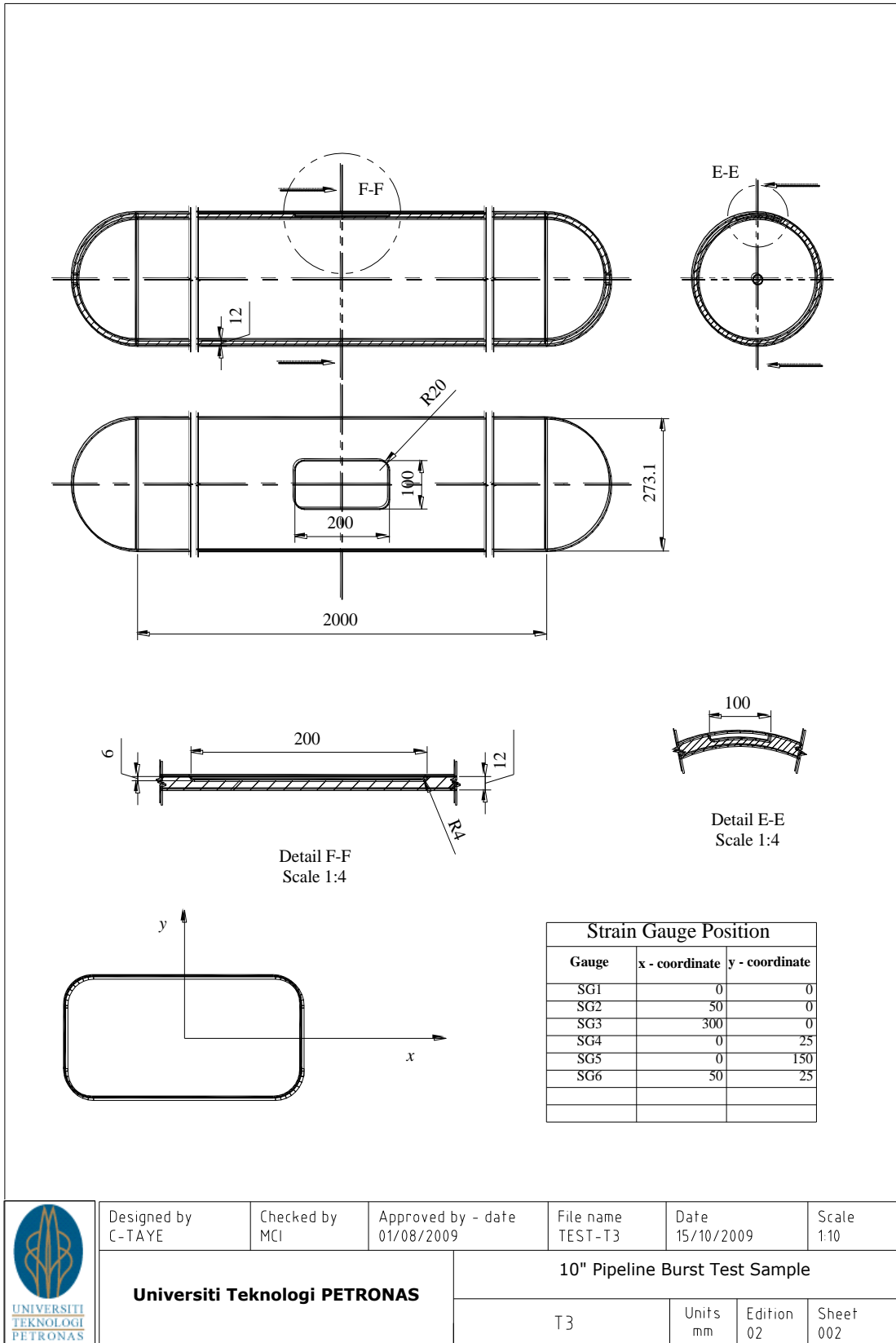


Figure B.2 Burst test sample drawing, T3

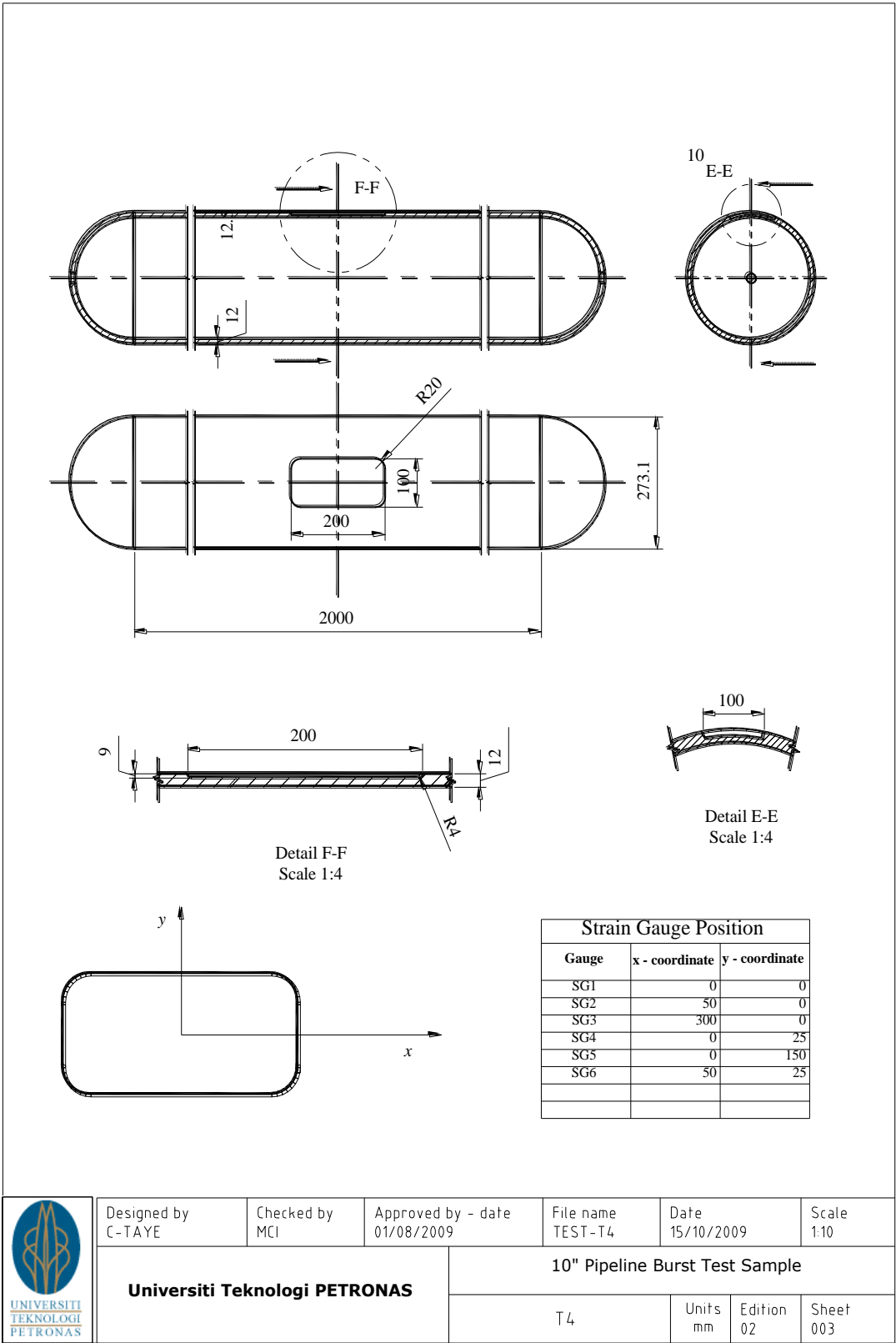


Figure B.3 Burst test sample drawing, T4

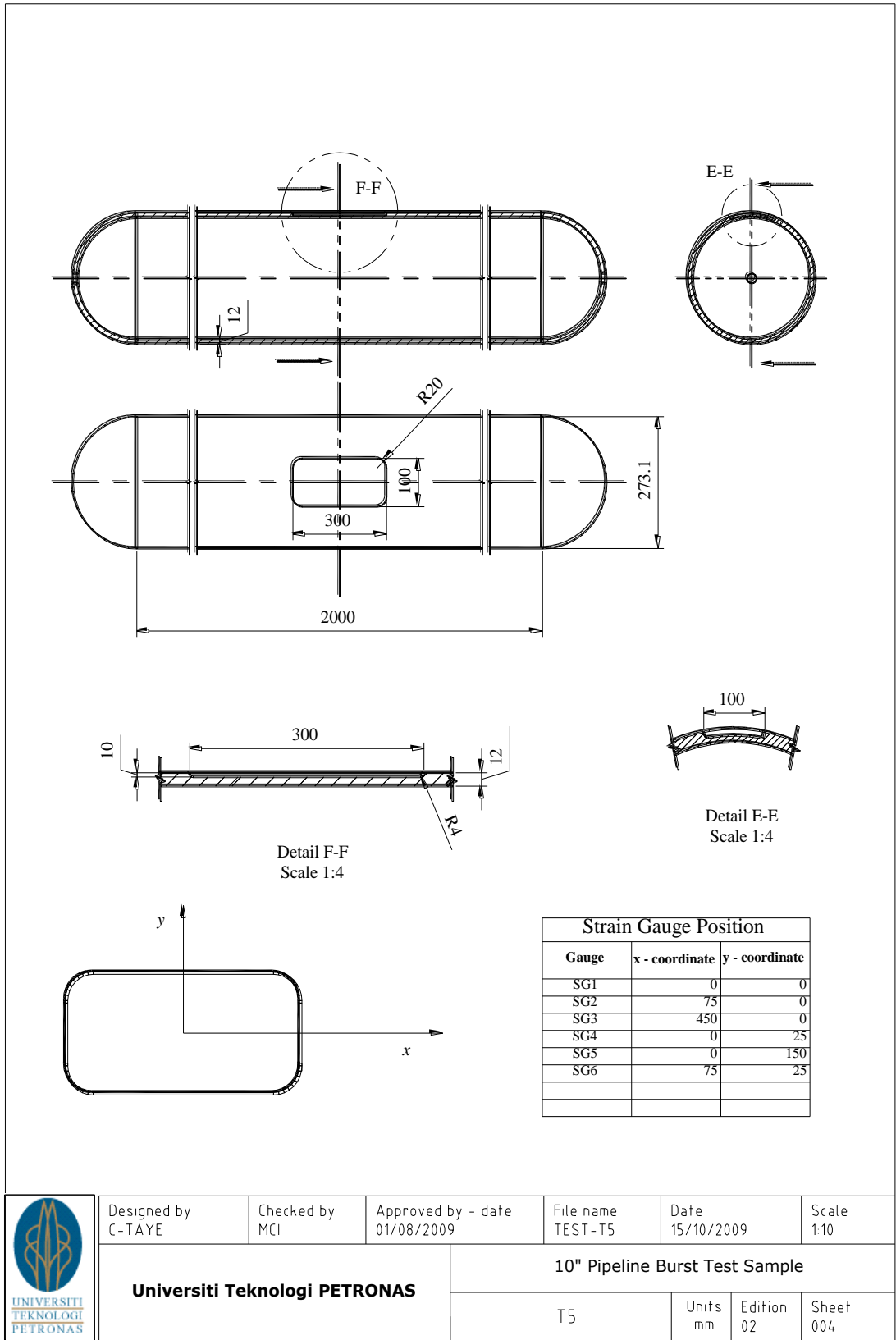


Figure B.4 Burst test sample drawing, T5

APPENDIX C
BURST TEST RECORDS

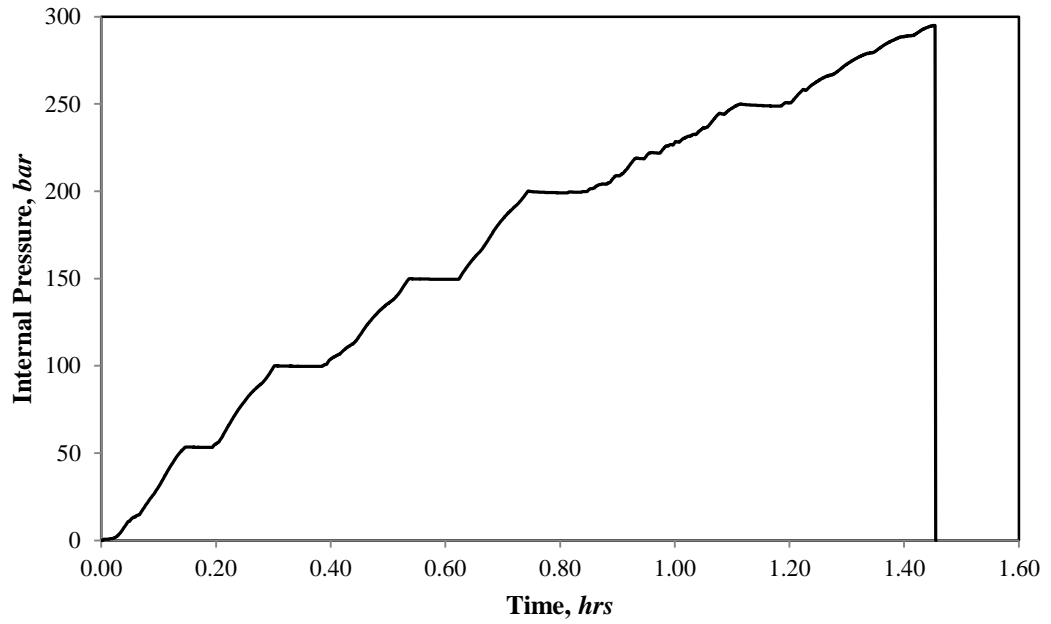


Figure C.1 Burst test, T3

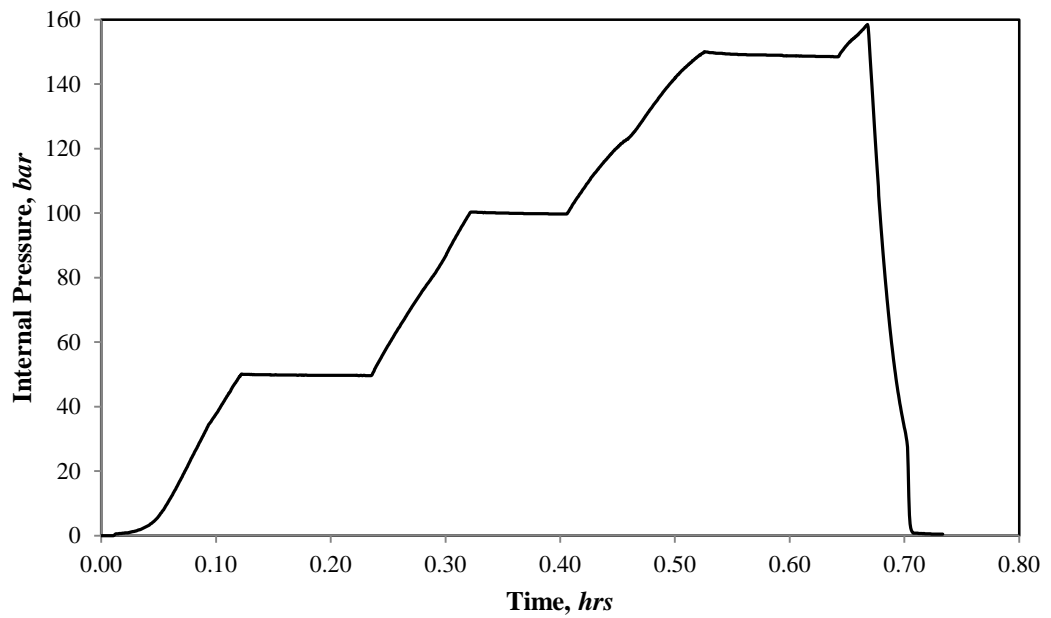


Figure C.2 Burst test, T4

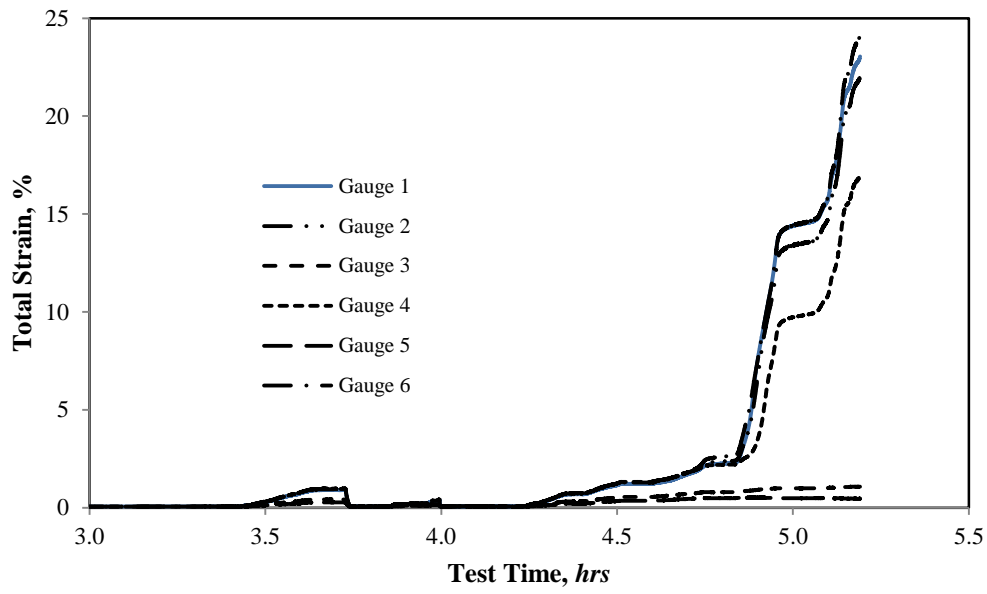


Figure C.3 Total strain distribution, T3

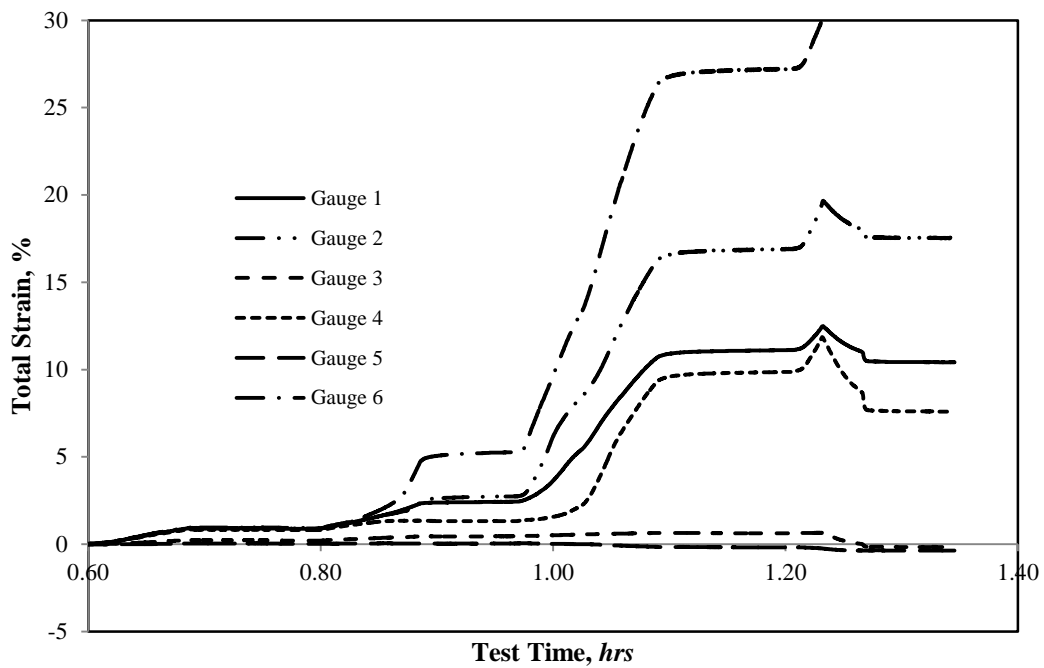


Figure C.4 Total strain distribution, T4

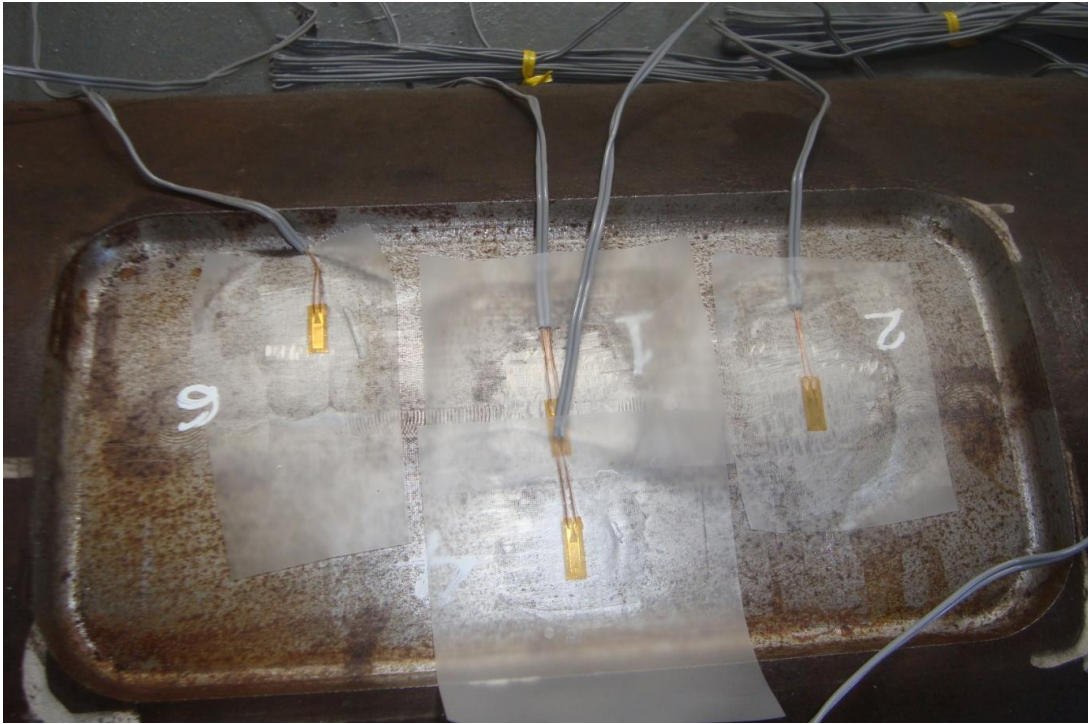
APPENDIX D
BURST TEST PHOTOS



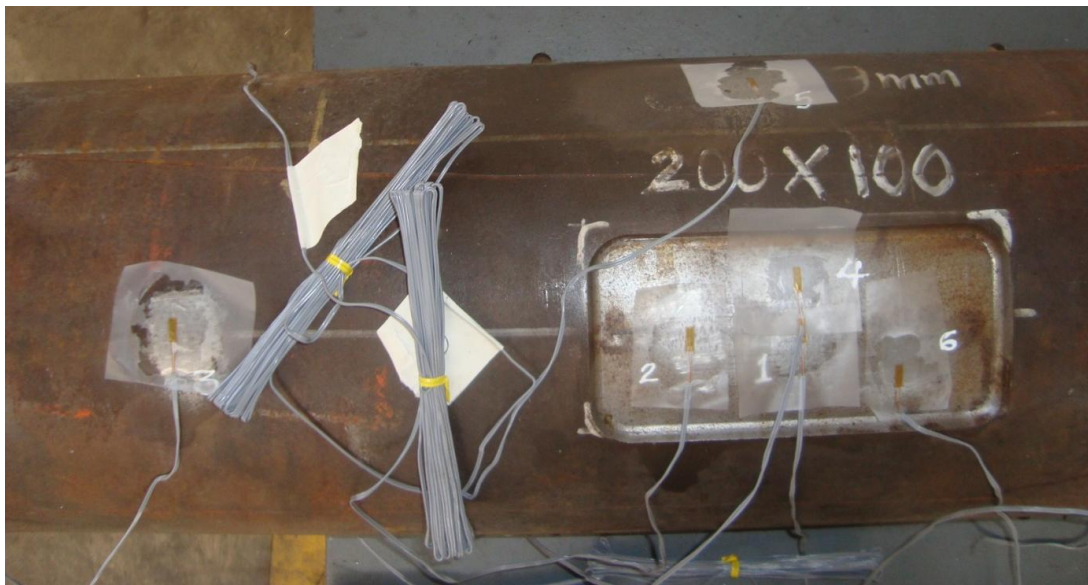
Plate D.1 Sections of abandoned pipeline



Plate D.2 Simulated defect



(a)



(b)

Plate D.3 Surface preparation and strain gauges placement



(a)

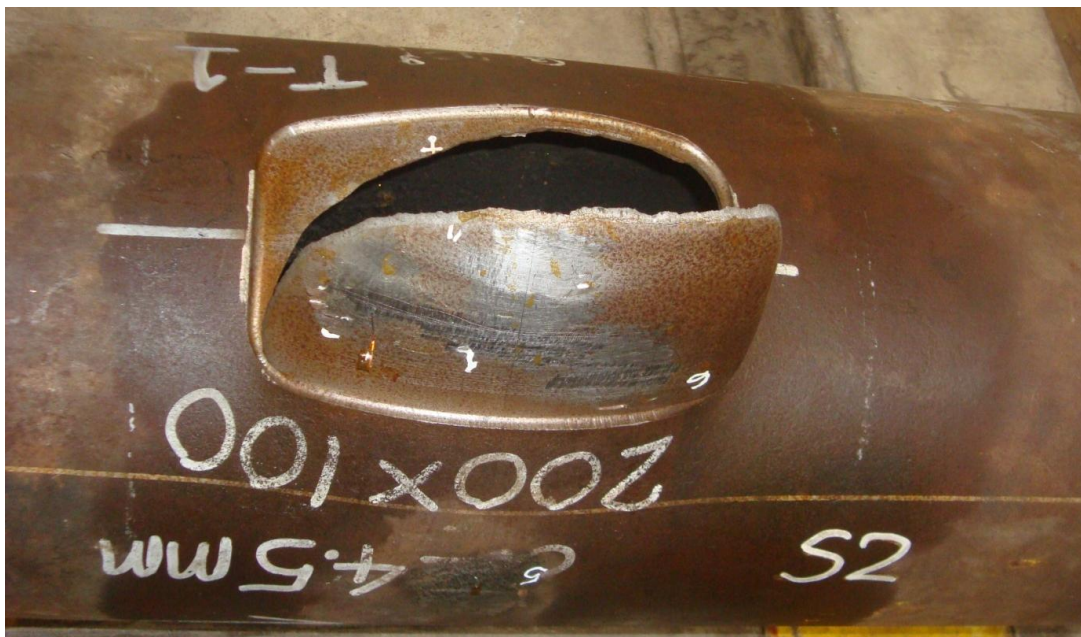


(b)

Plate D.4 Test sample setup: (a) Clamping on saddle support (b) Monitoring device



(a)



(b)

Plate D.5 Samples ruptured at the defect: (a) T3 and (b) T1

APPENDIX E

SAMPLE OF FE SIMULATION RESULTS

Table E.1 A sample of FE simulation results for plane strain defect model [$D = 274mm$, $t = 12mm$, $d/t = 0.5$ and $w/t = 10$]

P_{int} (MPa)	Internal Node		Mid Node		External Node	
	ε_{int}	σ_{int} (MPa)	ε_{mid}	σ_{mid} (MPa)	ε_{ext}	σ_{ext} (MPa)
0.03	0.000002	0.35	0.000003	0.72	0.000002	0.54
0.06	0.000003	0.70	0.000006	1.44	0.000005	1.08
0.10	0.000005	1.22	0.000011	2.52	0.000009	1.90
0.16	0.000009	2.01	0.000019	4.14	0.000014	3.12
0.26	0.000014	3.19	0.000030	6.56	0.000022	4.94
0.40	0.000022	4.98	0.000046	10.18	0.000035	7.69
0.61	0.000035	7.70	0.000070	15.59	0.000053	11.80
0.89	0.000051	11.31	0.000102	22.67	0.000078	17.22
1.17	0.000068	14.98	0.000134	29.70	0.000102	22.63
1.45	0.000084	18.69	0.000165	36.68	0.000126	28.05
1.73	0.000101	22.46	0.000197	43.62	0.000151	33.46
2.01	0.000118	26.26	0.000228	50.52	0.000175	38.88
2.29	0.000136	30.12	0.000259	57.37	0.000200	44.29
2.57	0.000153	34.01	0.000289	64.19	0.000224	49.71
2.85	0.000171	37.95	0.000320	70.96	0.000249	55.12
3.13	0.000189	41.93	0.000350	77.70	0.000273	60.53
3.41	0.000207	45.95	0.000381	84.40	0.000297	65.95
3.69	0.000226	50.01	0.000411	91.06	0.000322	71.36
3.97	0.000244	54.10	0.000441	97.68	0.000346	76.77
4.25	0.000263	58.23	0.000470	104.28	0.000371	82.19
4.53	0.000281	62.40	0.000500	110.84	0.000395	87.60
4.81	0.000300	66.61	0.000529	117.36	0.000419	93.01
5.09	0.000319	70.84	0.000559	123.86	0.000444	98.42
5.37	0.000339	75.11	0.000588	130.32	0.000468	103.83

Table E.1 A sample of FE simulation results for plane strain defect model [$D = 274mm, t = 12mm, d/t = 0.5$ and $w/t = 10$] (continued)

P_{int} (MPa)	Internal Node		Mid Node		External Node	
	ε_{int}	σ_{int} (MPa)	ε_{mid}	σ_{mid} (MPa)	ε_{ext}	σ_{ext} (MPa)
5.65	0.000358	79.41	0.000617	136.75	0.000493	109.25
5.93	0.000378	83.75	0.000646	143.15	0.000517	114.66
6.21	0.000397	88.11	0.000674	149.53	0.000541	120.07
6.49	0.000417	92.51	0.000703	155.88	0.000566	125.48
6.77	0.000437	96.93	0.000731	162.20	0.000590	130.89
7.05	0.000457	101.38	0.000760	168.49	0.000615	136.30
7.33	0.000477	105.86	0.000788	174.76	0.000639	141.71
7.61	0.000498	110.37	0.000816	181.00	0.000663	147.12
7.89	0.000518	114.90	0.000844	187.22	0.000688	152.53
8.17	0.000539	119.46	0.000872	193.41	0.000712	157.94
8.45	0.000559	124.04	0.000900	199.58	0.000737	163.35
8.73	0.000580	128.65	0.000928	205.73	0.000761	168.77
9.01	0.000601	133.28	0.000955	211.86	0.000785	174.18
9.29	0.000622	137.94	0.000983	217.96	0.000810	179.59
9.57	0.000643	142.61	0.001010	224.05	0.000834	185.00
9.85	0.000664	147.31	0.001038	230.11	0.000859	190.41
10.13	0.000686	152.04	0.001065	236.15	0.000883	195.82
10.41	0.000707	156.78	0.001092	242.17	0.000907	201.23
10.69	0.000729	161.54	0.001119	248.18	0.000932	206.64
10.97	0.000750	166.33	0.001146	254.16	0.000956	212.05
11.25	0.000772	171.13	0.001173	260.13	0.000981	217.46
11.53	0.000794	175.96	0.001200	266.07	0.001005	222.87
11.81	0.000815	180.80	0.001227	272.00	0.001029	228.28
12.09	0.000837	185.66	0.001253	277.92	0.001054	233.69
12.37	0.000859	190.54	0.001280	283.81	0.001078	239.10
12.65	0.000881	195.44	0.001306	289.69	0.001103	244.51
12.93	0.000904	200.36	0.001333	295.56	0.001127	249.92

Table E.1 A sample of FE simulation results for plane strain defect model [$D = 274mm$, $t = 12mm$, $d/t = 0.5$ and $w/t = 10$] (continued)

P_{int} (MPa)	Internal Node		Mid Node		External Node	
	ε_{int}	σ_{int} (MPa)	ε_{mid}	σ_{mid} (MPa)	ε_{ext}	σ_{ext} (MPa)
13.21	0.000926	205.29	0.001359	301.41	0.001151	255.33
13.49	0.000948	210.25	0.001386	307.23	0.001176	260.74
13.77	0.000971	215.26	0.001412	313.00	0.001200	266.15
14.05	0.000994	220.36	0.001437	318.69	0.001225	271.56
14.33	0.001017	225.60	0.001462	324.25	0.001249	276.97
14.61	0.001043	231.24	0.001486	329.41	0.001273	282.36
14.89	0.001070	237.18	0.001508	334.28	0.001298	287.75
15.17	0.001098	243.40	0.001528	338.89	0.001322	293.13
15.45	0.001127	249.93	0.001548	343.19	0.001346	298.51
15.73	0.001158	256.74	0.001566	347.23	0.001370	303.88
16.01	0.001191	264.01	0.001582	350.81	0.001395	309.24
16.29	0.001226	271.82	0.001596	353.88	0.001419	314.58
16.57	0.001263	280.07	0.001608	356.52	0.001443	319.92
16.85	0.001301	288.54	0.001619	358.94	0.001467	325.25
17.13	0.001342	297.63	0.001627	360.77	0.001491	330.56
17.41	0.001391	308.49	0.001627	360.88	0.001515	335.84
17.69	0.001447	320.80	0.001622	359.57	0.001538	341.07
17.97	0.001502	333.17	0.001615	358.21	0.001562	346.31
18.25	0.001558	345.57	0.001609	356.83	0.001585	351.54
18.53	0.001614	357.87	0.001603	355.54	0.001609	356.78
18.81	0.001669	370.13	0.001598	354.30	0.001633	362.03
19.09	0.001734	380.71	0.001591	352.77	0.001656	367.26
19.37	0.002021	380.83	0.001559	345.61	0.001780	380.73
19.65	0.002562	381.07	0.001605	355.95	0.002074	380.86
19.93	0.012075	385.27	0.008404	383.65	0.010457	384.56
20.21	0.023566	397.89	0.021752	389.95	0.022661	393.92
20.49	0.025035	404.31	0.022976	395.30	0.023983	399.71

Table E.1 A sample of FE simulation results for plane strain defect model [$D = 274mm, t = 12mm, d/t = 0.5$ and $w/t = 10$] (continued)

P_{int} (MPa)	Internal Node		Mid Node		External Node	
	ε_{int}	σ_{int} (MPa)	ε_{mid}	σ_{mid} (MPa)	ε_{ext}	σ_{ext} (MPa)
20.77	0.026406	410.31	0.024284	401.03	0.025321	405.56
21.05	0.027782	416.33	0.025597	406.77	0.026665	411.44
21.33	0.029160	422.36	0.026912	412.53	0.028010	417.33
21.61	0.030535	428.38	0.028226	418.28	0.029353	423.21
21.89	0.031909	434.39	0.029540	424.03	0.030696	429.08
22.17	0.033379	439.92	0.030894	429.95	0.032101	435.09
22.45	0.034987	445.85	0.032385	436.25	0.033659	440.95
22.73	0.036636	451.94	0.033956	442.05	0.035268	446.89
23.01	0.038300	458.09	0.035550	447.93	0.036895	452.90
23.29	0.039978	464.29	0.037159	453.87	0.038537	458.96
23.57	0.041652	470.47	0.038759	459.78	0.040173	465.00
23.85	0.043488	475.76	0.040384	465.79	0.041849	471.19
24.13	0.045907	481.25	0.042460	473.43	0.044155	477.27
24.41	0.048733	487.66	0.045136	479.50	0.046918	483.54
24.69	0.051741	494.48	0.048023	486.05	0.049858	490.21
24.97	0.054730	501.26	0.050890	492.55	0.052780	496.83
25.25	0.057687	507.96	0.053719	498.96	0.055669	503.38
25.53	0.060638	514.66	0.056538	505.36	0.058553	509.92
25.81	0.063800	520.53	0.059403	511.85	0.061495	516.60
26.09	0.068524	526.93	0.063497	520.12	0.065986	523.49
26.37	0.074277	534.72	0.068967	527.53	0.071603	531.09
26.65	0.080279	542.85	0.074716	535.31	0.077467	539.04
26.93	0.086565	550.40	0.080576	543.25	0.083494	546.93
27.21	0.094018	558.82	0.087565	551.53	0.090752	555.13
27.49	0.101970	567.79	0.095149	560.09	0.098517	563.89
27.77	0.111596	576.83	0.104013	569.75	0.107755	573.24
28.00	0.120732	585.36	0.112721	577.88	0.116666	581.56

Table E.2 A sample of FE simulation results for an axisymmetric defect model [$D = 274mm$, $t = 12mm$, $d/t = 0.5$ and $L/t = 15$]

P_{int} (MPa)	Internal Node		Mid Node		External Node	
	ϵ_{int}	σ_{int} (MPa)	ϵ_{mid}	σ_{mid} (MPa)	ϵ_{ext}	σ_{ext} (MPa)
0.03	0.000003	0.62	0.000003	0.60	0.000003	0.58
0.06	0.000006	1.23	0.000005	1.19	0.000005	1.15
0.10	0.000010	2.15	0.000009	2.08	0.000009	2.02
0.16	0.000016	3.54	0.000015	3.42	0.000015	3.32
0.26	0.000025	5.61	0.000025	5.43	0.000024	5.27
0.40	0.000039	8.73	0.000038	8.45	0.000037	8.19
0.61	0.000060	13.40	0.000058	12.97	0.000057	12.58
0.89	0.000088	19.55	0.000085	18.93	0.000083	18.35
1.17	0.000116	25.70	0.000112	24.88	0.000109	24.13
1.45	0.000144	31.85	0.000139	30.84	0.000135	29.91
1.73	0.000171	38.01	0.000166	36.79	0.000161	35.68
2.01	0.000199	44.16	0.000193	42.75	0.000187	41.46
2.29	0.000227	50.32	0.000220	48.71	0.000213	47.24
2.57	0.000255	56.47	0.000247	54.67	0.000239	53.02
2.85	0.000282	62.62	0.000273	60.62	0.000265	58.80
3.13	0.000310	68.78	0.000300	66.58	0.000291	64.57
3.41	0.000338	74.94	0.000327	72.54	0.000317	70.35
3.69	0.000366	81.09	0.000354	78.50	0.000343	76.13
3.97	0.000393	87.25	0.000381	84.46	0.000369	81.91
4.25	0.000421	93.41	0.000408	90.42	0.000395	87.69
4.53	0.000449	99.56	0.000435	96.38	0.000422	93.48
4.81	0.000477	105.72	0.000462	102.34	0.000448	99.26
5.09	0.000505	111.88	0.000488	108.31	0.000474	105.04
5.37	0.000532	118.04	0.000515	114.27	0.000500	110.82
5.65	0.000560	124.20	0.000542	120.23	0.000526	116.60
5.93	0.000588	130.36	0.000569	126.19	0.000552	122.39
6.21	0.000616	136.52	0.000596	132.16	0.000578	128.17

Table E.2 A sample of FE simulation results for an axisymmetric defect model [$D = 274\text{mm}$, $t = 12\text{mm}$, $d/t = 0.5$ and $L/t = 15$] (continued)

P_{int} (MPa)	Internal Node		Mid Node		External Node	
	ε_{int}	σ_{int} (MPa)	ε_{mid}	σ_{mid} (MPa)	ε_{ext}	σ_{ext} (MPa)
6.49	0.000643	142.68	0.000623	138.12	0.000604	133.95
6.77	0.000671	148.84	0.000650	144.09	0.000630	139.74
7.05	0.000699	155.00	0.000677	150.05	0.000656	145.52
7.33	0.000727	161.16	0.000704	156.02	0.000682	151.31
7.61	0.000755	167.33	0.000730	161.98	0.000708	157.09
7.89	0.000782	173.49	0.000757	167.95	0.000735	162.88
8.17	0.000810	179.65	0.000784	173.91	0.000761	168.67
8.45	0.000838	185.81	0.000811	179.88	0.000787	174.45
8.73	0.000866	191.98	0.000838	185.85	0.000813	180.24
9.01	0.000894	198.14	0.000865	191.81	0.000839	186.03
9.29	0.000921	204.31	0.000892	197.78	0.000865	191.82
9.57	0.000949	210.47	0.000919	203.75	0.000891	197.60
9.85	0.000977	216.64	0.000946	209.72	0.000917	203.39
10.13	0.001005	222.81	0.000973	215.69	0.000943	209.18
10.41	0.001033	228.97	0.001000	221.66	0.000969	214.97
10.69	0.001060	235.14	0.001027	227.63	0.000996	220.76
10.97	0.001088	241.31	0.001053	233.60	0.001022	226.55
11.25	0.001116	247.48	0.001080	239.57	0.001048	232.34
11.53	0.001144	253.64	0.001107	245.54	0.001074	238.13
11.81	0.001172	259.81	0.001134	251.51	0.001100	243.93
12.09	0.001199	265.98	0.001161	257.49	0.001126	249.72
12.37	0.001227	272.15	0.001188	263.46	0.001152	255.51
12.65	0.001255	278.32	0.001215	269.43	0.001178	261.30
12.93	0.001283	284.49	0.001242	275.41	0.001205	267.10
13.21	0.001311	290.66	0.001269	281.38	0.001231	272.89
13.49	0.001339	296.84	0.001296	287.36	0.001257	278.69
13.77	0.001366	303.01	0.001323	293.33	0.001283	284.48

Table E.2 A sample of FE simulation results for an axisymmetric defect model [$D = 274\text{mm}$, $t = 12\text{mm}$, $d/t = 0.5$ and $L/t = 15$] (continued)

P_{int} (MPa)	Internal Node		Mid Node		External Node	
	ε_{int}	σ_{int} (MPa)	ε_{mid}	σ_{mid} (MPa)	ε_{ext}	σ_{ext} (MPa)
14.05	0.001394	309.18	0.001350	299.31	0.001309	290.28
14.33	0.001422	315.35	0.001377	305.28	0.001335	296.07
14.61	0.001450	321.53	0.001404	311.26	0.001361	301.87
14.89	0.001478	327.70	0.001431	317.23	0.001387	307.66
15.17	0.001506	333.87	0.001458	323.21	0.001414	313.46
15.45	0.001534	340.05	0.001485	329.19	0.001440	319.26
15.73	0.001561	346.22	0.001512	335.17	0.001466	325.06
16.01	0.001589	352.40	0.001538	341.15	0.001492	330.85
16.29	0.001617	358.58	0.001565	347.12	0.001518	336.65
16.57	0.001645	364.75	0.001592	353.10	0.001544	342.45
16.85	0.001673	370.93	0.001619	359.08	0.001570	348.25
17.13	0.001701	377.11	0.001646	365.06	0.001597	354.05
17.41	0.001732	380.71	0.001676	371.75	0.001626	360.56
17.69	0.001778	380.73	0.001720	380.29	0.001668	369.81
17.97	0.002097	380.87	0.002017	380.83	0.001942	380.80
18.25	0.003511	381.49	0.003324	381.36	0.003164	381.34
18.53	0.006756	382.92	0.006297	382.56	0.005961	382.57
18.81	0.013850	386.06	0.012762	385.30	0.012069	385.27
19.09	0.024737	403.01	0.022767	394.07	0.021583	389.47
19.22	0.027215	413.85	0.025195	404.74	0.023903	399.36
19.34	0.028378	418.94	0.026339	409.77	0.024999	404.15
19.47	0.029408	423.45	0.027349	414.20	0.025966	408.39
19.66	0.030822	429.64	0.028734	420.28	0.027296	414.21
19.94	0.032857	437.99	0.030723	429.01	0.029207	422.57
20.22	0.034787	445.12	0.032614	436.92	0.031026	430.53
20.50	0.036743	452.34	0.034526	444.00	0.032868	438.03
20.78	0.038792	459.91	0.036522	451.38	0.034792	445.13

Table E.2 A sample of FE simulation results for an axisymmetric defect model [$D = 274\text{mm}$, $t = 12\text{mm}$, $d/t = 0.5$ and $L/t = 15$] (continued)

P_{int} (MPa)	Internal Node		Mid Node		External Node	
	ε_{int}	σ_{int} (MPa)	ε_{mid}	σ_{mid} (MPa)	ε_{ext}	σ_{ext} (MPa)
21.06	0.040910	467.73	0.038585	459.01	0.036781	452.48
21.34	0.043052	474.77	0.040670	466.72	0.038794	459.91
21.62	0.045263	479.79	0.042812	474.12	0.040859	467.54
21.90	0.047704	485.32	0.045159	479.45	0.043117	474.92
22.18	0.050514	491.70	0.047847	485.54	0.045703	480.79
22.46	0.053511	498.49	0.050718	492.06	0.048467	487.05
22.74	0.056631	505.57	0.053715	498.86	0.051355	493.60
23.02	0.059794	512.74	0.056758	505.76	0.054291	500.26
23.30	0.063011	519.46	0.059864	512.81	0.057292	507.07
23.58	0.066449	524.12	0.063177	519.60	0.060492	514.32
23.86	0.070443	529.53	0.067010	524.79	0.064190	521.05
24.14	0.074943	535.62	0.071324	530.63	0.068356	526.70
24.42	0.079642	541.99	0.075843	536.75	0.072725	532.62
24.70	0.084550	548.13	0.080576	543.17	0.077308	538.83
24.98	0.089741	553.99	0.085589	549.22	0.082168	545.41
25.26	0.095250	560.21	0.090917	555.24	0.087338	551.28
25.54	0.100965	566.66	0.096459	561.50	0.092722	557.35
25.82	0.106852	572.40	0.102177	567.91	0.098285	563.63
26.10	0.113127	578.26	0.108279	573.67	0.104224	569.95
26.38	0.119685	584.38	0.114664	579.63	0.110446	575.76
26.66	0.126298	590.84	0.121113	585.67	0.116737	581.63
26.94	0.132846	597.31	0.127509	591.98	0.122980	587.55
27.22	0.139298	603.69	0.133813	598.22	0.129140	593.65
27.50	0.145919	607.49	0.140285	604.29	0.135465	599.90
27.78	0.153060	611.50	0.147260	608.20	0.142289	605.46
28.00	0.159152	614.89	0.153217	611.54	0.148125	608.73

Table E.3 A sample of FE simulation results for a flat-bottomed rectangular defect model [$D = 274mm$, $t = 12mm$, $d/t = 0.5$, $L/D = 0.75$ and $w/t = 10$]

P_{int} (MPa)	Internal Node		Mid Node		External Node	
	ε_{int}	σ_{int} (MPa)	ε_{mid}	σ_{mid} (MPa)	ε_{ext}	σ_{ext} (MPa)
0.07	0.000007	1.46	0.000007	1.45	0.000007	1.45
0.14	0.000013	2.91	0.000013	2.91	0.000013	2.90
0.24	0.000023	5.10	0.000023	5.09	0.000023	5.08
0.39	0.000038	8.38	0.000038	8.36	0.000038	8.35
0.62	0.000060	13.30	0.000060	13.26	0.000060	13.25
0.96	0.000093	20.68	0.000093	20.62	0.000093	20.60
1.48	0.000143	31.75	0.000143	31.66	0.000143	31.63
2.16	0.000209	46.33	0.000208	46.19	0.000208	46.14
2.84	0.000275	60.92	0.000274	60.73	0.000274	60.66
4.88	0.000472	104.72	0.000471	104.35	0.000470	104.18
5.56	0.000538	119.33	0.000536	118.89	0.000535	118.69
6.24	0.000604	133.95	0.000602	133.43	0.000601	133.19
6.92	0.000670	148.57	0.000667	147.98	0.000666	147.69
7.60	0.000736	163.19	0.000733	162.53	0.000731	162.18
8.28	0.000802	177.82	0.000799	177.07	0.000797	176.68
8.96	0.000868	192.45	0.000864	191.62	0.000862	191.17
9.64	0.000934	207.09	0.000930	206.18	0.000927	205.67
10.32	0.001000	221.74	0.000995	220.73	0.000993	220.16
11.00	0.001066	236.38	0.001061	235.28	0.001058	234.64
11.68	0.001132	251.03	0.001127	249.84	0.001123	249.13
12.36	0.001198	265.69	0.001192	264.39	0.001189	263.61
13.04	0.001264	280.35	0.001258	278.95	0.001254	278.10
13.72	0.001330	295.02	0.001324	293.51	0.001319	292.58
14.40	0.001397	309.69	0.001389	308.07	0.001385	307.06
15.08	0.001463	324.36	0.001455	322.63	0.001450	321.54
15.76	0.001529	339.04	0.001521	337.20	0.001515	336.01
16.44	0.001595	353.72	0.001586	351.76	0.001581	350.49

Table E.4 A sample of FE simulation results for a flat-bottomed rectangular defect model [$D = 274\text{mm}$, $t = 12\text{mm}$, $d/t = 0.5$, $L/D = 0.75$ and $w/t = 10$] (continued)

P_{int} (MPa)	Internal Node		Mid Node		External Node	
	ε_{int}	σ_{int} (MPa)	ε_{mid}	σ_{mid} (MPa)	ε_{ext}	σ_{ext} (MPa)
17.12	0.001661	368.40	0.001652	366.33	0.001646	364.96
17.80	0.001752	380.71	0.001737	380.70	0.001726	380.70
18.48	0.002558	381.06	0.002557	381.06	0.002557	381.04
19.16	0.003858	381.59	0.003908	381.60	0.003979	381.60
19.84	0.005589	382.29	0.005735	382.31	0.005959	382.36
20.52	0.007999	383.27	0.008282	383.32	0.008755	383.47
21.20	0.011557	384.77	0.012015	384.87	0.012838	385.16
21.88	0.016493	386.91	0.017155	387.10	0.018401	387.56
22.56	0.021802	390.05	0.022726	393.81	0.024139	399.87
23.24	0.025310	405.23	0.026282	409.41	0.027757	415.73
23.92	0.028607	419.68	0.029614	424.03	0.031113	430.45
24.60	0.032006	434.51	0.033011	438.28	0.034506	443.67
25.28	0.035705	448.32	0.036688	451.91	0.038126	457.10
25.96	0.039500	462.36	0.040441	465.81	0.041789	470.67
26.64	0.043946	476.67	0.044846	478.69	0.046190	481.64
27.32	0.049480	489.24	0.050309	491.11	0.051550	493.83
28.00	0.055456	502.81	0.056193	504.47	0.057314	506.93
28.68	0.061899	517.44	0.062500	518.59	0.063503	519.97
29.36	0.070971	530.17	0.071456	530.83	0.072322	531.93
30.04	0.080893	543.62	0.081216	544.06	0.081905	544.93
30.72	0.092945	557.55	0.093084	557.71	0.093579	558.21
31.40	0.106795	572.30	0.106713	572.23	0.106973	572.42
32.08	0.123164	587.69	0.122814	587.35	0.122800	587.28
32.76	0.140513	604.42	0.139873	604.00	0.139578	603.83
33.44	0.169923	620.77	0.168944	620.24	0.168172	619.77
34.00	0.207153	636.68	0.205869	636.17	0.204545	635.59

APPENDIX F

FE SIMULATION RESULTS

Table F.1 FE results summary for plane strain models ($D = 274mm$ and $t = 12mm$)

d/t	No 1-9		No 1a-9a		No 10-18		No 19-27		No 19a-27a	
	(w/t = 1.0)		(w/t = 2.0)		(w/t = 3.0)		(w/t = 5.0)		(w/t = 15.0)	
	$P_b(bar)$	RSF	$P_b(bar)$	RSF	$P_b(bar)$	RSF	$P_b(bar)$	RSF	$P_b(bar)$	RSF
0.10	48.80	0.98	47.80	0.96	47.40	0.95	47.30	0.95	47.00	0.94
0.20	45.90	0.92	42.95	0.86	43.40	0.87	42.80	0.86	42.60	0.85
0.30	41.05	0.82	39.20	0.78	39.10	0.78	39.10	0.78	38.20	0.76
0.40	36.35	0.73	33.70	0.67	33.75	0.68	33.60	0.67	32.85	0.66
0.50	27.70	0.55	28.15	0.56	28.15	0.56	28.10	0.56	27.70	0.55
0.60	22.40	0.45	22.55	0.45	22.60	0.45	22.40	0.45	22.30	0.45
0.70	17.20	0.34	17.00	0.34	16.90	0.34	16.95	0.34	16.85	0.34
0.80	11.35	0.23	11.35	0.23	11.30	0.23	11.30	0.23	11.30	0.23
0.90	5.70	0.11	5.70	0.11	5.70	0.11	5.70	0.11	5.75	0.12

Table F.2 FE results summary for axisymmetric models ($D = 274mm$ and $t = 12mm$)

d/t	No 28-36		No 37-45		No 46-54		No 46b-54b		No 47a-54a	
	(L/t = 1.0)		(L/t = 3.0)		(L/t = 5.0)		(L/t = 15.0)		(L/t = 25.0)	
	$P_b(bar)$	RSF	$P_b(bar)$	RSF	$P_b(bar)$	RSF	$P_b(bar)$	RSF	$P_b(bar)$	RSF
0.10	45.15	0.90	45.00	0.90	44.20	0.88	43.05	0.86	42.45	0.85
0.20	45.25	0.91	44.20	0.88	42.45	0.85	39.35	0.79	38.30	0.77
0.30	45.10	0.90	43.05	0.86	40.90	0.82	35.60	0.71	34.15	0.68
0.40	44.70	0.89	41.45	0.83	38.35	0.77	31.10	0.62	29.45	0.59
0.50	44.30	0.89	39.55	0.79	35.80	0.72	26.40	0.53	24.65	0.49
0.60	43.00	0.86	37.40	0.75	32.75	0.66	21.40	0.43	19.80	0.40
0.70	41.00	0.82	35.20	0.70	29.05	0.58	16.00	0.32	14.85	0.30
0.80	38.20	0.76	33.15	0.66	25.15	0.50	10.60	0.21	9.95	0.20
0.90	31.15	0.62	30.25	0.61	21.50	0.43	5.25	0.11	5.00	0.10

Table F.3 FE results summary for flat-bottomed rectangular defects: effect of defect width ($D = 274mm$, $t = 12mm$ and $d/t = 0.5$)

w/t	No 55-61		No 62-68	
	$(L/D = 0.75)$		$(L/D = 1.50)$	
	$P_b(bar)$	RSF	$P_b(bar)$	RSF
1	33.70	0.67	30.60	0.61
2	33.35	0.67	29.95	0.60
3	33.25	0.67	30.00	0.60
4	33.30	0.67	30.05	0.60
6	33.10	0.66	30.10	0.60
10	32.35	0.65	29.55	0.59
15	32.10	0.64	29.05	0.58

Table F.4 FE results summary for flat-bottomed rectangular defects: effect of defect length ($D = 274mm$, $t = 12mm$ and $w/t = 6.0$)

L/D	No 69-76		No 77-84		No 85-92	
	$(d/t = 0.30)$		$(d/t = 0.50)$		$(d/t = 0.70)$	
	$P_b(bar)$	RSF	$P_b(bar)$	RSF	$P_b(bar)$	RSF
0.25	42.25	0.85	37.50	0.75	35.05	0.70
0.50	39.50	0.79	34.90	0.70	29.20	0.58
0.75	38.00	0.76	33.05	0.66	25.40	0.51
1.00	37.45	0.75	31.55	0.63	22.95	0.46
1.25	37.25	0.75	30.45	0.61	21.35	0.43
1.50	37.15	0.74	29.95	0.60	20.40	0.41
1.75	37.15	0.74	29.40	0.59	19.60	0.39
2.00	37.10	0.74	29.10	0.58	19.00	0.38

Table F.5 FE results summary for flat-bottomed rectangular defects: effect of defect depth ($D = 274mm$, $t = 12mm$ and $w/t = 6.0$)

d/t	No 94-101 ($L/D = 0.75$)		No 103-110 ($L/D = 1.50$)	
	$P_b(bar)$	RSF	$P_b(bar)$	RSF
0.20	41.60	0.83	41.40	0.83
0.30	37.95	0.76	37.15	0.74
0.40	35.35	0.71	34.20	0.68
0.50	33.00	0.66	30.10	0.60
0.60	29.50	0.59	25.25	0.51
0.70	25.40	0.51	20.45	0.41
0.80	20.60	0.41	16.95	0.34
0.90	14.12	0.28	9.20	0.18

APPENDIX G

LIST OF PUBLICATIONS

Cited Journals

1. Belachew, C.T., Ismail, M.C. and Karuppanan, S., 2011. Strength Assessment of Corroded pipelines- Burst Test, Oil & Gas Journal. (Under Revision)
2. Belachew, C.T., Ismail, M.C. and Karuppanan, S., 2011. Strength Assessment of Corroded pipelines- Finite Element Simulations and Parametric Studies, Oil & Gas Journal. (Under Revision)
3. Belachew, C.T., Ismail, M.C. and Karuppanan, S., 2011. Burst Strength Analysis of Corroded pipelines by Finite Element Method. Journal of Applied Science.
4. Shafiq, N., Ismail, M.C., Belachew, C.T. and Nuruddin, M.F., 2010. Burst Test, Finite Element Analysis and Structural Integrity of Pipeline System, Petromin Pipeliner

Project Reports

1. Belachew, C.T., et al., Failure Analysis of PMO PL24 Corroded Pipeline. 2009, Universiti Teknologi PETRONAS for Group Technology Solutions Research and Technology Division PETRONAS: Perak Malaysia

Conferences

1. Burst strength analysis of corroded pipelines by finite element method. A conference of world engineering, science and technology congress, ESTCON 2010, 15-17 June 2010, Kuala Lumpur Convention Centre, Malaysia
2. Effect of corrosion defect on burst pressure of pipelines: Numerical studies and validation. Malaysia International Non-Destructive Testing Conference and Exhibition 2009 (MINDTCE 09), 20-21 July 2009, The Legend Hotel, Kuala Lumpur, Malaysia

3. Effect of corrosion defects on burst strength of pipelines. NACE East Asian and Pacific Regional Conference and Exposition 2009. Nov 23 -25, 2009, Prince Hotel, Kuala Lumpur, Malaysia.
4. Capacity assessment of corroded pipelines using available codes. National Postgraduate Conference on Engineering, Science and technology (NPC 2009), 25-26 March 2009, Universiti Teknologi PETRONAS, Malaysia
5. Evaluation of available codes for capacity assessment of corroded pipelines. 10th Malaysian Specialist Engineers Meeting (MSEM 2009), “Enhancing Integrity, Nurturing World-Class capability”, 3-4 February 2009, Palace of The Golden Horses, Selangor, Malaysia